

Naval Surface Warfare Center Carderock Division

West Bethesda, MD 20817-5700

NSWCCD-61-TR-2001/21

November 2001

Survivability, Structures, and Materials Directorate
Technical Report

Development of Innovative Nondestructive Evaluation Technologies for the Inspection of Cracking and Corrosion Under Coatings

by

Kirsten G. Lipetzky and Michele R. Novack
Naval Surface Warfare Center, Carderock Division

Ignacio Perez and William R. Davis
Naval Air Warfare Center, Aircraft Division



Approved for public release; distribution is unlimited.

Naval Surface Warfare Center
Carderock Division
West Bethesda, MD 20817-5700

NSWCCD-61-TR-2001/21

November 2001

Survivability, Structures, and Materials Directorate
Technical Report

**Development of Innovative Nondestructive
Evaluation Technologies for the Inspection
of Cracking and Corrosion Under Coatings**

by

Kirsten G. Lipetzky and Michele R. Novack
Naval Surface Warfare Center, Carderock Division

Ignacio Perez and William R. Davis
Naval Air Warfare Center, Aircraft Division

REPORT DOCUMENTATION PAGE

Form Approved
OMB No. 0704-0188

Public reporting burden for this collection of information is estimated to average 1 hour per response, including the time for reviewing instructions, searching existing data sources, gathering and maintaining the data needed, and completing and reviewing this collection of information. Send comments regarding this burden estimate or any other aspect of this collection of information, including suggestions for reducing this burden to Department of Defense, Washington Headquarters Services, Directorate for Information Operations and Reports (0704-0188), 1215 Jefferson Davis Highway, Suite 1204, Arlington, VA 22202-4302. Respondents should be aware that notwithstanding any other provision of law, no person shall be subject to any penalty for failing to comply with a collection of information if it does not display a currently valid OMB control number. **PLEASE DO NOT RETURN YOUR FORM TO THE ABOVE ADDRESS.**

REPORT DATE (DD-MM-YYYY) 29-11-2001		2. REPORT TYPE Final		3. DATES COVERED (From - To) 1 Jan 99 – 21 Mar 00	
4. TITLE AND SUBTITLE DEVELOPMENT OF INNOVATIVE NONDESTRUCTIVE EVALUATION TECHNOLOGIES FOR THE INSPECTION OF CRACKING AND CORROSION UNDER COATINGS				5a. CONTRACT NUMBER N0001499WX21013/AA	
				5b. GRANT NUMBER	
				5c. PROGRAM ELEMENT NUMBER 63716D	
				5d. PROJECT NUMBER	
6. AUTHOR(S) KIRSTEN G. LIPETZKY, MICHELE R. NOVACK, IGNACIO PEREZ, AND WILLIAM R. DAVIS				5e. TASK NUMBER	
				5f. WORK UNIT NUMBER 1-6150-356	
				8. PERFORMING ORGANIZATION REPORT NUMBER NSWCCD-61-TR-2001/21	
7. PERFORMING ORGANIZATION NAME(S) AND ADDRESS(ES) AND ADDRESS(ES) NAVAL SURFACE WARFARE CENTER CARDEROCK DIVISION (CODE 615) 9500 MACARTHUR BOULEVARD WEST BETHESDA MD 20817				NAVAL AIR WARFARE CENTER AIRCRAFT DIVISION MATERIALS DIV., CODE 4.3.4.2 PATUXENT RIVER MD 20670	
9. SPONSORING / MONITORING AGENCY NAME(S) AND ADDRESS(ES) SERDP PROGRAM OFFICE SUITE 303 901 NORTH STUART STREET ARLINGTON, VIRGINIA 22203				10. SPONSOR/MONITOR'S ACRONYM(S) SERDP	
				11. SPONSOR/MONITOR'S REPORT NUMBER(S) SERDP #PP1134	
12. DISTRIBUTION / AVAILABILITY STATEMENT Approved for public release; distribution is unlimited.					
13. SUPPLEMENTARY NOTES					
14. ABSTRACT Three different innovative nondestructive evaluation technologies were developed and evaluated for the ability to detect fatigue cracks and corrosion hidden under painted aluminum panels. The three technologies included real-time ultrasound imaging, thermal imaging, and near-field microwave imaging. With each of these nondestructive inspection methods, subtasks were performed in order to optimize each methodology.					
15. SUBJECT TERMS nondestructive evaluation ultrasound imaging thermal imaging microwave imaging					
16. SECURITY CLASSIFICATION OF:			17. LIMITATION OF ABSTRACT SAR	18. NUMBER OF PAGES 115	19a. NAME OF RESPONSIBLE PERSON Kirsten G. Lipetzky
a. REPORT UNCLASSIFIED	b. ABSTRACT UNCLASSIFIED	c. THIS PAGE UNCLASSIFIED			19b. TELEPHONE NUMBER (include area code) 301.227-5074

CONTENTS

	<u>Page</u>
CONTENTS	iii
FIGURES	v
TABLES	viii
ADMINISTRATIVE INFORMATION	ix
PROJECT BACKGROUND	1
EXPECTED PAYOFF	2
OBJECTIVE	2
TECHNICAL APPROACH	3
<i>Sample Preparation</i>	4
<i>Real-Time Ultrasound Imaging</i>	7
<i>Thermal Imaging</i>	7
<i>Active thermography</i>	7
<i>Sonic thermography</i>	7
<i>Near-Field Microwave Imaging</i>	8
SUMMARY	9
<i>Real-Time Ultrasound Imaging</i>	9
<i>Thermal Imaging</i>	9
<i>Near-Field Microwave Imaging</i>	10
RESULTS AND DISCUSSION	10
<i>Real-Time Ultrasound Imaging</i>	10
<i>Through transmission</i>	11
<i>Reflection</i>	14
<i>Angle beam</i>	16
<i>Thermal Imaging</i>	18
<i>Modeling thermal field transient interaction with corrosion pits</i>	18
<i>Optimization of the thermographic imaging system</i>	22
<i>Active thermography</i>	23
<i>Inductive heating</i>	24
<i>Laser diode excitation</i>	25
<i>Pulse thermography</i>	26
<i>Sonic excitation</i>	28
<i>Near-Field Microwave Imaging</i>	29
<i>Open-ended coaxial probe</i>	30
<i>Open-ended rectangular probe</i>	30
<i>Detection of fatigue cracks</i>	31
<i>Detection of corrosion</i>	37

CONTENTS (Cont.)

	<u>Page</u>
<i>OTHER PROJECT ACCOMPLISHMENTS</i>	<i>40</i>
<i>CONCLUSIONS</i>	<i>40</i>
<i>TRANSITION PLAN</i>	<i>41</i>
<i>REFERENCES</i>	<i>43</i>
<i>APPENDIX A</i>	<i>A-1</i>
<i>APPENDIX B</i>	<i>B-1</i>
<i>APPENDIX C</i>	<i>C-1</i>

FIGURES

<u>Figure</u>		<u>Page</u>
1.	The various types of corrosion that can be found on a typical riveted structure.	3
2.	A typical metallographic image showing exfoliation corrosion of 7075 T6 aluminum. (Cross-sectional view; magnification 100x).....	5
3.	Corrosion severity versus number of fields in the sample versus Time.....	6
4.	Percent corrosion (area loss) versus time (weeks) in a salt fog environment for 7075 T6 aluminum sheet.	6
5.	Immersion tank and early through transmission real-time equipment	11
6.	Through transmission real-time ultrasound image of a composite panel with included flaws showing the detail available at high inspection speed.....	12
7.	Through transmission real-time ultrasound image of a plastic millimeter scale	12
8.	Detection of light corrosion in aluminum 7075 T6 panel.....	13
9.	Acoustocam through transmission real-time ultrasound imaging system in C-shaped frame.....	13
10.	Schematic drawing of beam splitter reflection camera.....	14
11.	Photograph of Acoustocam beam splitter camera.....	15
12.	Corrosion pits (1 mm diameter) detected using Acoustocam beam splitter camera viewed from the front surface of the sample through paint.....	15
13.	Schematic of re-designed beam splitter reflection camera	15
14.	Honeycomb sample (left) and debonding (right) that has occurred within the sample as detected using the reflection Acoustocam system.	16
15.	Modeling was used to examine the beam inside a plate during one side inspection using the oblique angle reflection method.....	16
16.	Schematic of oblique angle reflection camera for real-time ultrasound imaging.	17
17.	Photograph of prototype oblique angle reflection camera.....	17

FIGURES (Cont.)

<u>Figure</u>	<u>Page</u>
18. Corrosion hidden under paint as imaged with the angle beam reflection camera.	17
19. Angle beam image of a flat bottom hole showing the multiple images that occur.....	18
20. This figure shows the building blocks of the simple calorimetric model. Two different materials with different density and specific heat comprise the panel.	20
21. Graph showing the thermal imaging detectability regions in parameter space for two different aluminum panel thicknesses.....	20
22. Aluminum panels with flat bottom holes used to characterize the response of the thermographic system. The panel on the left is 1/8” thick and has 40 flat bottom holes of different radii and depths. The panel on the right is 1/16” thick and has 12 flat bottom holes with much smaller diameters.	22
23. Thermographic inspection system developed by Thermal Wave Imaging, Inc..	23
24. Aluminum panel with a fatigue crack in the center.....	24
25. Experimental setup for the inductive heating excitation method of thermal imaging.....	24
26. Thermal contrast generated across the fatigue crack by inductive heating.	25
27. Experimental setup for laser diode heating excitation method of thermal imaging.....	26
28. Thermal contrast generated across the fatigue crack by laser diode excitation. .	26
29. Schematic diagram of the experimental setup for pulse thermography.	27
30. The image on the left shows an optical photograph of an F-18 intake panel in which areas of previously detected corrosion have been ground out. The panel was discolored and had numerous stains. The white areas observed in the thermographic image on the right show regions where corrosion was detected under paint using an optimized pulse thermography system (3 kJ flash energy, 6 oz. Uncooled camera, optimized signal processing).....	27

FIGURES (Cont.)

<u>Figure</u>		<u>Page</u>
31.	Large composite thermographic image of F-18 intake panel created from 8 smaller individual images.	28
32.	Experimental setup for the sonic excitation method of thermal imaging.	29
33.	Thermal contrast generated on the fatigue crack specimen by sonic excitation.	29
34.	Schematic drawing of open-ended coaxial microwave probe.	30
35.	Schematic of open-ended rectangular waveguide used for detecting fatigue cracks and corrosion under paint.	31
36.	Crack characteristic signal at 11.3 GHz for a slot with a width of ~0.200 mm and with different depths, coax inner radius of 0.5 mm and outer radius of 1.5 mm.	32
37.	Crack characteristic signal at 11.3 GHz for a slot with a width of ~0.200 mm and with different depths, coax inner radius of 1.0 mm and outer radius of 4.0 mm.	32
38.	Crack characteristic signal for a fatigue crack with a width of ~3 μ m and at a frequency of 11.3 GHz.	33
39.	Crack characteristic signal for covered crack with one and two layers of tissue paper.	33
40.	Crack characteristic signal for covered crack with three and four layers of tissue paper.	34
41.	Influence of frequency and incident power on covered crack detection for a slot with a width of 0.15 mm and a depth of 0.75 mm and coating (tape) thickness of 0.11 mm.	34
42.	Higher order mode signals generated by the open-ended rectangular waveguide probe for a crack in a brass sample with a width of ~0.1 mm and a depth of 0.9 mm at a frequency of 31.5 GHz.	36
43.	Sample plates C (left) and B (right) showing corrosion before being painted, with areas scanned highlighted.	37
44.	Image acquired using an open-ended rectangular waveguide probe of the top-middle strip of the front of panel B, at a frequency of 24.1 GHz and at a standoff distance of 0 mm (i.e. in contact). (Note: Dimensions are in mm)..	38

FIGURES (Cont)

<u>Figure</u>		<u>Page</u>
45.	Image acquired using an open-ended rectangular waveguide probe of the top-middle strip of the front of panel B, at a frequency of 24.1 GHz and at a standoff distance of 5 mm. (Note: Dimensions are in mm).....	38
46.	Image acquired using an open-ended rectangular waveguide probe of the top strip of the front of panel C, at a frequency of 24.1 GHz and at a standoff distance of 5 mm. (Note: Dimensions are in mm).....	39
47.	Image acquired using an open-ended rectangular waveguide probe of the middle strip of the front of panel C, at a frequency of 33.5 GHz and at a standoff distance of 2 mm. (Note: Dimensions are in mm).	39
48.	Image acquired using an open-ended rectangular waveguide probe of the top-middle strip of the front of panel C, at a frequency range of 33.5 GHz and at a standoff distance of 2 mm. (Note: Dimensions are in mm).	39

TABLES

<u>Table</u>		<u>Page</u>
1.	Corrosion, fatigue, and various manufactured samples.....	5
2.	Comparison of all thermal imaging techniques studied under the SERDP program.	9

ADMINISTRATIVE INFORMATION

The work described in this report was funded by the SERDP Program Office, Office of Naval Research, Arlington, VA. under the program titled Innovative Technologies for the Inspection of Cracking and Corrosion Under Coatings, PP-1134 (Program Element 63716D). This report was written by personnel at the Carderock Division, Naval Surface Warfare Center (NSWCCD), West Bethesda, MD Welding & NDE Branch (Code 615), under the supervision of Johnnie J. DeLoach. The report is a compilation of work performed by the various program investigators. The author has made every attempt to incorporate all available sources of information and materials generated from the program, including annual reports, status reports, program reviews, published papers, and personal communications.

This page intentionally left blank

PROJECT BACKGROUND

This project responded to the well documented, tri-service need for NDE technology to both support condition-based maintenance programs for military assets and, more importantly, minimize or mitigate the various streams of VOC and HAP pollutants and other hazardous wastes which create significant environmental compliance burdens for DOD. These basic issues are faced by other federal agencies as well as commercial industries, but the sheer volume of ferrous and non-ferrous metallic weapon platforms and military infrastructure has always presented a formidable life-cycle management problem due to the ever-present natural tendency for metals to degrade in the operating environment.

Conventionally, the problems of corrosion (chemical degradation) and fatigue cracking (mechanical degradation) have been addressed with the use of surface coatings (e.g. organic solvent-based paints) and periodic NDE inspections (e.g. eddy current or magnetic particle methods). These practices have evolved over the years with the introduction of technologies offering better performance, but they always remained a significant portion of the maintenance budget for each system and played a major factor in overall system readiness especially since conventional NDE methods have required the removal of surface coatings in order to effectively conduct interrogations of the metallic substrate. With the dawn of environmental compliance mandates, attention has focused on the significant volume of air pollutants and hazardous waste by-products generated by aircraft, ground vehicle, and even shipboard maintenance practices. The disposal costs for these wastes is in the millions of dollars and is increasing.

In July 1997, the SERDP Coatings & Coatings Removal Workshop reviewed the Joint-Service user requirements and formulated the following *high priority* needs:

- “NDE of Paint and Corrosion Under Paint” - techniques needed to determine the extent of corrosion damage to aluminum structure beneath coatings systems without requiring the removal of the coating.
- “Pre-Evaluation Technique/Process to Determine if a Coating Needs to be Removed” - coatings are often stripped from weapons systems in order to evaluate the substrate characteristics, not because of poor coating performance. Capability to inspect “through the coating” would decrease the frequency the number of stripping and repainting cycles.

In addition, the Joint Air Force/FAA/NASA Aging Aircraft Plan, has noted the following similar need:

- Improved non-visual techniques for finding hidden corrosion using a variety of techniques. Must have the capability to discover and roughly quantify hidden corrosion without requiring disassembly of the aircraft. (20% of all needs relating to aging aircraft are for corrosion detection. As a result, new methods of NDE for hidden corrosion are the #2 strategic priority of the Aging Aircraft Plan. “Green” coating systems are the #1 priority)

These needs also tie-in with the FY98 Defense Technology Area Plan, Defense Technology Objective (DTO) MP.07.01—Material and Processes for Metal Cleaning, Corrosion Control, and Coatings. This DTO is from the Civil Engineering & Environmental Quality Sub-area, Pollution Prevention Sub-Sub-area. The objective is to research and develop innovative technologies for preventing pollution while maintaining warfighting capabilities. Current efforts focus on the development of “green” paints, coatings, surface preparations and treatments, and the associated enabling technologies. The February ’98 TARA briefing identified *early corrosion detection capability as a “hot need” and nondestructive analytical techniques as the respective new thrust area*. According to the presenters at the briefing, *“the ability to detect and repair corrosion areas prior to severe degradation will improve operational readiness and reduce operational maintenance cost by 25%.”*

EXPECTED PAYOFF

Reduced frequency of depaint/paint operations leading to significant cost savings, reduced environmental pollution, and enhanced operational availability. Economic benefits will result by reducing the amount of work required to continually strip/repaint, and aircraft would be more available for field operations, thus enhancing force readiness. “Inspection-through-paint” is a prerequisite for long coating system life, and selective stripping of topcoats without removal of corrosion protection layers and the achievement of true condition-based maintenance.

OBJECTIVE

The objective of this program was to develop and evaluate three innovative technologies for their viability as nondestructive evaluation tools for the detection of cracks and corrosion under surface coatings in aircraft and ground vehicle applications. The technologies had been developed in the private sector under either private or Navy SBIR program funding and had shown promise for meeting the technical and sometimes unique logistical needs of DOD aircraft and ground vehicle applications. The technologies included:

- Ultrasound Imaging (Imperium, Inc.)
- Thermal Imaging (Thermal Wave Imaging, Inc. and Wayne State University/Institute for Manufacturing Research)
- Near-Field Microwave Imaging (Texas Research Institute/Austin and Colorado State University/Advanced Microwave Nondestructive Test Lab)

In particular, these technologies were selected for their potential to inspect areas rather than points (translating into efficient levels of inspection scan rates), portability to the job site, overall projected economy to implement, and relative technological maturity. For example, the feasibility of using microwaves to locate hidden corrosion under shipboard paint had already been demonstrated under a Navy contract, however, the technology was in need of transition funding to build prototypes for a commercial hardware offering. Microwave detection of cracks under paint on steel substrates had been addressed in the university environment, and was ready

to transition to practice. The head start advantage of this technology did not mean it was without risk, but it also meant that a product with positive environmental impact could be produced in the SERDP time frame if the risks were overcome.

While not always apparent, there was a sense of urgency for addressing this SERDP need. Goals were in place to *reduce paint stripping and application toxic waste by 50% by FY2001*. And, as in most research in support of pollution prevention, the economic incentives were reductions in operational and environmental compliance costs, disposal costs, workplace exposures to hazardous materials, and long-term liabilities and clean-up costs.

TECHNICAL APPROACH

No matter how good a coating system is, over time it will degrade and the corrosive environment will leak in. This is especially true in aircraft structures where, due to fatigue, UV radiation, and high loads, the coating embrittles. Accelerated fatigue develops predominantly around high flex area at joints and around rivets. In Figure 1 cracks are shown developing around rivets and along a butt joint. Once a crack is formed in the coating, the environment will leach in and corrosion will start to develop. Depending on the material, coating, location, and structure, different types of corrosion will develop such as pitting corrosion, exfoliation, filiform, crevice, and third layer. Most of the effects of corrosion remain hidden from the naked eye until the damage is so significant that the entire structure is placed in danger and major overhaul of the structure is required. Corrosion substantially reduces the strength of materials either by thinning the material, by plastically deforming the materials due to accumulation of debris or by introducing stress raisers. In every case the strength of the structure is significantly reduced. Early detection and quantification of corrosion without removing the paint system can significantly enhance the life of these structures while minimizing the environmental impact.

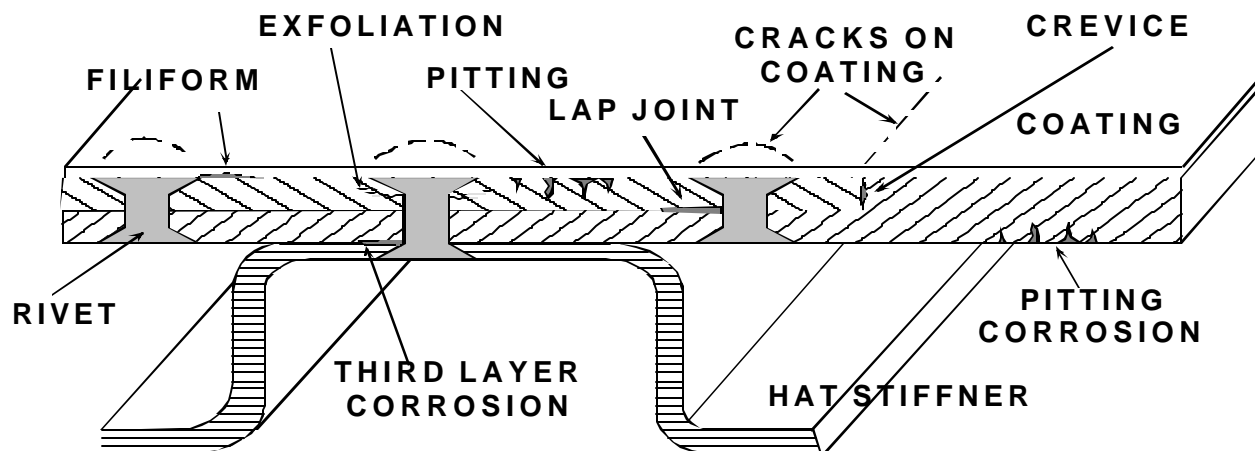


Figure 1. The various types of corrosion that can be found on a typical riveted structure.

In order to properly detect corrosion and diagnose the severity and the impact that it might have on the structure, advanced nondestructive evaluation (NDE) methods are required as well as corrosion models that correlate the NDE signal with the severity of corrosion. In this

program three NDE techniques for the detection of corrosion were evaluated, namely Ultrasound Imaging, Thermal Imaging, and Near-Field Microwave Scanning. These techniques were also believed to be effective in detecting cracks under coatings and were investigated for that purpose as well. In a parallel effort to NDE technique development, models were developed to correlate with the output signature of the various techniques.

Sample Preparation

Corrosion, fatigue, and other manufactured samples were fabricated from aluminum alloy 7075 T6 plate. Alloy 7075 T6 was selected based on the fact that it is a common alloy used in the aircraft industry and was also known to corrode fairly rapidly (a benefit when producing artificially corroded samples). A list of the types of samples that were manufactured appears in Table 1.

A salt fog environment was used to induce corrosion in some of the plates manufactured for this study. The degree of corrosion could be controlled by the duration of the exposure of a plate to the salt fog environment. In addition, it was possible to restrict the corrosion to certain areas on a plate by protecting the majority of a given sample with MIL-P-85582 primer (waterborne, Type 1 Class C—a chromate primer) and MIL-PRF-85285 topcoat (aviation gray paint) and leaving the remaining portion of the sample uncoated and susceptible to the salt fog environment.

The corrosion rate of the samples was studied by metallographically examining the samples that had been corroded in the salt fog environmental chamber for various time periods. The area of each corrosion pit was measured and recorded utilizing a computer based metallographic image analysis system. A typical metallographic image is shown in Figure 2. The quantitative study of corrosion rates yielded information about both pit formation and overall corrosion rate. Figure 3 provides a graphical presentation of the size and number of pits observed as a function of exposure time in the salt fog environment. Initially the corrosion pits were small and scattered evenly about a given sample. (See the four-week exposure distribution in Figure 3.) As the exposure time increased there was no increase in the distribution of the small pits but an increase was observed in the number of large pits. (See the seven-week exposure distribution in Figure 3). Advanced corrosion regions contained pits on the order of 0.020 inch diameter and larger.

Table 1. Corrosion, fatigue, and various manufactured samples.

Corrosion Samples
<ul style="list-style-type: none"> ✱ Set 1 - Heavy corrosion, salt fog plus SO₂ (all paint came off) ✱ Set 2 - Light corrosion, salt fog (paint still on samples) ✱ Set 3 - Bare panels without protection
Manufactured Samples
<ul style="list-style-type: none"> ✱ Crack Samples <ul style="list-style-type: none"> ✱ F1-F4 Fatigue cracks approx. 1" long in 0.062" plate ✱ Flat Bottom Holes (FBH) <ul style="list-style-type: none"> ✱ A1 2" x 4" x 1/16" plate, 0.187" diameter hole 0.005"/0.007" deep inside/outside ✱ A2 3" x 3 3/4" x 1/16" plate, 0.187" diameter hole 0.012"/0.012" deep inside/outside ✱ A3 2 3/4" x 4" x 1/8" plate, 0.187" diameter hole 0.01"/0.025" deep inside/outside ✱ Painted Samples <ul style="list-style-type: none"> ✱ P1 5 1/2" x 7 1/2" x 1/8" plate, 20 each 0.03" diameter holes 0.01"/0.05" deep under 0,2,4, and 6 mils of paint ✱ P2 5 1/2" x 7 1/2" x 1/16" plate, 20 each 0.03" diameter holes 0.01"/0.05" deep under 0,2,4, and 6 mils of paint ✱ Plug Specimens ✱ Welded Specimens

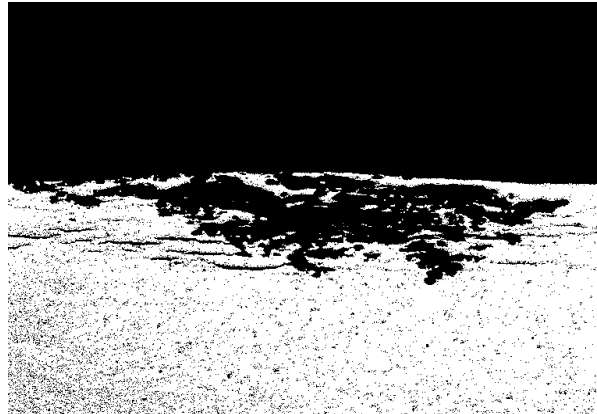


Figure 2. A typical metallographic image showing exfoliation corrosion of 7075 T6 aluminum. (Cross-sectional view; magnification 100x)

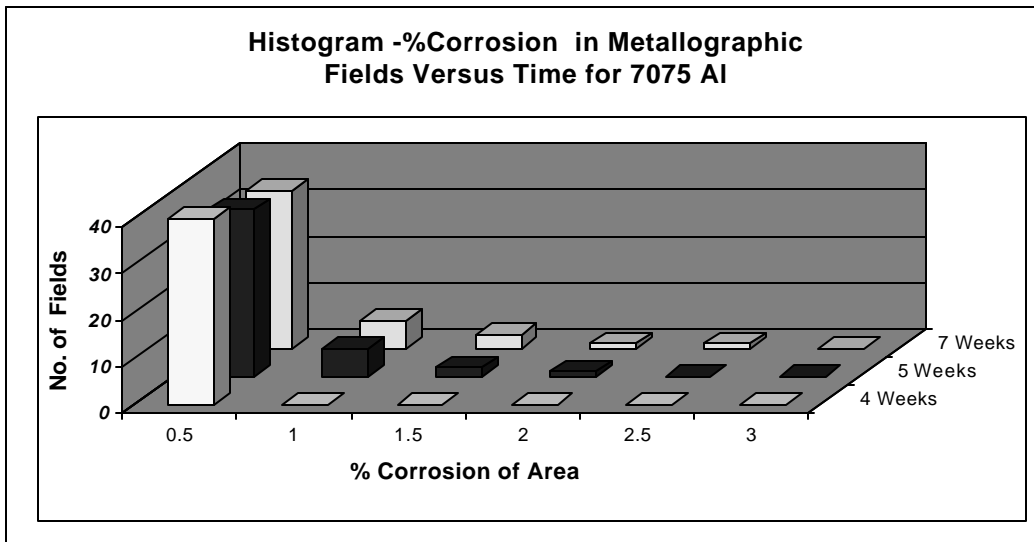


Figure 3. Corrosion severity versus number of fields in the sample versus time.

The study of the growth rate of the pits with regard to mean, average, and maximum value clearly demonstrated the formation of small numbers of larger pits as time progressed. The average corrosion severity (% area loss), as calculated, increased only slowly while the maximum corrosion severity increased at a much greater rate as the smaller number of pits grew rapidly. See Figure 4 for clarification.

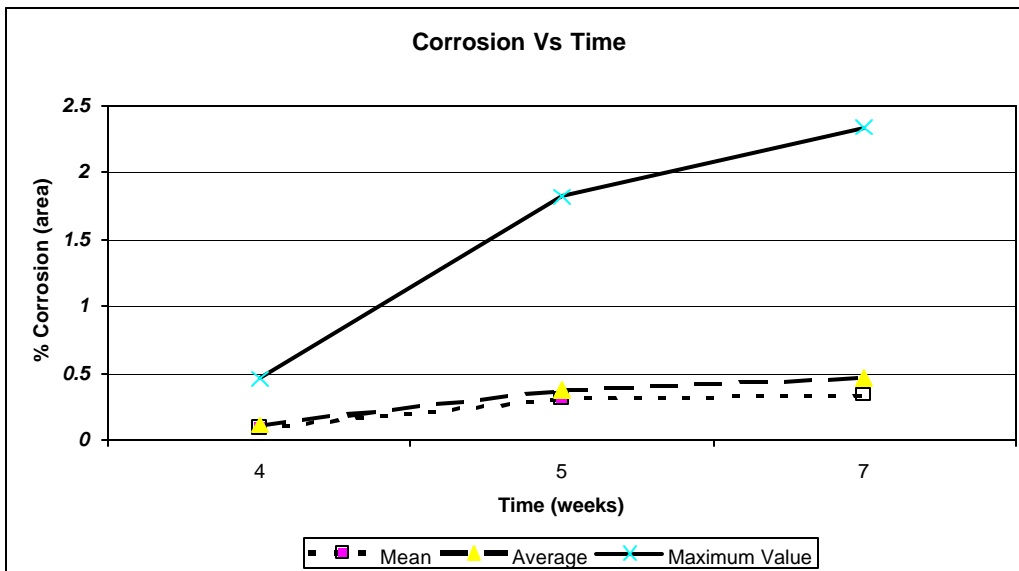


Figure 4. Percent corrosion (area loss) versus time (weeks) in a salt fog environment for 7075 T6 aluminum sheet.

Several samples were manufactured to replicate fine fatigue cracks and center thickness exfoliation corrosion. Fatigue cracks were grown from small stress intensifiers such as tool cuts in the aluminum sheet; the cracks were grown by utilizing fatigue machines to elastically stress

the samples. Several methods for producing exfoliation corrosion samples were attempted. Unsuccessful methods included joining two thin plates together with one of the plates having surface discontinuities (flat bottom holes) on it. Methods for joining the two plates included grease, glue, and metal filled epoxy cement. One method that appeared to be highly successful was drilling a flat bottom hole in a sample and then welding over the hole making sure that the depth of the weld pool didn't reach the bottom of the drilled hole. This resulted in a solid sample with a centerline discontinuity, simulating exfoliation corrosion.

Samples were also manufactured to simulate single corrosion pits under paint. Flat bottom holes with dimensions 0.03 inches in diameter and depths varying from 0.010 inches to 0.05 inches were placed in an array. The samples were then coated with standard paint in such a way that one set of holes having the full range of depths was covered by one paint thickness (2 mils), two paint thicknesses (4 mils), and three paint thicknesses (6 mils).

Real-Time Ultrasound Imaging

In order to perform real-time ultrasound imaging, a concept was developed by Imperium Inc. wherein sound waves could be imaged in a water media using a modified infrared charge coupled device (CCD) [1-5]. Since then, continued development of the "Acoustocam" system has taken place in partnership with Naval Aviation (NAVAIR) through small business innovative research (SBIR) contracts and the current SERDP project.

The basis of the real-time ultrasound imaging technology is a newly developed and patented two-dimensional piezo microelectronic array that generates high resolution subsurface c-scan images over an area in real-time. This is in contrast to present c-scan systems based on a point-by-point scans, which are time consuming and require an immersion system. Entire areas can be imaged with the new portable system in the same amount of time it would be necessary to acquire data from a single point with a standard c-scan system. Investigation and development during the two year period of the SERDP program resulted in three major inspection methods for real-time ultrasound imaging: through transmission, reflection, and angle beam.

Thermal Imaging

Thermal imaging is a nondestructive evaluation technique that relies upon heat transfer characteristics of a given material to discriminate between various regions in a sample. That is, when a material is heated by external sources (for example, flash lamps or ultrasonic frictional heating), anomalies within the material will exhibit temperature differentials that can be detected by an infrared camera.

Active thermography

Active thermography was the approach taken by Thermal Wave Imaging to look for hidden corrosion and fatigue cracks under paint. The principle behind active thermographic techniques is to use external sources to generate heat in a sample and image the sample with an infrared camera both prior to and following the application of the external source in order to record changes in surface temperature. Three main tasks were outlined as to the approach to take

in order to fully evaluate and implement active thermography for the inspection of hidden corrosion and fatigue cracks under paint. The first task involved developing an understanding of the interaction between the thermal field transients and the corrosion pits by expanding on thermal models developed at Naval Air Warfare Center Aircraft Division (NAWC-AD) for the related problem of detection of hidden corrosion under lap-joints. The second task focused on optimizing a hand held thermographic imaging system for detection of corrosion and cracks under coatings. The final task was to experimentally verify the capabilities of the new thermographic system for the detection of corrosion and cracks under paints and determine the sensitivity of the system.

Sonic thermography

Sonic thermography was the approach taken by Wayne State University to look for fatigue cracks under paint. Sonic thermography is performed by utilizing high amplitude sonic waves (typically generated from a 20 kHz ultrasonic horn) to induce vibrations within a sample thereby causing frictional heating at the crack interface; an infrared camera is used as the detector to look for temperature differentials. Because the high amplitude sonic waves spread throughout the entire sample and are not affected by the specimen's surface, there is no need to remove coatings prior to inspection.

Near-Field Microwave Imaging

Microwave crack detection techniques have received considerable attention in the past few years [6-20]. These techniques rely on investigating the reflection properties of metallic surfaces using open-ended microwave probes such as coaxial and waveguide aperture probes. The presence of a surface crack changes the reflection properties of the metallic surface. Detecting these changes, as well as their properties, render such a crack detected and its geometrical properties evaluated. One of the most important features associated with these microwave nondestructive testing and evaluation techniques is their ability to detect cracks under dielectric coatings such as paint, primer and dielectric composites, in addition to detecting cracks filled with such materials. Therefore, these techniques render paint removal unnecessary.

Open-ended rectangular waveguide probes have been used in the past to detect the presence of corrosion in steel plates under layers of paint and primer, as well as under thick composite laminate coatings [21-22]. A microwave signal reflects completely off of a metal surface, regardless of the type of metal. Therefore, the distinction between the SERDP investigation and that of corrosion in steel plates lies solely in the potential difference between the dielectric properties of rust (Fe_2O_3) and aluminum oxide (Al_2O_3).

To determine the potential of microwave crack detection and hidden corrosion techniques, the use of two specific approaches were proposed by Colorado State University and Texas Research Institute Austin, Inc., namely, open-ended rectangular waveguide (higher-order mode) and open-ended coaxial probe techniques. These are both considered to be sensitive approaches for detecting tight surface cracks and hidden corrosion with their respective advantages and limitations.

SUMMARY

Real-Time Ultrasound Imaging

The real-time ultrasonic imaging system developed by Imperium, Inc. in collaboration with NAWC-AD has far exceeded all goals and demonstrated the feasibility of detection of light corrosion and fatigue cracks under paint utilizing a highly portable system. The system works through paint and is capable of detecting corrosion as light as 0.5% weight loss in flat (sheet) material. Three different portable units were developed for real-time ultrasound imaging, these include the through transmission system, the pulse-echo (beam splitter) system, and the oblique angle beam system. Two major accomplishments resulted from this work: (1) the first commercial aerospace unit for through transmission real-time ultrasound imaging is being fabricated for Boeing/Vertol Philadelphia, and (2) application has been made for the issuance of a patent based on the oblique angle beam system.

Thermal Imaging

The thermal imaging techniques pursued by Thermal Wave Imaging and Wayne State University were fairly successful in their ability to detect light corrosion and fatigue cracks under paint. The table below summarizes the capabilities of each of the thermographic techniques investigated as well as the advantages and disadvantages of each technique.

Table 2. Comparison of all thermal imaging techniques studied under the SERDP program.

Technique	Corrosion Detection	Crack Detection	Advantages	Disadvantages
Pulse Heating	Y	Sometimes	Wide area, non-contact, curvature tolerant	Requires absorbing surface
UT Excitation	not tried	Y	Wide area, strong contrast	Coupling effects, point of contact
Induction Heating	N	Y	Non-contact	Coupling variation, uniformity control
Laser Diode Heating	N	Y	Non-contact, curvature tolerant	Requires absorbing surface, low power

Of the three active thermography techniques that were evaluated, the pulse thermography technique shows the most promise for transitioning into the field. The pulse thermography system developed by Thermal Wave Imaging, Inc. under the SERDP program was designed to be fully portable and has proven to have sensitivity sufficient to detect corrosion hidden under paint. Furthermore, the ability to inspect large areas by building mosaics of many smaller individual thermographic images is viewed as being very beneficial to field inspection units. The main shortcoming of the pulse thermography system is the inability to consistently locate fatigue cracks owing to low thermal contrast between the crack and the base material. In contrast, the sonic thermography system developed by Wayne State University is very capable of locating fatigue cracks in samples, however, studies still need to be performed to determine the effectiveness of sonic thermography for the detection of hidden corrosion.

Near-Field Microwave Imaging

Extensive sets of measurements over a wide range of cracks were conducted by Colorado State University using coaxial and open-ended rectangular (higher order mode) waveguide probes. Both coated and uncoated fatigue cracks and slots were studied in this investigation. The results indicate that both probes have high potential for detecting cracks under coatings such as paint and primer. Each probe possesses its unique advantages and disadvantages. The coaxial probe was shown to easily be able to detect tight cracks under coatings of about 0.15 mm at relatively low microwave frequencies (X-band). The coaxial probe was also found to be less susceptible to edge effect issues. The open-ended rectangular (higher order mode) waveguide probe also showed the ability to detect similar cracks under like coatings, however, the issues of edge effects and small changes in the standoff distance seem to be more of a concern when using this probe.

The results of the investigation by Colorado State University and Texas Research Institute showed that there exists a high potential for detecting corrosion in aluminum under a layer of paint and primer using near-field microwave NDT techniques with open-ended rectangular waveguide probes. This was shown in both the theoretical simulations and experimental investigations performed using laboratory designed measurement systems.

The dielectric properties of paint, primer and naturally produced aluminum oxide were measured over a wide range of microwave frequencies (2.6-18 GHz). These materials were found to have low permittivities and low loss factors. Also, it was found that dielectric properties of aluminum oxide, paint and primer are very similar to each other. This is important since it is easier to detect corrosion under paint when the dielectric properties have a greater difference when compared to each other, as is the case with steel corrosion.

RESULTS AND DISCUSSION

Real-Time Ultrasound Imaging

The basis of the real-time ultrasound imaging technology is a newly developed and patented two-dimensional piezo-microelectronic array that generates high-resolution subsurface c-scan images over an area in real-time. This is in contrast to present c-scan systems based on a point-by-point scan, which is time consuming.

When measuring ultrasound energy reflected from targets of interest, particular interest is placed on the surface uniformity of the reflecting target. Specular reflection occurs when the roughness of the target is less than the wavelength of the ultrasound in the medium in which the ultrasound is propagating. For example, if the energy is reflected from a smooth back surface of the target, the energy will be reflected specularly. On the other hand, if the surface is appreciably corroded, scattering will take place. An internal crack will also act as a scattering source.

Scattered energy is typically difficult to detect by a point detector since most of the energy will not strike the detector. However, if a lens is incorporated in the ultrasound camera, the ultrasound receiver will collect much of the energy. Thus, it is quite possible for the ultrasound camera system to detect energy scattered from internal faults that could not otherwise be measured.

Through transmission

Initial work in the area of real-time ultrasound inspection was performed using through transmission techniques. In the through transmission technique a sound beam (coming from an ultrasonic transducer) is passed through a sample from one side and detected by the ultrasound camera on the other side of the sample. Early equipment required the use of an immersion tank so that the transducer, test sample, and camera diaphragm could be immersed in water to permit efficient transmission and detection of the sonic waves. A photograph of the system and immersion tank is shown in Figure 5.

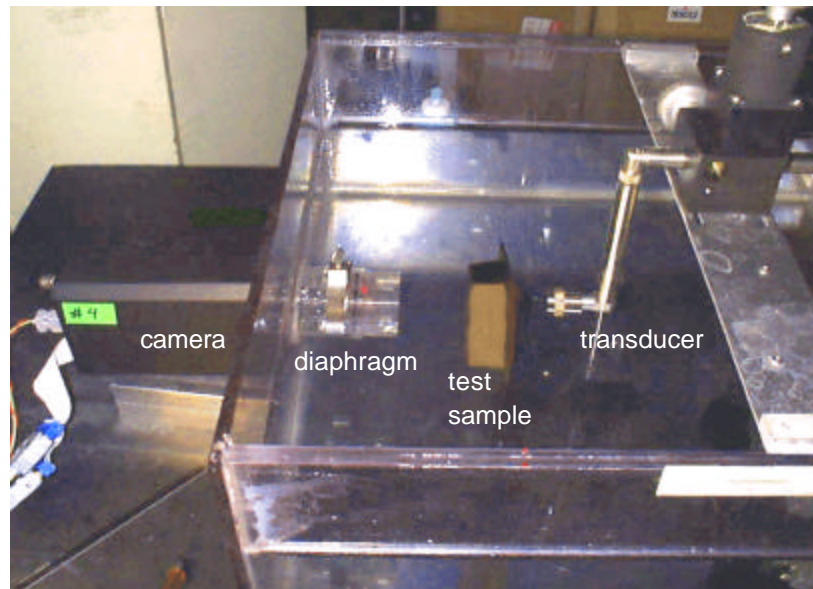


Figure 5. Immersion tank and early through transmission real-time equipment.

Set-up of the immersion tank involved mounting an aqualene diaphragm on one end of the tank as the ultrasound camera was manufactured with a block of aqualene cemented on the imaging chip. In order to obtain an image, a suitable liquid or gel was applied to the outside surface of the diaphragm and the camera was moved into contact with the diaphragm. An immersible transducer (Panametrics A409S-SB 5 MHz usually) was aimed directly into the camera chip and the test sample (target) was positioned near the transducer. The lens array of the camera was then adjusted to focus slightly in front of the transducer. Early through transmission results showed excellent clarity and the ability to penetrate composites up to an inch thick, showing details as fine as the fibers themselves. See Figure 6.

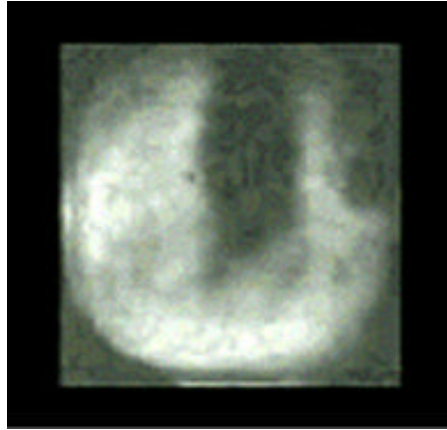


Figure 6. Through transmission real-time ultrasound image of a composite panel with included flaws showing the detail available at high inspection speed.

Improvements gained through study of the physical principles of ultrasound and application to the imaging of ultrasonic waves led to continuous improvements in the techniques used. Higher resolution and clarity were achieved by making modifications to various components in the imaging system, including modifications to the 100 series Acoustocam camera chip, physical coupling, lenses, and transducers. By way of example, the resolution of a millimeter scale focused in through transmission is shown in Figure 7. This resolution and clarity far exceeds anything achieved to date by other ultrasonic methods and the speed of inspection is without comparison.

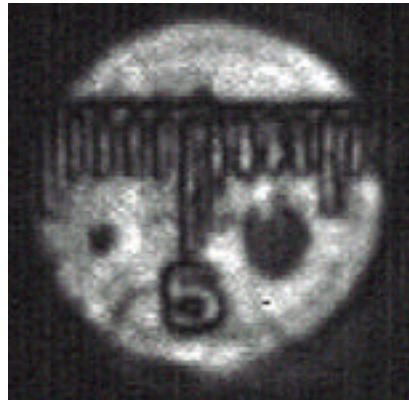


Figure 7. Through transmission real-time ultrasound image of a plastic millimeter scale.

The detection of very light corrosion in the through transmission mode was easy to accomplish through many layers of paint on either the front or back surface. (See Figure 8.) The one drawback of this system was the requirement that the test component, camera diaphragm and transducer all needed to be immersed in water. Few components in the aerospace industry lend themselves to total immersion and as such Imperium Inc. worked on the fabrication of a fixture

for the inspection of parts by through transmission without a water tank. The fixture consists of a large C-shaped frame with the transducer on one side and the camera on the other (Figure 9). Although the use of a couplant (thin film of water or gel) is still necessary in order for the sound energy to pass through the sample from the transducer to the camera diaphragm, the new system is far more amenable to the inspection of aerospace components and other parts where total water submersion may not be possible.



Figure 8. Detection of light corrosion in aluminum 7075 T6 panel.



Figure 9. Acoustocam through transmission real-time ultrasound imaging system in C-shaped frame.

The through transmission method for real-time ultrasound imaging has gained the quickest success and approval by the aerospace industry. In fact, Boeing Vertol is currently evaluating Imperium's Acoustocam through transmission system for use in inspecting small composite parts for delaminations and defects in the production environment.

Reflection

The reflection method of real-time ultrasonic inspection developed during the SERDP program has progressed from a concept to a reality. The inspection camera developed is portable and has a diaphragm on the end that can be pushed against a slightly wetted surface to image the interior of a part. A schematic drawing and a photograph of the beam splitter reflection camera are shown in Figure 10 and Figure 11 respectively, and its operation is described below. In the reflection method the sound generated from an unfocused transducer is redirected into the test sample at the 50/50 beam splitter. The sound propagates into the test sample and upon encountering a discontinuity (e.g. corrosion or crack) or the back wall of the test sample is reflected back into the camera. The sound beam then travels through the beam splitter and focusing lenses to the camera chip. Inspection of corrosion samples prepared in the laboratory shows that corrosion pits one to three mm in diameter are capable of being detected without paint removal from either the front surface (Figure 12) or the back surface of the test sample in real-time.

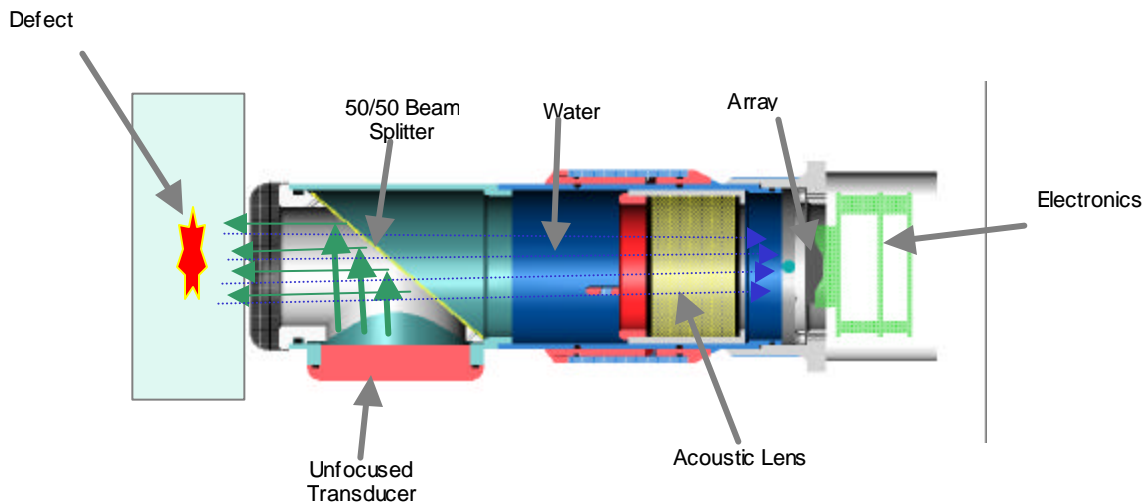


Figure 10. Schematic drawing of beam splitter reflection camera.



Figure 11. Photograph of Acoustocam beam splitter camera.

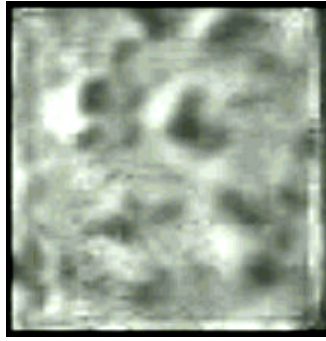


Figure 12. Corrosion pits (1 mm diameter) detected using Acoustocam beam splitter camera viewed from the front surface of the sample through paint.

During the course of the SERDP program many changes were made to advance the technology for real-time reflection ultrasound imaging. The electronics necessary to operate the beam splitter Acoustocam reflection camera shrank from a large rack mount panel to a package the size of a pack of playing cards mounted on the end of the unit. Changes in lens design helped to achieve higher resolution and changes in the beam splitter panel increased the clarity and strength of the received signal. A schematic of the re-designed beam splitter Acoustocam reflection camera is shown in Figure 13.

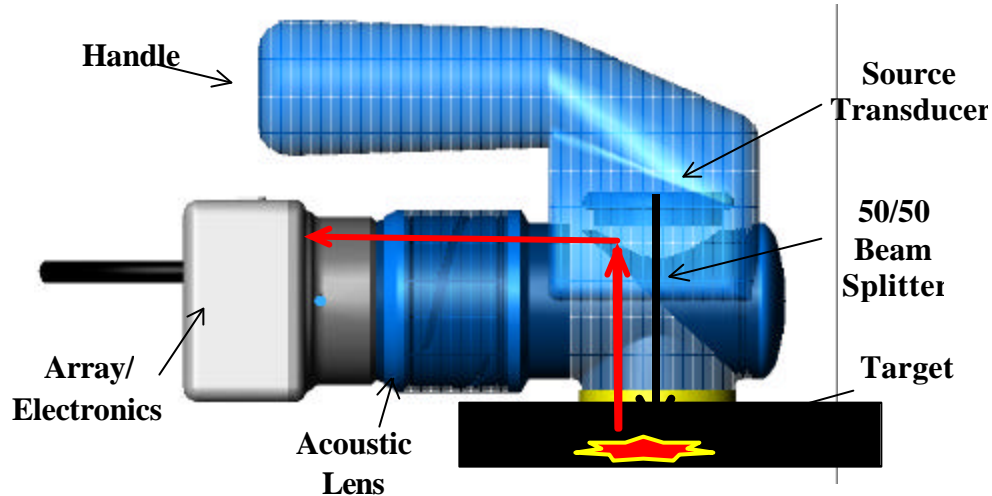


Figure 13. Schematic of re-designed beam splitter reflection camera.

The reflection method is best suited for the inspection of components where only one side of the component is available to the inspector. The real-time reflection ultrasound camera has been found to be of great utility in the inspection of composite components as well as metallic ones. One such application is the inspection of honeycomb panels for locating areas of delamination caused by fabrication problems, fatigue, or water intrusion (Figure 14). Inspection of such components is quite difficult for techniques based on point inspection methods such as the focused beam c-scan ultrasonic method that uses a small ultrasonic beam and scans very

slowly over a structure to allow a computer to build up a picture of the interior. The Acoustocam reflection method is analogous to a visual inspection in which one looks into the interior with a field of view greater than one inch in diameter. The speed of the inspection is very rapid compared to all other existing ultrasonic inspection methods.

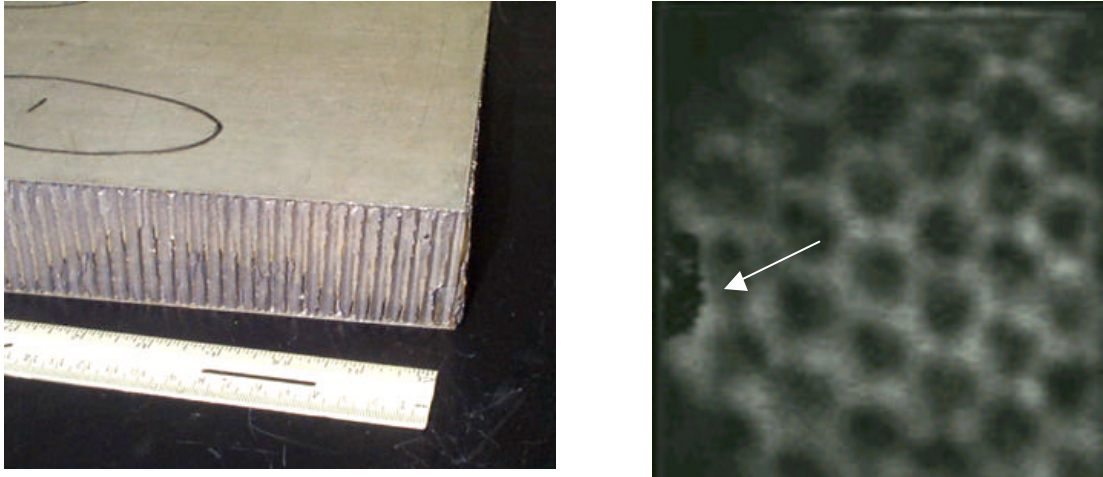


Figure 14. Honeycomb sample (left) and debonding (right) that has occurred within the sample as detected using the reflection Acoustocam system.

Angle beam

The inspection of very thin metallic sheets (0.06 inches up to 0.125 inches thick) was shown to be difficult for the reflection method of ultrasound imaging to undertake; this was due to the extremely short time delay between the front and back surfaces of the thin sheets. By injecting the sound beam into the metallic sheet at an appreciable angle it was found to cause multiple reflections progressing along the sheet with the end result of illuminating a large region of the sample with sound energy (Figure 15). A prototype angle beam ultrasound camera was fabricated at the Becker Labs of the Naval Air Warfare Center Aircraft Division (Figures 16-17) and has proven that rapid ultrasound imaging of thin sheet is practicable and is unaffected by painted coatings (Figure 18).

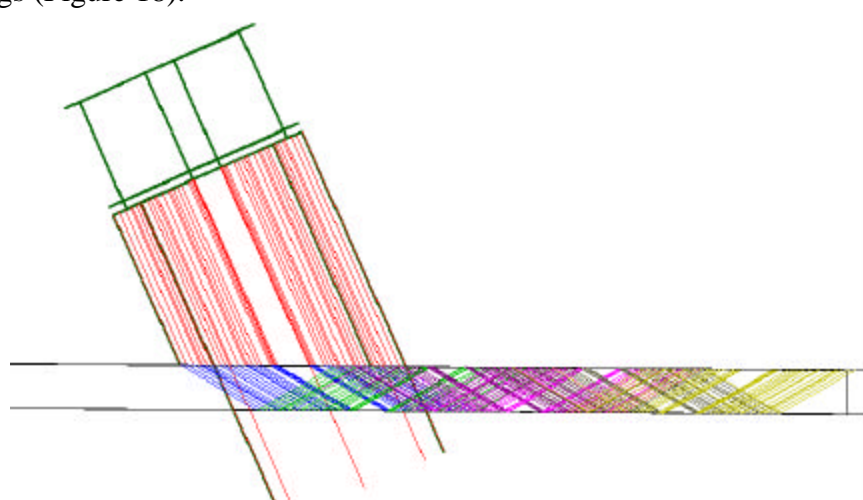


Figure 15. Modeling was used to examine the beam inside a plate during one side inspection using the oblique angle reflection method.

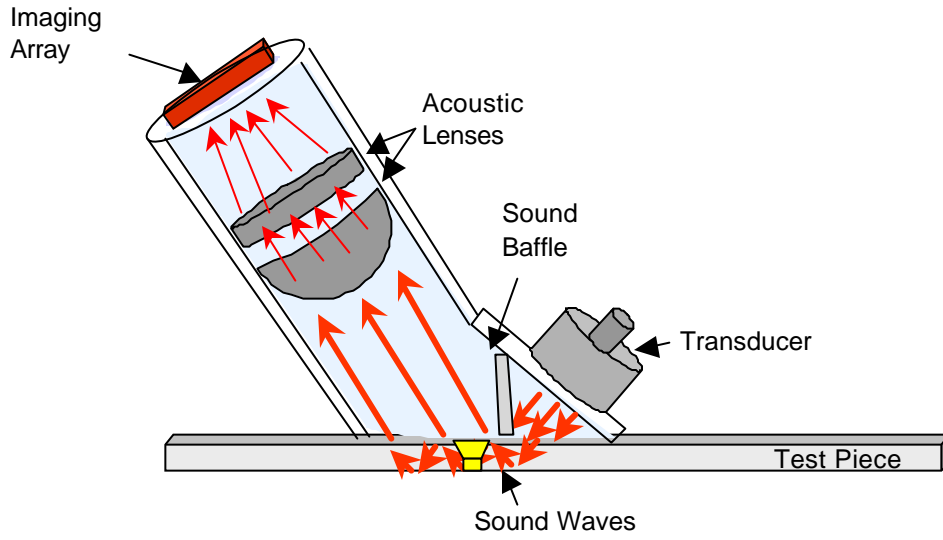


Figure 16. Schematic of oblique angle reflection camera for real-time ultrasound imaging.

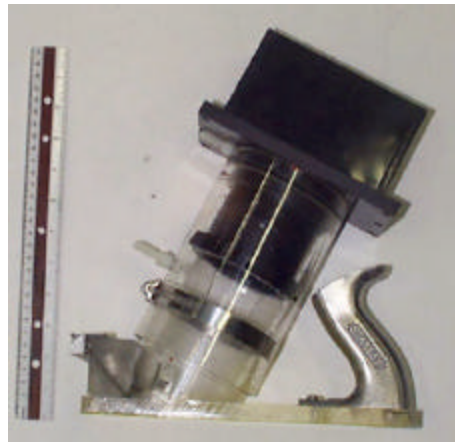


Figure 17. Photograph of prototype oblique angle reflection camera.



Figure 18. Corrosion hidden under paint as imaged with the angle beam reflection camera.

The Acoustocam system was shown to be able to respond to the dynamic range of the multiple bounces with an image very similar to that of a through transmission image with the exception that recurring images of a defect are observed in the oblique angle reflection mode owing to the fact that the sound beam continues to reflect. (See Figure 19). The concept, however, has proven to be viable for the inspection of corrosion under painted coatings at high speed and with high sensitivity. Application has been made for the issuance of a patent based on the oblique angle beam system [23].



Figure 19. Angle beam image of a flat bottom hole showing the multiple images that occur.

Thermal Imaging

Thermal imaging is a nondestructive evaluation technique that relies upon heat transfer characteristics of a given material to discriminate between various regions in a sample. That is, when a material is heated by external sources (for example, flash lamps or ultrasonic frictional heating), anomalies within the material will exhibit temperature differentials that can be detected by an infrared camera.

Three main tasks were outlined as to the approach to take in order to fully evaluate and implement thermal imaging for the inspection of hidden corrosion and fatigue cracks under paint. The first task involved developing an understanding of the interaction between the thermal field transients and the corrosion pits by expanding on thermal models developed at Naval Air Warfare Center Aircraft Division (NAWC-AD) for the related problem of detection of hidden corrosion under lap-joints. The second task focused on optimizing a hand held thermographic imaging system for detection of corrosion and cracks under coatings (Thermal Wave Imaging). The final task was to experimentally verify the capabilities of the thermographic systems for the detection of corrosion and cracks under paint and determine the sensitivity of the systems (Thermal Wave Imaging and Wayne State University).

Modeling thermal field transient interaction with corrosion pits

The effects that materials and process parameters have on thermal contrast have been previously determined [24-26]. These parameters include the amount of heat (Q) deposited on

the surface the sample, of the pit size (A) and depth (h), of the substrate thickness (t_o), of the lateral thermal conductivity (k_l), of the coating thermal properties and of the heating rate (Q/δ). This combined effect can be summarized in the following formula and the following statements:

$$\Delta T = \frac{Q}{\rho c} \left(\frac{1}{d} - \frac{1}{t_o} \right) \left[\frac{k_n R^2}{4k_L} \left(\frac{t_o}{d(t_o - d)} \right)^2 \right]^{\frac{1}{1 - \frac{k_n R^2}{4k_L} \left(\frac{t_o}{d(t_o - d)} \right)^2}}$$

- The contrast temperatures (T) increase linearly with the amount of energy deposited per unit area (Q).
- The higher the specific heat-density of a material ($c \uparrow$) the smaller the contrast temperatures becomes (T \downarrow)
- The closer the defect is to the surface ($d \rightarrow 0$) the larger that the front contrast temperature becomes ($T_{\text{front}} \rightarrow \infty$) while the back contrast temperature is independent of d.
- As the defect depth approaches the panel thickness ($d \rightarrow t_o$) the front contrast temperature vanishes ($T_{\text{front}} \rightarrow 0$) while the back contrast temperature is constant.
- For a given defect depth d, the thicker the panel ($t_o \rightarrow \infty$) the larger the front contrast
- As defects approach to the surface ($d \rightarrow 0$) or as they approach the far end ($d \rightarrow t_o$), the lateral heat effects tend to disappear ($f_{\text{lateral}}(d) \rightarrow 1$) and the contrast is given by

$$\Delta T = \frac{Q}{\rho c} \left(\frac{1}{d} - \frac{1}{t_o} \right)$$

- When the defect size decreases ($R \rightarrow 0$) or the lateral conductivity increases ($k_L \rightarrow \infty$), then the lateral heat factor vanishes ($f_{\text{lateral}}(d) \rightarrow 0$) and the thermal contrast disappears (T $\rightarrow 0$)
- When the lateral conductivity decreases ($k_L \rightarrow 0$) or the defect size increases ($R \rightarrow \infty$) then we approach lateral isolation ($f_{\text{lateral}}(d) \rightarrow 1$) and the contrast becomes $\Delta T = \frac{Q}{\rho c} \left(\frac{1}{d} - \frac{1}{t_o} \right)$
- When the thickness of the panel becomes very large ($t_o \rightarrow \infty$) then the contrast temperature has the limiting value given by $\Delta T = \frac{Q}{\rho c} \frac{1}{d} \left(\frac{R^2}{4d^2} \right)^{\frac{1}{1 - \frac{R^2}{4d^2}}}$
- The higher the specific heat-density product of the second layer ($c_2 \uparrow$) and/or the smaller the specific heat-density product of the first layer ($c_1 \downarrow$) the larger the contrast temperature becomes (T_{front} \uparrow)
- The optimum heating time is given by $\tau_1 = \frac{\rho c}{k} \left(\frac{d(t_o - d)}{t_o} \right)^2$
- If the heating time exceeds the quantity given by $\tau_2 = \frac{\rho c}{k_L} \frac{R^2}{2}$, then the thermal contrast will be exponentially diminished.

All the parameters provided in the previous statements and in the equations are represented in Figure 20. One of the key results of all this modeling is the capability to generate a detectability map. This type of map shows the region in the parameter space (defect depth vs. defect diameter) where defects (corrosion pits) can be detected and regions where they cannot be

detected for a given experimental condition. Figure 21 shows a typical example of a detectability curve for two different aluminum panels. The x-axis represents the flaw diameter (2R). The y-axis represents the defect depth (d). The broken straight lines represent two panel thicknesses. The broken straight line with the label $t=1/16''$ represents an aluminum panel thickness of $1/16'' = 0.0625''$. A point below that line will characterize a defect of specific length and depth in that panel. The broken curve shown on that same graph and located just under the straight line separates that surface area into two regions. One region is labeled detectable region while the remaining region is labeled the undetectable region. The detectable region represents the defects that can be detected thermographically with the infrared system at NAWC-AD. The undetectable region represents the defects that cannot be detected thermographically with the system at NAWC-AD.

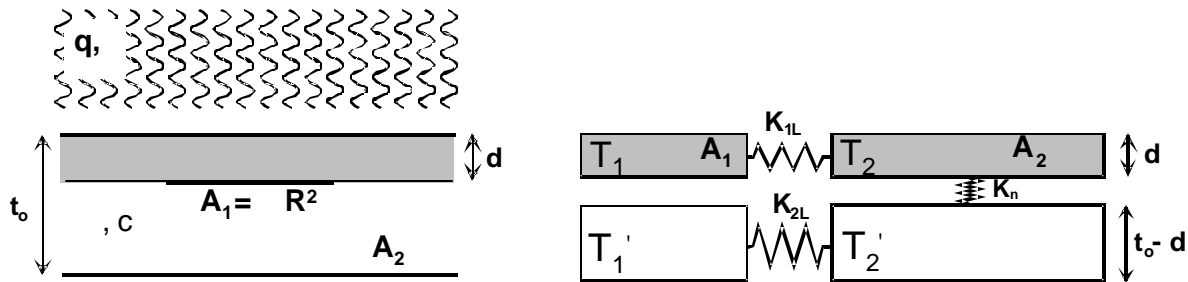


Figure 20. This figure shows the building blocks of the simple calorimetric model. Two different materials with different density and specific heat comprise the panel.

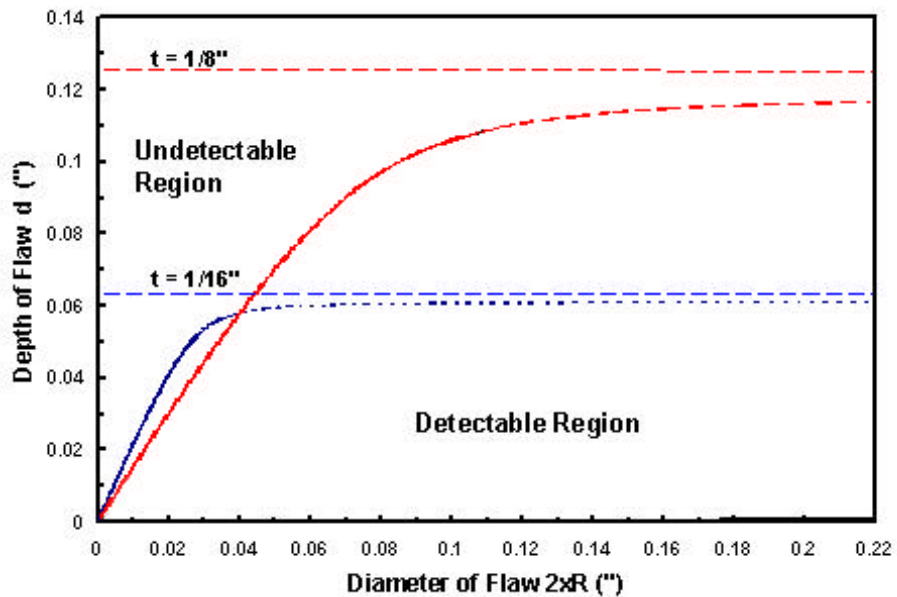


Figure 21. Graph showing the thermal imaging detectability regions in parameter space for two different aluminum panel thicknesses.

From Figure 21, it becomes clear that not all of the pits will be thermographically detectable. The following remarks can be made by analyzing Figure 21:

- No matter how large the defect might be, there is a defect depth (or defect shallowness) below which defects cannot be detected. For 1/16" thick aluminum panels that depth corresponds to approximately 5% mass loss. For a 1/8" thick aluminum panels that corresponds approximately 10% mass loss. The only way by which shallower defects might be detected would be by increasing the amount of energy deposited on the surface.
- As the defect cross section decreases, a point is reached where the detectability limit changes from being flat and constant to rapidly decreasing towards zero. In the case of a 1/16" thick aluminum panel that transition point corresponds to approximately $2R = 40$ mil. For a panel that is 1/8" thick the transition point where the detectability starts departing from a constant value is approximately 100-mil diameter.
- As the panel thickness increases the ratio of "detectable" to "non-detectable" regions decreases as well as the transition point from constant detectability limit to rapidly decreasing detectability increases becomes larger. Both of these limitations reduce the effectiveness of corrosion detection for thick materials.
- In order to improve the detectability region curve for a material, larger amounts of energy need to be deposited on the surface of the panels.

Figure 22 below shows two panels with flat bottom holes (FBH) used to characterize the response of the thermographic system. The panel on the left is a 1/8" thick panel while the panel on the right is a 1/16" thick panel. The panel on the left has a total of 40 FBH while that on the right has a matrix of 12 FBH. The largest flat bottom hole on the left panel was 1" in diameter while the smallest hole diameter was 1/8" diameter. The brightest regions correspond to 80% mass removal while the dimmest regions correspond to 10% mass removal. The largest flat bottom hole on the right panel was 1/16" in diameter while the smallest diameter was 1/32" diameter. The brightest regions correspond to 80% mass removal while the dimmest regions correspond to 40% mass removal. It is clear from the panel on the right that the smaller the diameter of your FBH the smaller the contrast, in fact, the 3/64" diameter and the 1/32" diameter can not be seen in the image at any of the depths studied.

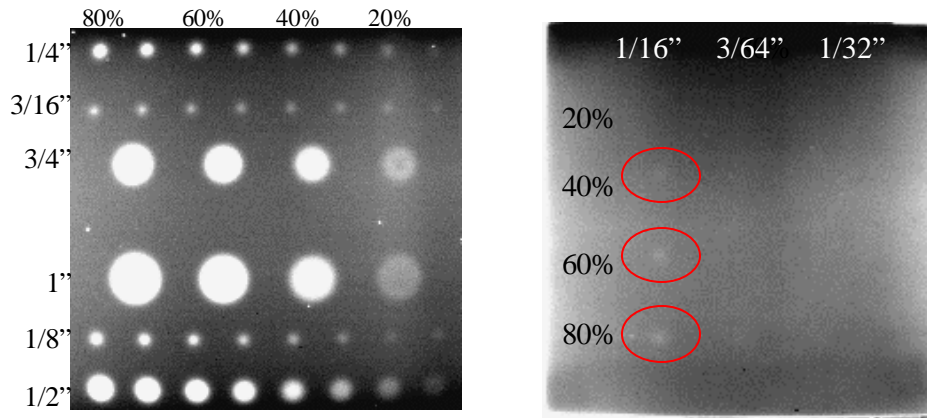


Figure 22. Aluminum panels with flat bottom holes used to characterize the response of the thermographic system. The panel on the left is 1/8" thick and has 40 flat bottom holes of different radii and depths. The panel on the right is 1/16 " thick and has 12 flat bottom holes with much smaller diameters.

Optimization of the thermographic imaging system

Thermal Wave Imaging completed the development of an advanced portable thermographic imaging system with Navy SBIR Phase II funding. A photo of the complete system is shown in Figure 23. The system has many advantages compared with previous generations including, improved lateral resolution, controls that are accessible from the camera head, an LCD display panel located on the camera head, lighter weight, and the system allows for single operator use. In addition, Thermal Wave Imaging developed sophisticated software with automatic detection, segmentation, and classification algorithms for corrosion inspection. Improvements were also made in the data processing, functionality, and storage capabilities of the thermographic system. The advanced portable thermographic imaging system was used in the SERDP program to evaluate the use of thermal imaging for the detection of hidden corrosion and fatigue cracks.



Figure 23. Thermographic inspection system developed by Thermal Wave Imaging, Inc.

Thermal Wave Imaging has investigated several methodologies for conducting active thermography studies for the detection of corrosion and fatigue cracks hidden under paint. These methodologies include, asymmetric inductive heating, asymmetric laser diode heating, sonic excitation heating, and thermal pulse excitation heating. The first two methods rely upon depositing energy near the crack in an asymmetric pattern so as to initiate lateral heat flow. Under these conditions it is expected that a crack will offer the maximum thermal resistance and therefore the largest likelihood that a thermal contrast will develop across the crack.

Figure 24 shows a fatigue crack that was generated in the laboratory for the purpose of comparing all the thermographic excitation techniques. A 1/16" x 3" x 12" aluminum panel was cut with a Dremel® tool to introduce a small notch in the center of the panel. The sample was placed under bending loads in a fatigue machine until fatigue cracks developed. Figure 24 shows the Dremel® notch and two cracks emanating from the tips of the mark. The fatigue cracks are barely visible to the eye and require special illumination to make them visible. The total length of the crack is approximately 1/2" and it is not a through crack.

Active thermography

Active thermography was the approach taken by Thermal Wave Imaging, Inc. to look for hidden corrosion and fatigue cracks under paint. The principle behind active thermographic techniques is to use external sources to generate heat in a sample and image the sample with an infrared camera both prior to and following the application of the external source in order to record changes in surface temperature. Three methods for performing active thermography were evaluated by Thermal Wave Imaging, Inc.: inductive heating, laser diode heating, and pulse thermography. These methods are described in detail below along with the capabilities/shortcomings of each technique.

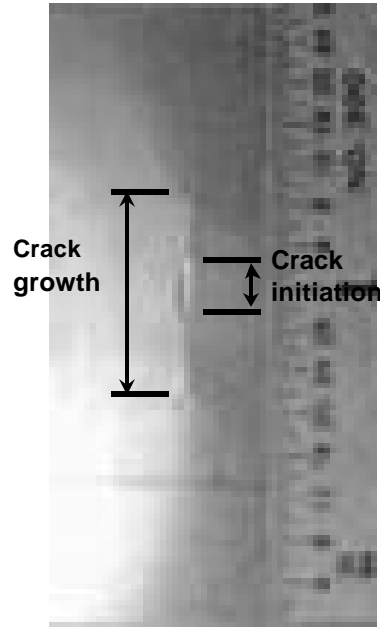


Figure 24. Aluminum panel with a fatigue crack in the center.

Inductive heating

Figure 25 shows the experimental setup used for the inductive heating method of thermographic imaging. The key component is the induction head and the induction coil at the center of the photograph (the power supply is not shown). The induction coil consisted of two loops of thin wall copper tube through which water flowed for cooling purposes. A typical thermographic image of the fatigue crack specimen as acquired using inductive heating is shown in Figure 26.

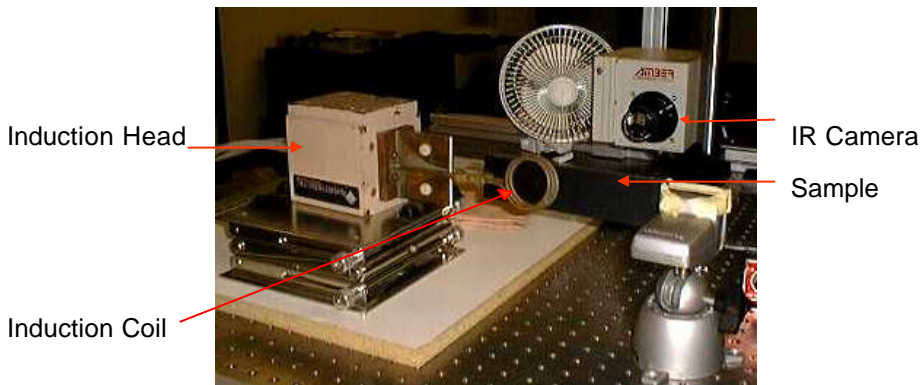


Figure 25. Experimental setup for the inductive heating excitation method of thermal imaging.

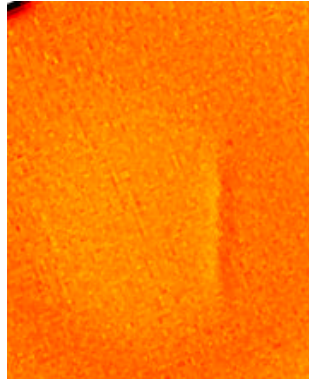


Figure 26. Thermal contrast generated across the fatigue crack by inductive heating.

Several problems were identified with the induction method of thermal excitation. First, the power requirements were significant making the equipment too heavy to be considered portable. The high power requirements mandated that the induction coil be cooled, adding weight and other complications (rigid coil, water tubing) to the system. The rigidity of the coil did not allow for small coils, and therefore small localized heating effects. As a result the thermal gradients were not large in general, leading to small thermal contrast. Finally, with the high power requirements, electrical shock protection became an issue. In general it was determined that the induction thermal excitation method would require significant developmental work in order to increase sensitivity and, as such, other thermal excitation methods were investigated.

Laser diode excitation

Figure 27 shows the experimental setup used for the asymmetric laser diode heating method; the key component of the system is the relatively economic laser diode shown in the photograph. The laser is located behind the camera lens. It should be noted that the power supply for the laser is not shown in Figure 27. Figure 28 represents the thermal contrast image obtained from the fatigue specimen following data massaging. This technology has several advantages and some disadvantages compared to the inductive heating method. One advantage of the laser diode heating method is that the laser diode and power supply are small which allow the system to be portable. Due to the inherent collimation of laser beams, the heated area can be relatively small, and the thermal gradients can be high enough to produce thermal contrast. The major problem with this type of system is the power of the laser diode, which tends to be small leading to small thermal contrast over large areas.

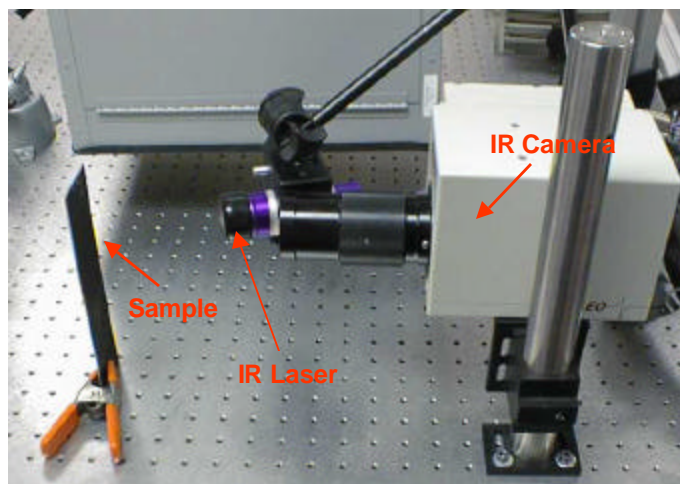


Figure 27. Experimental setup for laser diode heating excitation method of thermal imaging.

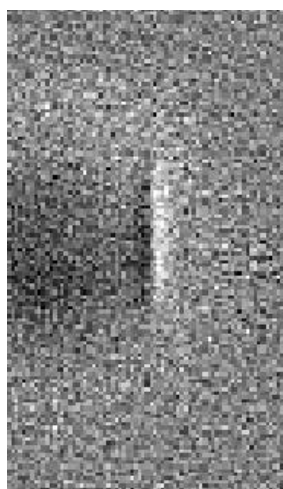


Figure 28. Thermal contrast generated across the fatigue crack by laser diode excitation.

Pulse thermography

A schematic diagram of the pulse thermography approach is shown in Figure 29. The basic concept of this heating method is to use a strong thermal pulse in conjunction with infrared imaging proceeding and following the pulse to record differences in surface temperatures.

Several issues needed to be resolved before the pulse thermography system could be used to look for the effects of corrosion hidden under paint. Detector saturation due to flash heating initially masked the corrosion under the paint, therefore the flash energy was reduced and the dynamic range of the camera

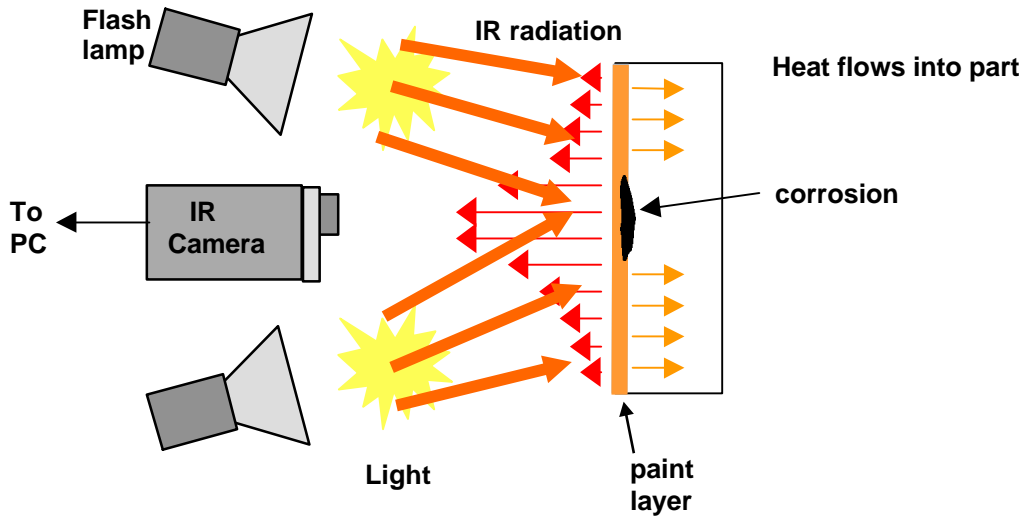


Figure 29. Schematic diagram of the experimental setup for pulse thermography.

was matched to the early time domain only (later time domains require higher flash energy). In addition, changes needed to be made in order to distinguish corrosion from flash reflection artifacts. These changes involved using thermal decay characteristics to identify reflection and corrosion signatures. As a result of these modifications it was possible to identify regions of hidden corrosion under painted surfaces; see Figure 30. Furthermore, as can be seen in Figure 31, it was possible to image large specimens by building a large composite image from smaller individual pulse thermographic images.

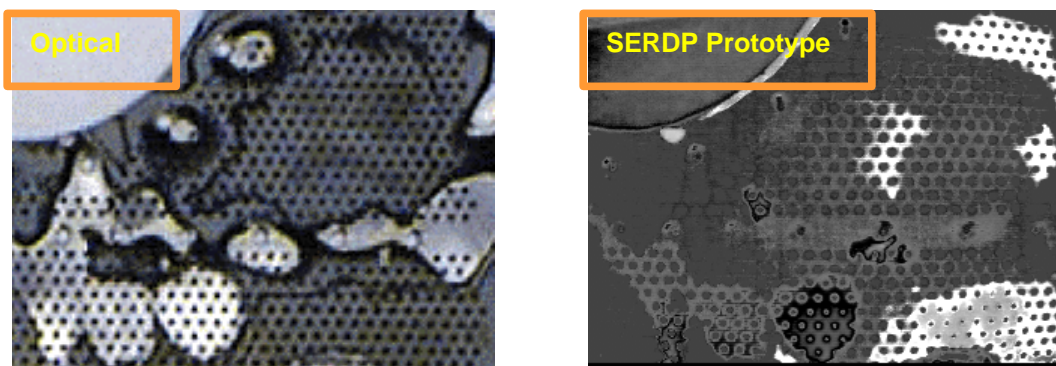


Figure 30. The image on the left shows an optical photograph of an F-18 intake panel in which areas of previously detected corrosion have been ground out. The panel was discolored and had numerous stains. The white areas observed in the thermographic image on the right show regions where corrosion was detected under paint using an optimized pulse thermography system (3 kJ flash energy, 6 oz. uncooled camera, optimized signal processing).

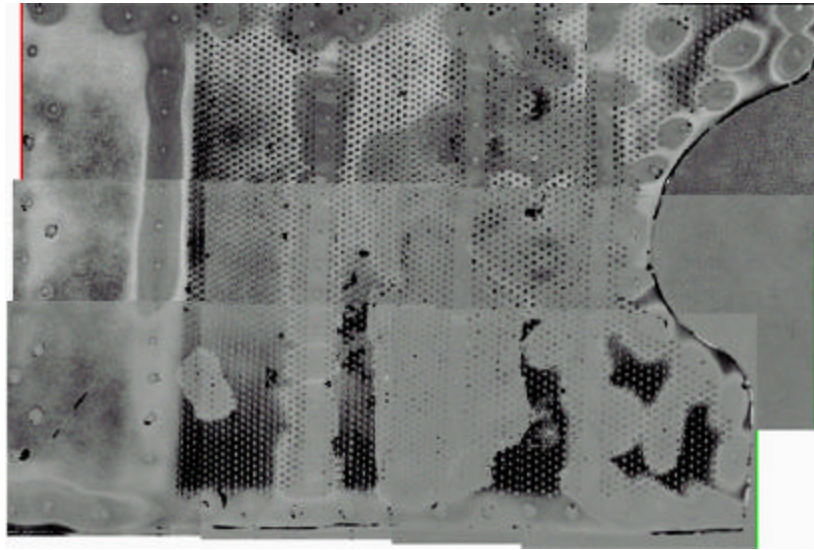


Figure 31. Large composite thermographic image of F-18 intake panel created from 8 smaller individual images.

Sonic excitation

Sonic thermography was the approach taken by Wayne State University to look for fatigue cracks hidden under paint. Sonic thermography is performed by utilizing high amplitude sonic waves (typically generated from a 20 kHz ultrasonic horn) to induce vibrations within a sample thereby causing frictional heating at an interface (e.g. a crack); an infrared camera is used as the detector to look for temperature differentials. Because the high amplitude sonic waves spread throughout the entire sample and are not affected by the specimen's surface, there is no need to remove coatings prior to inspection. In addition large areas with complex curvature can be imaged with the system in the same amount of time that it takes to acquire a single point with a standard c-scan system.

Figure 32 shows the experimental setup used for the sonic excitation method. The main component of this system is the ultrasonic horn used to impart the sonic energy. Figure 33 shows a thermal image acquired from the fatigue crack specimen after only 2 seconds of excitation with the ultrasonic horn. Clearly thermal contrast is very good.

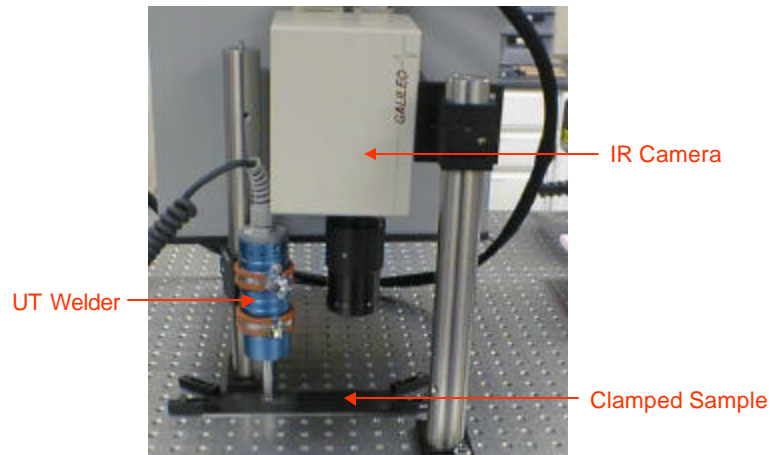


Figure 32. Experimental setup for the sonic excitation method of thermal imaging.

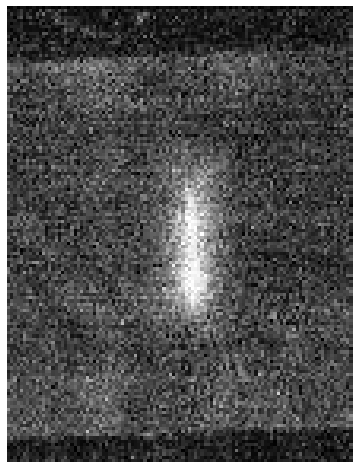


Figure 33. Thermal contrast generated on the fatigue crack specimen by sonic excitation.

Near-Field Microwave Imaging

The presence of surface discontinuities such as cracks or corroded regions change the reflection properties of a metallic surface, by using microwaves to detect these changes and the associated materials properties the discontinuity is distinguished and its geometrical properties evaluated. One of the most important features associated with microwave nondestructive testing and evaluation techniques is the ability to detect cracks and corrosion under dielectric coatings such as paint, primer and dielectric composites, in addition to detecting cracks filled with such materials. Therefore, nondestructive microwave inspection techniques render paint removal unnecessary.

To determine the potential of microwave crack detection and hidden corrosion techniques, the use of two specific approaches were proposed by Colorado State University, namely, open-ended coaxial probe and open-ended rectangular waveguide (higher-order mode) techniques. Both of these techniques are considered to be sensitive approaches for detecting tight surface cracks and hidden corrosion with their respective advantages and limitations.

Open-ended coaxial probe

Figure 34 shows the side and plan views of an open-ended coaxial microwave probe [18]. In general, when open-ended aperture probes interact with material media the aperture fields are perturbed as a function of the properties of the medium they are interacting with. Consequently, a certain amount of the incident fields will be reflected back into the probe. The properties of this reflected signal, directly or its comparison with the incident signal (reflection coefficient) or its combination with the incident signal (standing wave), can provide information about the presence of the material and any anomalies in it as well as giving information about the properties of the anomaly (such as crack dimensions). The distribution of the electromagnetic fields at the aperture of a given open-ended probe significantly influences its interaction with a given anomaly.

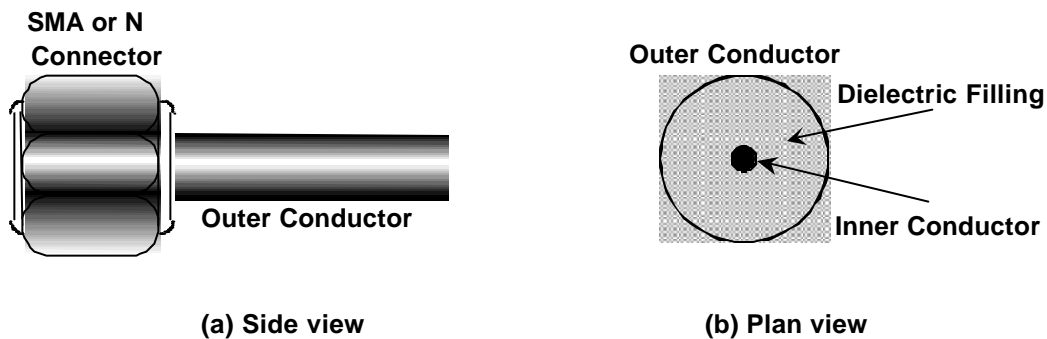


Figure 34. Schematic drawing of open-ended coaxial microwave probe.

When the coax is terminated in a metal plate (conducting plate) the entire incident signal gets reflected back into the coax. As the crack appears in the aperture, the electric field distribution (and hence induced surface currents) is perturbed, which subsequently change the properties of the reflected signal. As more of the crack enters the aperture more of this perturbation is experienced. As the crack passes over the inner conductor the opposite is experienced [18]. The change in reflected signal can be detected in several fashions. One may measure the reflection coefficient at the coaxial aperture and use the change in its phase or magnitude as a means for detecting a surface crack. It is also possible to use systems sensitive to phase or amplitude of reflection coefficient that produce a dc voltage proportional to the change in the phase or magnitude of reflection coefficient. For the experiments conducted in the SERDP program the latter method of detection of change in reflection signal was utilized.

Open-ended rectangular probe

Figure 35 shows a side view of the open-ended rectangular waveguide probe. In the same manner as described with the open-ended coaxial probe, when an open-ended rectangular waveguide is terminated by a metal plate the incident signal goes through a complete reflection. The incident signal is that of the dominant TE₁₀ mode in a rectangular waveguide [8, 15]. However, when there is a crack in the metal plate the surface currents on the metal plate are disturbed and high-order modes are generated. The presence of these modes changes the properties of the reflected signal, hence changes the reflection coefficient (in particular its phase) [8, 15]. The change in phase can be detected somewhere in the waveguide away from the metal plate. This type of crack detection is known as the dominant mode approach. However, it is also possible to detect the presence of the evanescent higher-order modes by placing a small probing antenna near the waveguide aperture. These modes possess all three electric field components. Thus, when the antenna probe is directed along the x-axis it picks up electric field components in that direction. In the absence of a crack there are no high-order modes generated. However, in the presence of a crack higher-order modes are generated and picked up by the small antenna placed along the narrow dimension of the aperture. This signal is then detected using a diode detector.

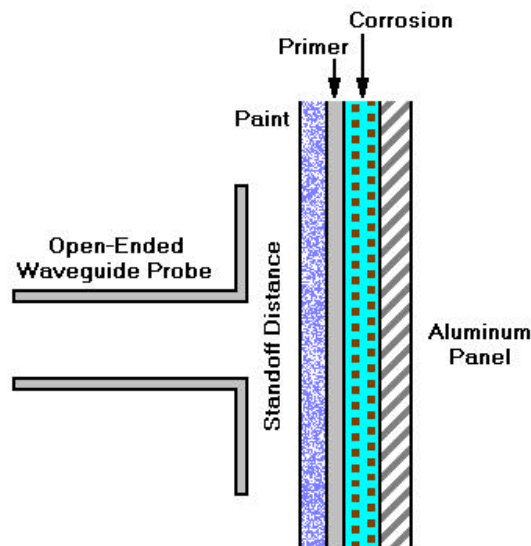


Figure 35. Schematic of open-ended rectangular waveguide used for detecting fatigue cracks and corrosion under paint.

Detection of fatigue cracks

Due to the fact that samples were not supplied by the sponsor of this research samples were manufactured by investigators at Colorado State University. Cracks of varying sizes were generated in aluminum plates using jeweler saws (more like slots). Some of the samples were fatigued in order to grow the cracks to better mimic fatigue cracks of concern in the field. In

order to simulate paint of varying thicknesses, specimens were covered with tissue paper, tape and paint.

During the scanning process using the open-ended coaxial probe, the phase change in the reflection coefficient with respect to when the crack is out of the coax aperture, or the voltage proportional to this was recorded. This voltage as a function of the scanning distance is called the *crack characteristic signal*. Figures 36 and 37 show the influence of crack size and coaxial aperture dimension on the crack characteristic signal for two cracks/slots (not covered with paint) with the same width (~ 0.200 mm) but different depths (0.5 mm and 0.75 mm) at a frequency of 11.3 GHz.

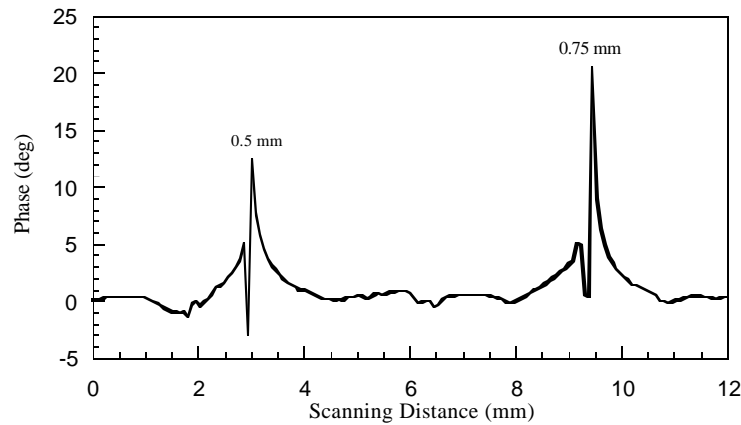


Figure 36. Crack characteristic signal at 11.3 GHz for a slot with a width of ~ 0.200 mm and with different depths, coax inner radius of 0.5 mm and outer radius of 1.5 mm.

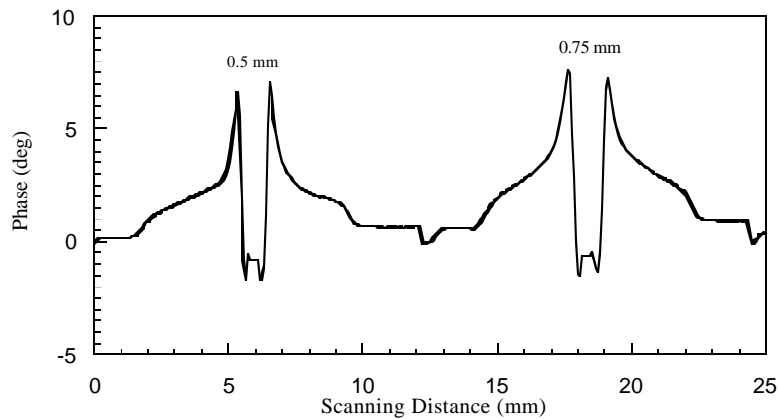


Figure 37. Crack characteristic signal at 11.3 GHz for a slot with a width of ~ 0.200 mm and with different depths, coax inner radius of 1.0 mm and outer radius of 4.0 mm.

To show the potential of this method for detecting tight surface cracks, a fatigue specimen with a 3 μm -wide crack was inspected using the smaller coaxial probe (0.5 mm inner radius and 1.5 mm outer radius) and at a frequency of 11.3 GHz. Figure 38 shows the results of the scan; as can be seen the technique is clearly capable of detecting very tight fatigue cracks.

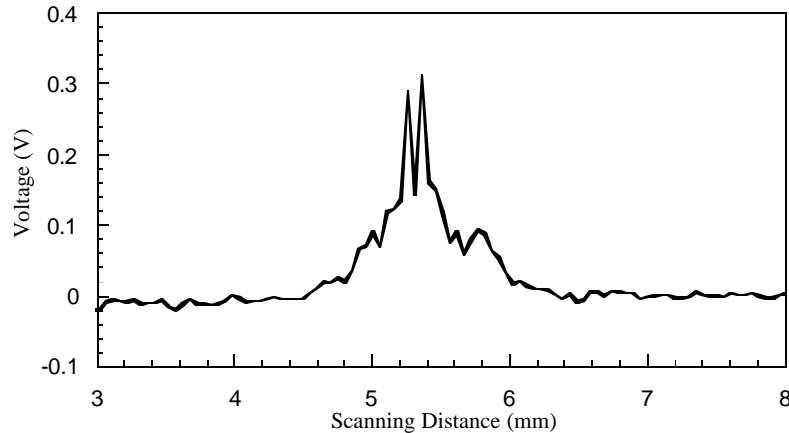


Figure 38. Crack characteristic signal for a fatigue crack with a width of $\sim 3 \mu\text{m}$ and at a frequency of 11.3 GHz.

The primary goal of this investigation was to detect fatigue cracks that were covered by paint, therefore, to simulate varying paint thickness, sheets of 0.025 mm thick tissue paper was used to cover cracks that were subsequently scanned. Figures 39 and 40 show the results for a crack/slot with a width of 0.25 mm and a depth of 1.0 mm at a frequency of 10.5 GHz for four different tissue paper thicknesses. It is obvious that as the coating thickness increases, the dynamic range of the detected signal decreases. Another point to note is that there is now only one peak in the crack characteristic signal while there are two peaks for the case when there is no coating. This is due to the fact that the crack no longer directly interacts with the inner conductor of the coaxial probe and consequently, the two peaks that were seen previously are combined into one.

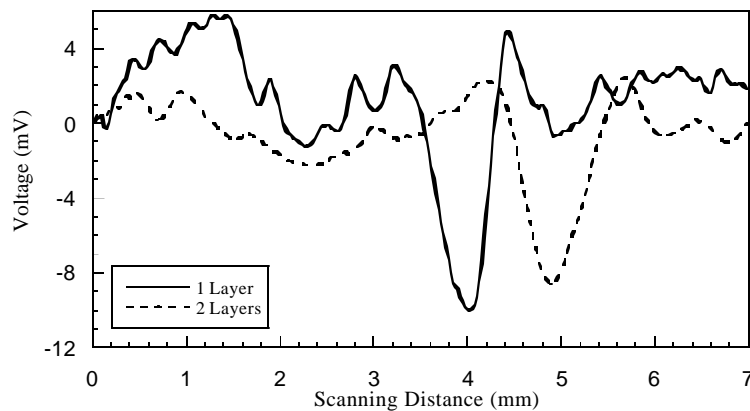


Figure 39. Crack characteristic signal for covered crack with one and two layers of tissue paper.

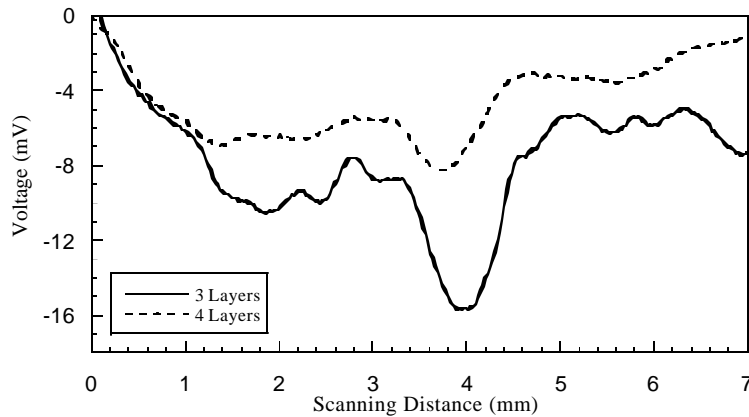


Figure 40. Crack characteristic signal for covered crack with three and four layers of tissue paper.

Figure 41 shows the effects of frequency and incident power in covered crack detection. At a frequency of 11.37 GHz the detected dynamic range is larger than that at a frequency of 10.33 GHz. Measurements show that the optimal frequency for detection depends on the combination of the different crack sizes and the coax size. Regarding incident power, if the power is too low the electric field may not be able to penetrate through the paint and reflect back to the coax aperture. In this case the crack will not be seen. Examining the signals at 11.37 GHz and different power input (dB) in Figure 41, it can be seen that the dynamic range increases with increasing incident power.

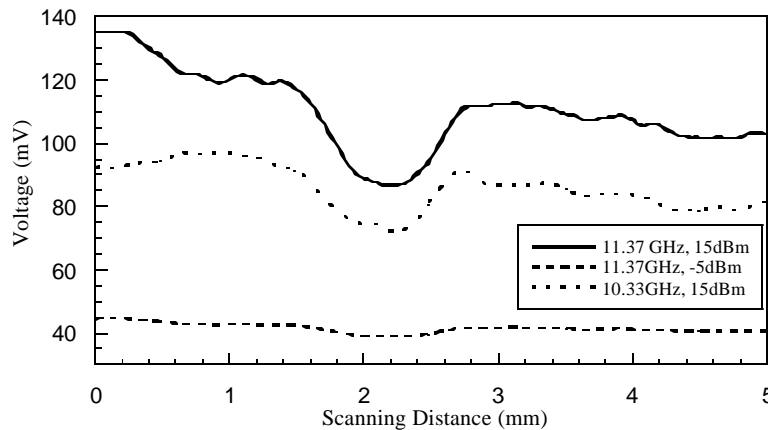


Figure 41. Influence of frequency and incident power on covered crack detection for a slot with a width of 0.15 mm and a depth of 0.75 mm and coating (tape) thickness of 0.11 mm.

When a rectangular waveguide, operating in its dominant mode (TE_{10}), is terminated with a metal plate, it is effectively short-circuited and there is no electric field component along the direction of the broad side of the rectangular waveguide. However, if there is a crack in the metal plate, the crack changes the reflection properties of the plate and hence the waveguide is

no longer short-circuited, the electric field is disturbed, and higher-order modes are generated. This causes an electric field component in the direction along the broad side of the waveguide. By detecting this electric field, the presence of a crack can be indicated. This is a very sensitive method for detecting cracks. Such a probe was used to examine the potential of this method for detecting covered cracks as well.

Similar to the coaxial probe approach, measurements were conducted by moving the aperture of the open-ended rectangular probe along the surface under inspection. The recorded voltage is related to the power associated with the presence of high-order modes as a result of the presence of a crack in a metal plate. Measurements were conducted in the Ka-band frequency range (26.5 - 40 GHz) that was previously determined to be a suitable frequency range for this purpose [7].

For the open-ended rectangular waveguide crack characteristic signal, there are issues concerning the flange edge effect. When there is no dielectric layer between the waveguide and the metal plate, we expect two peaks as the two edges of the waveguide aperture come across the crack. However, when there is a dielectric layer between the waveguide and the metal plate, there may exist an electric field propagating in the dielectric layer, and the detected signal changes four times as the two edges of the flange and two edges of the aperture scan across the crack [7, 17]. The relative amplitude of the multiple peaks depends on the operating frequency, dielectric property and thickness of the coating, and also the probe location.

Figure 42 shows the results when scanning a slot on a brass sample at a frequency of 31.5 GHz. Figure 42 (a) is for the case when the crack is uncovered. The air gap between the waveguide and the metal plate cause the multiple peaks (more than two). Figure 42 (b) and 42 (c) show the results from scanning the same crack under coating (clear tape) thickness of 0.05 mm and 0.15 mm. For all three cases shown in Figure 42, the signal level is low in the region where the crack is outside of the waveguide aperture. Theoretically if there is no coating there should be no signal detected and the signal-to-noise ratio is infinity. The high signal-to-noise level is the most prominent characteristic of the open-ended rectangular waveguide probe [7]. Also, the multiple peaks increase the probability of crack detection.

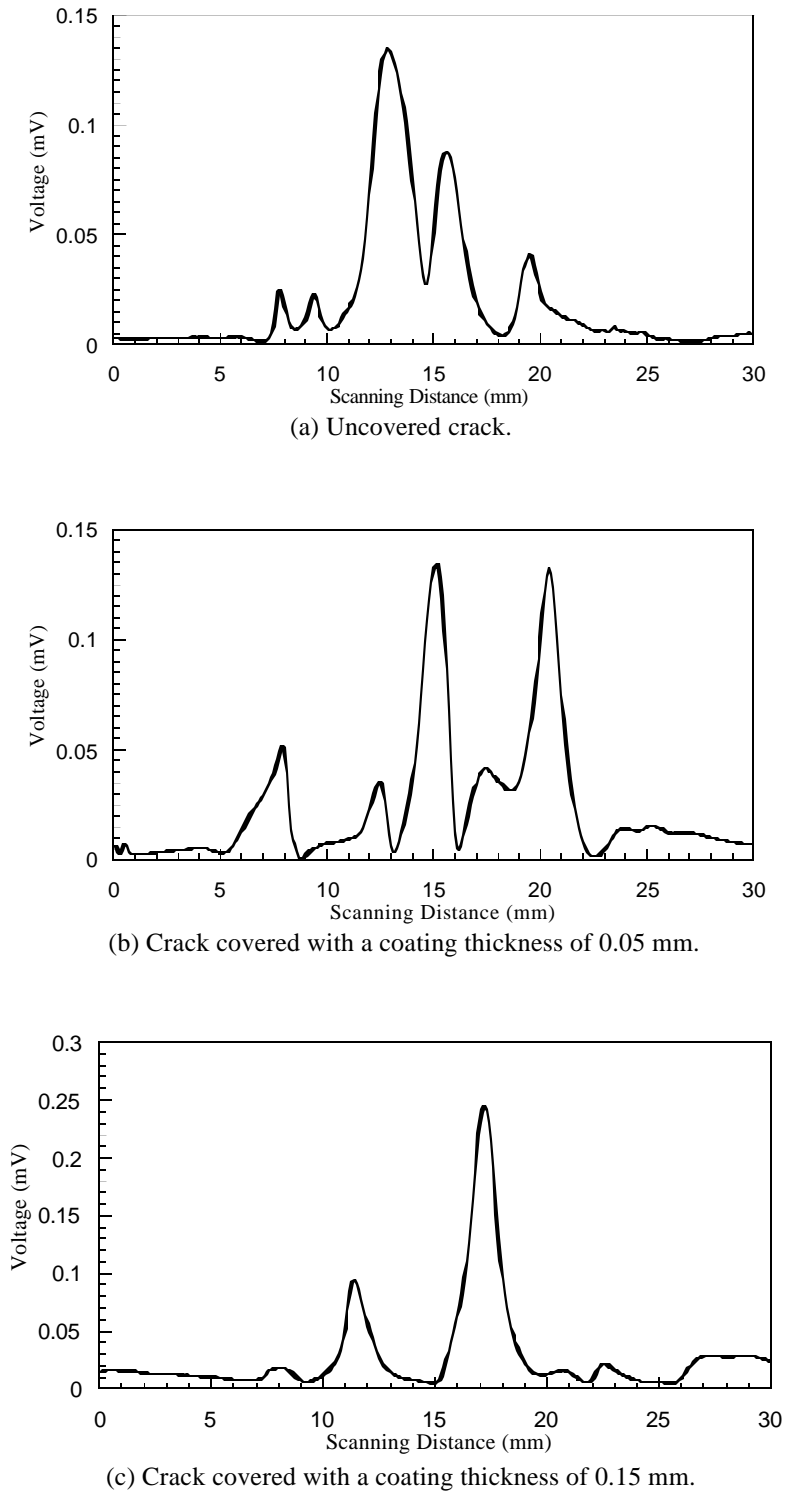


Figure 42. Higher order mode signals generated by the open-ended rectangular waveguide probe for a crack in a brass sample with a width of ~ 0.1 mm and a depth of 0.9 mm at a frequency of 31.5 GHz.

Extensive sets of measurements over a wide range of cracks were conducted using coaxial and open-ended rectangular (higher order mode) waveguide probes. Both coated and uncoated fatigue cracks and slots were studied in this investigation. The results indicate that both probes have high potential for detecting cracks under coatings such as paint and primer. Each probe possesses its unique advantages and disadvantages. The coaxial probe was shown to easily be able to detect tight cracks under coatings of about 0.15 mm at relatively low microwave frequencies (X-band). The coaxial probe was also found to be less susceptible to edge effect issues. The open-ended rectangular (higher order mode) waveguide probe also showed the ability to detect similar cracks under like coatings, however, the issues of edge effects and small changes in the standoff distance seem to be more of a concern when using this probe.

Detection of corrosion

Three aluminum plates were prepared for the experimental investigation of detecting hidden corrosion using open-ended rectangular waveguide probes. One panel, used as the control sample, was free of corrosion. The other two panels (B and C) were halfway submerged in salt water in order to generate corrosion products (Figure 43). Both halves of the plate contained some corrosion products, however, the bottom halves of the plate contained pitting due to the presence of salt products, while the top half remained smooth. Excess salt was removed from the plates, and they were then sand blasted to remove the corrosion. Both the front and back panels of the plates had masks placed on them to retain areas of corrosion during sand blasting. The fronts of the panels were left with a strip of corrosion about 3 inches wide running down the center of the plate from top to bottom, and the backs of the panels were masked so that there was a square of corrosion on the pitted area. The plates were then primed and painted.

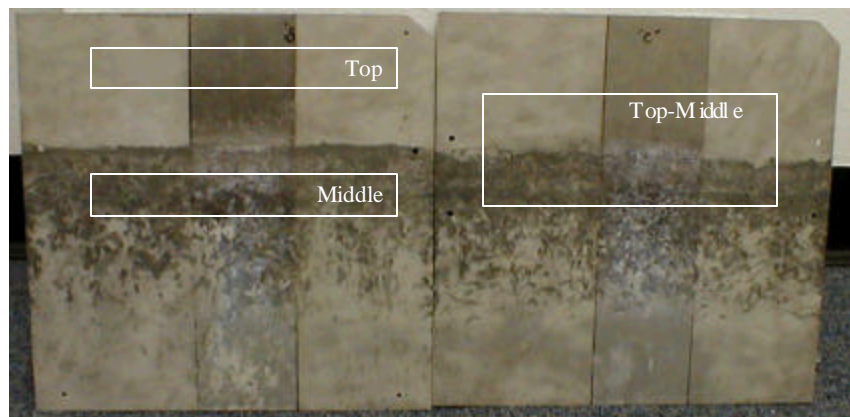


Figure 43. Sample plates C (left) and B (right) showing corrosion before being painted, with areas scanned highlighted.

The experimental investigation involved performing two-dimensional area scans with an open-ended waveguide probe. The areas scanned included strips along the top of the plate (where no pitting was present), strips along the middle of the plate (where pitting was present), strips along both the top and middle of the plate (where there contained areas with and without pitting). Scans of the entire plate were also performed. These scans were performed using different frequencies of operation, as well as adjusting the standoff distance of the waveguide probe [27].

Figure 44 shows an area scan of the top-middle strip of the front of panel B. The darker area of the image represents the corroded area in the panel. Pitting can also be seen in the lower half of the image. The frequency of operation was 24.1 GHz (K-band), and the waveguide probe was in contact with the surface (i.e. no standoff). Figure 45 shows the same scan as Figure 44, except the standoff distance was 5 mm in this case. Here, however, the lighter areas represent corrosion. Figure 46 shows an area scan of the top strip of the front of panel C. The frequency of operation was 24.1 GHz, and standoff distance was 5 mm. Again, the lighter area represents corrosion. Figure 47 shows an area scan of the middle strip of the front of panel C. Here, the darker area represents corrosion, and pitting can be easily seen. The frequency of operation was 33.5 GHz (K-band), and the standoff distance was 2 mm. Figure 48 shows an area scan of the top-middle strip of the front of panel C. The frequency of operation and standoff distance is the same as in Figure 47.

It was observed that as frequency of operation increased, the corroded area could be more easily distinguished from the non-corroded area. This observation matches the results from the theoretical analysis. Also, since the waveguide aperture is smaller at higher frequencies, pitting can be seen in greater detail as higher frequency bands are used.

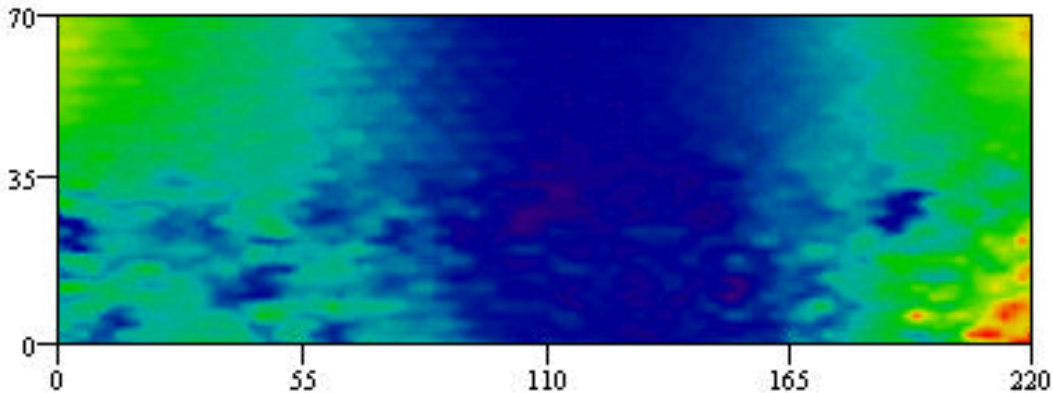


Figure 44. Image acquired using an open-ended rectangular waveguide probe of the top-middle strip of the front of panel B, at a frequency of 24.1 GHz and at a standoff distance of 0 mm (i.e. in contact). (Note: Dimensions are in mm).

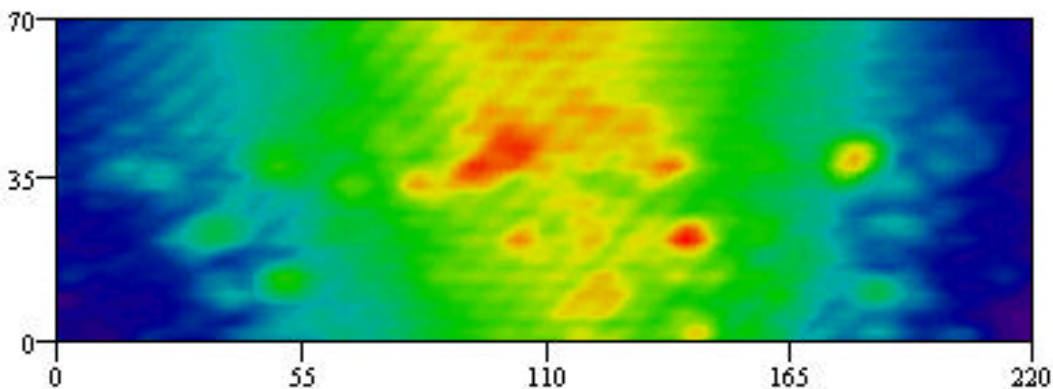


Figure 45. Image acquired using an open-ended rectangular waveguide probe of the top-middle strip of the front of panel B, at a frequency of 24.1 GHz and at a standoff distance of 5 mm. (Note: Dimensions are in mm).

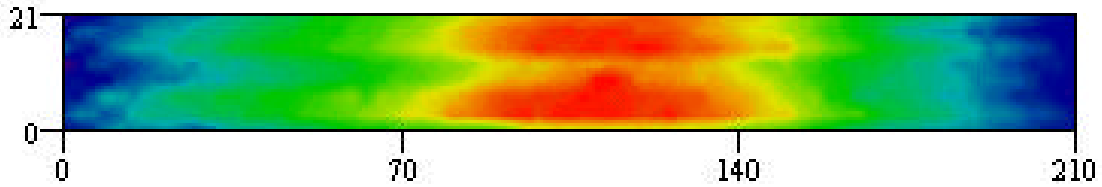


Figure 46. Image acquired using an open-ended rectangular waveguide probe of the top strip of the front of panel C, at a frequency of 24.1 GHz and at a standoff distance of 5 mm. (Note: Dimensions are in mm).

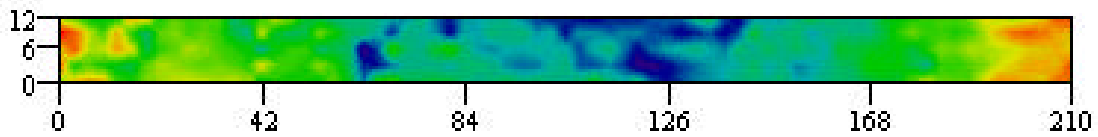


Figure 47. Image acquired using an open-ended rectangular waveguide probe of the middle strip of the front of panel C, at a frequency of 33.5 GHz and at a standoff distance of 2 mm. (Note: Dimensions are in mm).

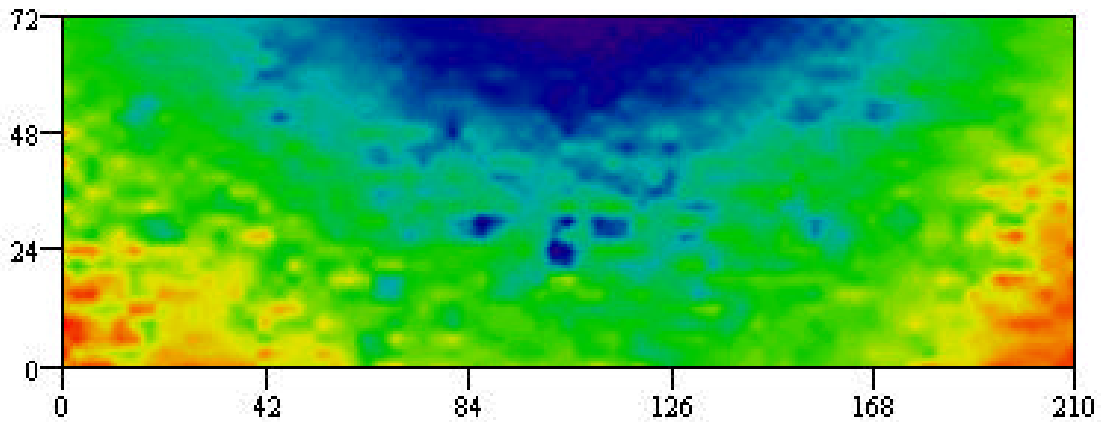


Figure 48. Image acquired using an open-ended rectangular waveguide probe of the top-middle strip of the front of panel C, at a frequency range of 33.5 GHz and at a standoff distance of 2 mm. (Note: Dimensions are in mm).

It was found that dielectric properties of aluminum oxide, paint and primer are very similar to each other. This is important since it is easier to detect corrosion under paint when the dielectric properties have a greater difference when compared to each other, as is the case with steel corrosion. Regardless, it was possible to detect corrosion in aluminum under a layer of paint and primer using near-field microwave nondestructive techniques with open-ended rectangular wave guide probes.

OTHER PROJECT ACCOMPLISHMENTS

This project, supported by the SERDP Program Office, has led to the advancement of nondestructive evaluation technologies for the inspection of fatigue cracks and corrosion hidden under coatings. This work has resulted in the publication of eight papers, the submission of three reports (not including the current document), and the presentation of nine technical talks at national and international conferences. An application has been made by Imperium, Inc. and the Naval Air Warfare Center Aircraft Division (NAWC-AD) for the issuance of a patent based on the oblique angle beam real-time ultrasound imaging system. Imperium is also fabricating the first through transmission real-time ultrasound imaging system for Boeing/Vertol in Philadelphia as a direct consequence of this work. Finally, Thermal Wave Imaging, Inc. developed and demonstrated a field portable pulse thermography unit for the inspection of corrosion hidden under paint.

CONCLUSIONS

Three different innovative nondestructive evaluation technologies were developed and evaluated for the ability to detect fatigue cracks and corrosion hidden under paint. The three technologies included real-time ultrasound imaging, thermal imaging, and near-field microwave imaging. With each of these nondestructive inspection methods, subtasks were performed in order to optimize each methodology.

For the ultrasound imaging technique three different configurations of camera were developed by Imperium, Inc. in order to acquire an image of a sample in real-time: through transmission, reflection (pulse-echo) and oblique angle beam. All of the camera systems were designed to be portable and all demonstrated the ability to detect light corrosion and fatigue cracks under paint. Two major accomplishments results from this work: (1) the first commercial aerospace unit for through transmission real-time ultrasound imaging is being fabricated for Boeing/Vertol Philadelphia, and (2) application has been made for the issuance of a patent based on the oblique angle beam system.

The thermal imaging techniques pursued by Thermal Wave Imaging and Wayne State University were fairly successful in their ability to detect light corrosion and fatigue cracks under paint. Thermal Wave Imaging evaluated the use of inductive heating, laser diode heating and pulse heating (flash lamps) as means to produce the heat gradients necessary to obtain thermographic images of test samples. The inductive heating and laser diode heating methods were more effective at detecting fatigue cracks than hidden corrosion, although both techniques had relatively low sensitivity owing to the low thermal contrast generated by the heat sources. The pulse heating technique was found to be very useful for the detection of hidden corrosion and showed the most promise for transitioning into the field owing largely to the portability of the system. The main shortcoming of the pulse thermography system was the inability of the system to consistently locate fatigue cracks owing to the low thermal contrast between the base metal and the crack. In contrast, the sonic thermography system developed by Wayne State University was very effective in locating fatigue cracks in samples. Studies still need to be performed to determine the capabilities of sonic thermography for the detection of hidden corrosion.

The results of the near-field microwave imaging investigation conducted by Colorado State University and Texas Research Institute showed that there exists a high potential for detecting corrosion in aluminum under a layer of paint and primer using open-ended rectangular waveguide probes. Colorado State University also successfully demonstrated the use of these probes and coaxial probes for locating cracks under coatings. Coaxial probes were found to be less susceptible to edge effect issues than the open-ended rectangular waveguide probes. While near-field microwave imaging techniques have demonstrated proof-of-principle concepts, further work is necessary before these techniques would be viable for field use.

TRANSITION PLAN

In order to support the transitioning of the technologies within this project, tasking was placed with four field activities: NADEP Jacksonville (FL), NADEP North Island (CA), Warner-Robins ALC (GA), and the Marine Corps Maintenance Center Albany (GA). An inspection requirements survey presented in Appendix A was developed and was completed by the Marine Corps Maintenance Center. Based on input from the Maintenance Center the questionnaire was to be revised and then sent to the other field activities. The revision was never completed and as a consequence the other field activities never received the survey. Appendix B contains the responses to the questionnaire sent to the Marine Corps Maintenance Center. A brief summary of the responses obtained from the Marine Corps Maintenance Center follows below.

The Marine Corps Maintenance Center did not identify paint removal as a requirement for performing nondestructive inspection on any of the ir platforms with the exception of the Light Armored Vehicle (LAV) where paint removal is required. In general, paint removal is dictated by the Statement-of-Work and not nondestructive inspection requirements. The LAV is repainted and inspected as a matter of course owing to its history of substrate stress and failure. In addition, paint removal is not performed chemically; rather paint is removed by blasting with glass or plastic grit. It was stated that there are situations under the IROAN Program (Inspect, Repair, Only As Necessary) where coating removal would not be necessary if the depots had an NDE technology that could inspect through the coating. The primary use of such NDE technology would be for the inspection of corrosion and cracks in the LAV. In general, the Marine Corps Maintenance Center would welcome any NDE technology that can locate corrosion and cracks, result in improved safety to the inspectors (as opposed to potential radiation hazards), and would eliminate the requirement for retaining a Level III inspector.

Of the three innovative nondestructive technologies developed and evaluated during the course of the SERDP program, the real-time ultrasound imaging and the pulse thermography system show the most promise for transitioning to the field. The through transmission approach to real-time ultrasound imaging has received considerable attention from the aerospace industry, in fact, Boeing/Vertol has accepted delivery of a through transmission unit to test composite components on the production line. The pulse thermography system is transitioning into the field because of successful demonstration of the abilities of the system to the aerospace community. NADEP Cherry Point NC has an older pulse thermography system that is currently

used for limited applications. The system developed under the SERDP program will allow for an expansion of these applications owing to the greater sensitivity of the new system as well as to its increased portability.

Sonic thermography has elicited a great deal of interest from the nondestructive evaluation community. Laboratory trials using actual aerospace components have been successful for the most part. Transitioning into the field, however, awaits the successful demonstration of a probability of detection determination in the case of a major application such as turbine engine components. Funding is being pursued in order to implement the transition of the technology.

The near-field microwave imaging program was capable of demonstrating proof-of-principle for using microwave techniques to inspect for fatigue cracks and corrosion hidden under paint. Additional work needs to be performed before the current systems (open-ended coaxial and open-ended rectangular waveguide probes) could be viable for field inspections.

REFERENCES

1. Lasser, M., Harrison, G. "A Novel High Speed, High Resolution Ultrasound Imaging System", QNDE Review of Progress In Quantitative NDE, Plenum Press, Volume 17B, pp. 1713-1719 (1997).
2. Lasser, M., Harrison, G., Kula, J., "Real-Time, Depth Sensitive C-scan Imaging System", 7th Annual research symposium transfer of emerging NDE technologies (1998).
3. Lasser, M., Lasser, B., Kula, J., Rohrer, G., "Latest Developments in Real-Time 2D Ultrasound Inspection for Aging Aircraft", 10th Annual AeroMat Conference & Exposition (1999).
4. Lasser, M., Lasser, B., Kula, J., Rohrer, G., "On-Line, Large Area Ultrasonic Imaging for Composite Manufacturing", American Society for Nondestructive Testing Conference (1999).
5. Lasser, M., "A Novel High Speed, High Resolution Ultrasound Imaging System", ASNT Fall Conference NDT- Keystone of Quality, published by ASNT, pp. 196-198 (1997).
6. Zoughi, R., S. Ganchev, C. Huber, E. Ranu and R. Runser, "A Novel Microwave Method for Filled and Covered Surface Crack Detection in Steel Bridges Including Crack Tip Identification," Final (Fourth Quarterly) Report, Federal Highway Administration (FHWA), Grant no. DTFH61-94-X-00023, p. 187, September 1995.
7. Qaddoumi, N., E. Ranu, R. Mirshahi, P. Stepanek, V. Otashevich, C. Huber and R. Zoughi, "Development of Equipment for and Quantitative Analysis of Microwave Detection and Evaluation of Fatigue Induced Surface Cracks in Steel," Final Report, Federal Highway Administration (FHWA), Grant no. DTFH61-94-X-00023, p. 519, January 1998.
8. Yeh, C., E. Ranu and R. Zoughi, "A Novel Microwave Method for Surface Crack Detection Using Higher Order Waveguide Modes," *Materials Evaluation*, vol. 52, no. 6, pp. 676-681, June 1994.
9. Huber, C. and R. Zoughi, "Higher Order Modes as Indicators of Surface Cracks Under Stratified Dielectric Coatings Using an Open-Ended Waveguide," *Proceedings of the Review of Progress in Quantitative NDE*, vol. 14A, pp. 637-642, 1995.
10. Yeh, C. and R. Zoughi, "A Novel Microwave Method for Detection of Long Surface Cracks in Metals," *IEEE Transactions on Instrumentation and Measurement*, vol. 43, no. 5, pp. 719-725, October 1994.
11. Yeh, C. and R. Zoughi, "Microwave Detection of Finite Surface Cracks in Metals Using Rectangular Waveguide Sensors," *Research in Nondestructive Evaluation*, vol. 6, no. 1, pp. 35-55, 1994.
12. Yeh, C. and R. Zoughi, "Sizing Technique for Surface Cracks in Metals," *Materials Evaluation*, vol. 53, no. 4, pp. 496-501, April 1995.
13. Huber, C., S.I. Ganchev, R. Mirshahi, J. Easter and R. Zoughi, "Remote Detection of Surface Cracks/Slots Using Open-Ended Rectangular Waveguide Sensors: An Experimental Investigation," *Nondestructive Testing & Evaluation*, vol. 13, pp. 227-237, 1997.
14. Ganchev, S., R. Zoughi, C. Huber, R. Runser and E. Ranu, "Microwave Method for Locating Surface Cracks Tips in Metals," *Materials Evaluation*, vol. 54, no. 5, pp. 598-603, May 1996.
15. Huber, C., H. Abiri, S. Ganchev and R. Zoughi, "Analysis of the Crack Characteristic Signal Using a Generalized Scattering Matrix Representation," *IEEE Transactions on Microwave Theory and Techniques*, vol. 45, no. 4, pp. 477-484, April 1997.

16. Huber, C., H. Abiri, S. Ganchev and R. Zoughi, "Modeling of Surface Hairline Crack Detection in Metals Under Coatings Using Open-Ended Rectangular Waveguides," *IEEE Transactions of Microwave Theory and Techniques*, vol. 45, no. 11, pp. 2049-2057, November 1997.
17. Qaddoumi, N., E. Ranu, J.D. McColskey, R. Mirshahi and R. Zoughi, "Microwave Detection of Stress Induced Fatigue Cracks in Steel and Potential for Crack Opening Determination," *Research in Nondestructive Evaluation*, vol. 12, no. 2, pp. 87-103, 2000.
18. Wang, Y. and R. Zoughi, "Interaction of Surface Cracks in Metals with Open-Ended Coaxial Probes at Microwave Frequencies," *Materials Evaluation*, vol. 58, no. 10, November 2000.
19. Zoughi, R., K. Hayes and S. Ganchev, "Microwave Detection of Hairline Surface-Breaking Cracks in Metals Using Open-Ended coaxial Sensors: Preliminary Results," *Proceedings of SPIE Symposium, Nondestructive Evaluation Techniques for Aging Infrastructure & Manufacturing Conferences*, vol. 2945, pp. 444-450, Scottsdale, AZ, December 2-5, 1996.
20. R. Zoughi, C. Huber, J. Easter and K. Hayes, "Microwave Detection of Surface Cracks in Metals Under Dielectric Coatings Using Open-Ended Coaxial Sensors: Preliminary Results," Special Topics Proceedings of *Nondestructive Evaluation of Infrastructure*, edited by H. Reis and B. Djordjevic, 1997.
21. Qaddoumi, N., L. Handjojo, T. Bigelow, J. Easter, A. Bray and R. Zoughi, "Microwave Corrosion Detection Using Open-Ended Rectangular Waveguide Sensors," *Materials Evaluation*, vol. 58, no. 2, pp. 178-184, February 2000.
22. Qaddoumi, N., A. Shroyer and R. Zoughi, "Microwave Detection of Rust Under Paint and Composite Laminates," *Research in Nondestructive Evaluation*, vol. 9, no. 4, pp. 201-212, 1997.
23. Davis, William R., "Method for Acoustic Imaging by Angle Beam," United States Patent Application 09/679,161 filed October 5, 2000 (Navy Case 80281).
24. Perez, I., Santos, R., Kulowitch, P., Ryan, M., "Calorimetric modeling of thermographic data," Proc. of the 1998 SPIE Thermosense XX Conference", Orlando, April 6 - 9, 1998.
25. Perez, I., Kulowitch, P., "Modeling of Pulsed Thermography in Anisotropic Media," 25th annual Progress in QNDE, Snowbird, Utah., July 19 - 24, 1998.
26. Perez, I., Davis, W.R., Kulowitch, P., "Thermographic modeling of water entrapment," Proc. of the 1999 SPIE, Thermosense XXI Conference, eds. D.H. LeMieux & J.R. Snell, Jr. April 1999, p32-39.
27. Wang, N., D. Hughes, K. Donnell, T. Case and R. Zoughi, "Feasibility Study of Corrosion Detection Under Paint in Aluminum Panels," Final Report, Texas Research Institute at Austin (TRI-Austin), July 2000.

APPENDIX A

The following is a survey that was written in order to support the transitioning of the nondestructive inspection methods developed and evaluated under the SERDP Program. The survey was sent to the Marine Corps Maintenance Center Albany (GA) and responses to this questionnaire appear in Appendix B. Based on input from the Maintenance Center the questionnaire was to be revised and then sent to the three other field activities: NADEP Jacksonville (FL), NADEP North Island (CA) and Warner-Robins ALC (GA). The revision was never completed and as a consequence the other field activities never received the survey.

NSWC Carderock / SERDP PP-1134 Crack and Corrosion Inspection Needs Survey for Field Activities

The following list of questions was developed as a basis for gathering information on inspection requirements and technology implementation constraints. While an effort was made to develop a list of comprehensive questions, the list is not necessarily all-inclusive. If there is additional information that you think may be useful, please include it along with your other responses.

1. Identify the types of aircraft or vehicles that are currently worked on at your facility.
2. What types of NDE inspections are performed on each of these vehicle types?
 - What is the purpose for conducting the inspection? When is the inspection conducted?
 - What is the substrate material?
 - What is the geometry of the inspection region?
 - Is any surface preparation required?
 - If there are corrosion issues, identify the corrosion type, etc.
 - If there are crack issues, identify the type, length, orientation or geometry.
3. Identify current inspection requirements that necessitate the removal of coatings. (ID inspection procedures and describe stripping requirements, if possible.)
 - Could coating removal be avoided if the NDE inspection technology could inspect through the coating?
4. For instances where coatings are removed:
 - What platforms/vehicles & how many are stripped per year?
 - What chemicals are used to strip? How many gallons per vehicle?
 - How much waste is generated? What is the disposal cost?
 - What are the outyear projections for these processes?
5. Identify an individual cognizant for pollution issues in your local environmental quality office and provide their contact information (phone, fax, email)
6. Identify the limits of current techniques and the resolution that will be required if a new inspection technology was to be introduced into service.

7. Identify constraints on new NDE system implementation:

- Acquisition cost
- Portability
- Size & dimensions
- Weight
- Power
- Safety
- Other

APPENDIX B

The following are responses to a questionnaire designed to assist the investigators of the SERDP Program with transition plans for implementing the technologies developed and evaluated during the course of this program. The responses come from the Marine Corps Maintenance Center Albany (GA).

NSWC Carderock / SERDP PP-1134 *Crack and Corrosion Inspection Needs Survey for Field Activities*

The following list of questions was developed as a basis for gathering information on inspection requirements and technology implementation constraints. While an effort was made to develop a list of comprehensive questions, the list is not necessarily all-inclusive. If there is additional information that you think may be useful, please include it along with your other responses.

1. Identify the types of aircraft or vehicles that are currently worked on at your facility.

Please refer to Table 1.

2. What types of NDE inspections are performed on each of these vehicle types?
 - What is the purpose for conducting the inspection? When is the inspection conducted?
 - What is the substrate material?
 - What is the geometry of the inspection region?
 - Is any surface preparation required?
 - If there are corrosion issues, identify the corrosion type, etc.
 - If there are crack issues, identify the type, length, orientation or geometry.

Please refer to Table 1.

3. Identify current inspection requirements that necessitate the removal of coatings (ID inspection procedures and describe stripping requirements, if possible).

- Could coating removal be avoided in the NDE inspection if technology could inspect through the coating?

Vehicle coating removal for the normal maintenance cycle is primarily driven by the Statements-Of-Work (SOWs), which require the removal of coatings. There are situations under the IROAN Program (Inspect, Repair, Only As Necessary) that coating removal would not be necessary if the depots had NDE technology that could inspect through the coating.

4. For instances where coatings are removed:

- What platforms/vehicles & how many stripped per year?

The primary focus of a new NDE system would be on the LAV. The five-year average would be in the 70-80 vehicles per year range. Other weapons platforms are also involved in this process on an "as required" basis, but virtually every LAV is inspected due to vehicle history.

- What chemicals are used to strip? How many gallons per vehicle?

Neither USMC maintenance center is currently using chemicals to strip paint. The preferred method is blasting.

- How much waste is generated? What is the disposal cost?

Maintenance Center Albany generated 36,404 lbs of plastic blast grit in FY98 and 25,179 lbs. of glass blast grit. Maintenance Center Barstow data was not forthcoming but it is estimated that they generated approximately 15-20% more because they paint more vehicles.

- What are out year projections for these processes?

The USMC maintenance centers do not anticipate utilizing any stripping method in out years that would involve chemicals to any great degree. It is possible that some form of high pressure water stripping could be utilized but not likely in the near future. The Applied Research Lab of Penn State University has a current research project underway funded by the ManTech Program to identify a commercially available, environmentally benign chemical paint stripper or process. Implementation would be dependent upon successful testing. The chemical paint stripping or alternative process would likely be used as pre-stripping paint softener to reduce our use of blast media.

5. Identify an individual cognizant for pollution issues in your local environmental quality office and provide their contact information (phone, fax, e-mail).

Lamaar Petties

Phone: (229) 639-6826

Fax: (229) 639-

E-Mail: pettiesl@matcom.usmc.mil

6. Identify the limits of current techniques and the resolution that will be required if a new inspection technology was to be introduced into service.

Current technology presents the following limitations:

THROUGHPUT - *The current process is labor intensive and as a result can create a vehicle throughput problem. It requires an intensive set-up and repositioning effort and the time required to "shoot" a vehicle is too long. Any new technology needs to improve on this problem.*

EFFICIENCY – *The cost of retaining a Level 3 inspector, film storage and handling, and manpower requirements are examples of our current technology's inefficiency. When shooting a vehicle, "guards" are posted to prevent inadvertent entry and exposure to the NDE area. These guards are an unnecessary expense and their time and effort could be better utilized. The cost of handling and storing film is a serious financial burden and any new technology that could reduce or eliminate this requirement would be welcomed. MCA is currently considering retaining the services of a Level 3 inspector specifically for the requirements of NDE. New technology that would eliminate this requirement would also be welcomed.*

SAFETY – *The fact that MCA posts guards during NDE operations is pretty indicative of the safety hazards present. Obviously, one of the driving factors of new technology has been the potential reduction or elimination of these hazards. The implementation of any new technology would almost certainly need to have the promise of improved safety issues.*

ACCURACY - *The USMC is facing some pretty serious cracking issues with the LAV armor plate. Putting troops in the field with the prospect of vehicle armor that has the potential to have unidentified cracks or suffering from reduced ballistic characteristics is a scenario that needs to be addressed.*

7. Identify constraints on new NDE system implementation:

- Acquisition cost
- Portability
- Size and dimensions
- Weight
- Power
- Safety
- Other

These constraints are discussed in Table 2.

Table 1. Vehicle Types and Inspection Data

VEHICLES	SUBSTRATE	CORROSION ISSUES	CORROSION TYPE	SURFACE PREP REQ.	CRACK ISSUES	ID TYPE, LENGTH, ORIENTATION, GEOMETRY
AAV	5083 Aluminum 1020 Steel	Yes	Primarily Stage 1-2, incidents of Stage 3 on steel components ¹	Paint is not removed ₃ for NDE purposes	No	Not an issue
LAV	00461 High Armor steel 1020 steel	Yes	Primarily Stage 1-2, incidents of Stage 3 on steel components ¹	Yes – paint must be removed	Yes	Figures identifying primary areas and length of cracks can be provided as an attachment if required ² .
M88	Primarily 1020 steel	Yes	Primarily Stage 1-2, incidents of Stage 3 on steel components ¹	Paint is not removed ₃ for NDE purposes	No	Not an issue
HMMWV	Primarily 1020 steel	Yes	Primarily Stage 1-2, incidents of Stage 3 on steel components ¹	Paint is not removed ₃ for NDE purposes	No	Not an issue
M-923 5-Ton Cargo Truck	Primarily 1020 steel	Yes	Primarily Stage 1-2, incidents of Stage 3 on steel components ¹	Paint is not removed ₃ for NDE purposes	No	Not an issue
M-105A2 Cargo Trailer	Primarily 1020 steel	Yes	Primarily Stage 1-2, incidents of Stage 3 on steel components ¹	Paint is not removed ₃ for NDE purposes	No	Not an issue
M1A1 Tank	High armor steel	Yes	Primarily Stage 1-2, incidents of Stage 3 on steel components ¹	Paint is not removed ₃ for NDE purposes	No	Not an issue
MK14 Trailer, Container	Primarily 1020 steel	Yes	Primarily Stage 1-2, incidents of Stage 3 on steel components ¹	Paint is not removed ₃ for NDE purposes	No	Not an issue

NOTES

1. There have been incidents of Stage 3 – 4 corrosion in certain areas: battery boxes, inaccessible areas of the frames, door jambs, etc.
2. Historical records have been kept going back several years on each LAV that has passed through the Albany Maintenance Center. These records include a graphical reproduction on the location, length, date, vehicle #, geometry, and disposition. The records are very detailed and have been retained in several notebooks.
3. Vehicle depainting is generally driven by the Statement-of-Work (SOW) not NDE requirements. Vehicles with a history of substrate stress and failure (LAV) are depainted and inspected as a matter of course.

Table 2. System Constraints

Acquisition Cost	Portability	Size / Dimension	Weight	Power	Safety	Other
<p>Don't know that there is a ceiling on this issue. Funding would be dependent on the functionality, flexibility, and safety of a new system. The costs of operating and maintaining current system is extremely expensive but an ROI assessment would have to be conducted.</p>	<p>Current system equipment has little or no portability. Portability would be a desired characteristic of new system but not required.</p>	<p>Current system has a dedicated facility. Size is not a big issue but new system should be able to utilize current facility without any major construction or refacilitization.</p>	<p>We are looking for something more portable and smaller than our current system. A new system that meets these desires would, by nature, be lighter.</p>	<p>Power should be commensurate with current requirements. The planned site survey would probably resolve this issue. We do not anticipate the power needs of any new technology being greater than our current process.</p>	<p>Current system has some serious safety issues and is one of the prime reasons that a new system is being evaluated. Any new system must be dramatically safer!</p>	<p>We are currently required to retain the services of a level III inspector. We are also handling and storing film. A reduction of these requirements would also be desirable.</p>

This page intentionally left blank

APPENDIX C

The following reports, presentations, and other associated professional works were produced during the course of the SERDP Project. Where available the reports appear in full.

Papers

Han, X., L.D. Favro, and R.L. Thomas, "Recent Developments in Thermosonic Crack Detection," *Review of Progress in Quantitative Nondestructive Evaluation*, Vol. 21, (to be published).

Ouyang, Z., L.D. Favro, R.L. Thomas, and X. Han, "Theoretical Modeling of Thermosonic Imaging of Cracks," *Review of Progress in Quantitative Nondestructive Evaluation*, Vol. 21, (to be published).

Perez, I. and X. Han, "Pulsed Thermographic Modeling," *Review of Progress in Quantitative Nondestructive Evaluation*, Vol. 21, (to be published).

Hughes, D., N. Wang, T. Case, K. Donnell, R. Zoughi, R. Austin, and M. Novack, "Microwave Nondestructive Detection of Corrosion Under Thin Paint and Primer in Aluminum Panels," *Subsurface Sensing Technologies and Applications*, Vol. 2, No. 4, pp. 435-451, October 2001.

Hughes, D., N. Wang, T. Case, K. Donnell, R. Zoughi, R. Austin, and M. Novack, "Detection of Corrosion in Aluminum Panels Under Paint and Primer," *Review of Progress in Quantitative Nondestructive Evaluation*, Vol. 20, edited by D.O. Thompson and D.E. Chimenti, 2001.

Wang, N., K. Donnell, M. Castle, R. Zoughi, and M. Novack, "Microwave Detection of Covered Surface Cracks in Metals," *Review of Progress in Quantitative Nondestructive Evaluation*, Vol. 20, edited by D.O. Thompson and D.E. Chimenti, 2001.

Davis, W.R. and B. Lasser, "Development of Real Time Ultrasonic Imaging," Proceedings of the 54th Meeting of the Machinery Failure Prevention Technology Society, 1-4 May 2000, Virginia Beach, Virginia.

Perez, I. and P. Kulowitch, "Thermography for Characterization of Corrosion Damage," Proceedings of the National Association of Corrosion Engineers (NACE) Expo 2000, 27-30 March 2000, Orlando, Florida.

Reports

Novack, M. and I. Perez, "Development of Innovative Nondestructive Evaluation Technologies for the Inspection of Cracking and Corrosion Under Coatings, SERDP PP-1134," FY00 Annual Report, March 2001.

Wang, N., K. Donnell, M. Castle and R. Zoughi, "Microwave Detection of Cracks in Painted Metallic Substrates," Final Report submitted to Michele Novack, October 2000.

Novack, M. and I. Perez, "Development of Innovative Nondestructive Evaluation Technologies for the Inspection of Cracking and Corrosion Under Coatings, SERDP PP-1134," FY99 Annual Report, March 2000.

Professional Presentations

Favro, Lawrence D. (Wayne State University), "Recent Developments in Thermosonic Crack Detection," 28th Annual Review of Progress in Quantitative Nondestructive Evaluation, Brunswick, Maine, 29 July - 3 August 2001.

Perez, Ignacio (Naval Air Warfare Center Aircraft Division), "Pulsed Thermographic Modeling," 28th Annual Review of Progress in Quantitative Nondestructive Evaluation, Brunswick, Maine, 29 July - 3 August 2001.

Ouyang, Zhong (Wayne State University), "Theoretical Modeling of Thermosonic Imaging of Cracks," 28th Annual Review of Progress in Quantitative Nondestructive Evaluation, Brunswick, Maine, 29 July - 3 August 2001.

Shepard, Steve (Thermal Wave Imaging, Inc.), "Thermographic Nondestructive Inspection of Metallic Aerospace Structures," 49th Annual Meeting of the Defense Working Group on Nondestructive Testing, hosted by the AF NDI Program Office and Keesler AFB, Biloxi, MS, 30 October-2 November 2000.

Chaudry, Brian (Thermal Wave Imaging, Inc.), "Application of Pulsed Thermography to Maintenance and Repair Inspections," Air Transport Association's 44th Annual Nondestructive Testing Forum, San Francisco, CA, 25-28 September 2000.

Wang, N. (Colorado State University), "Microwave Detection of Covered Surface Cracks in Metals," 27th Annual Review of Progress in Quantitative Nondestructive Evaluation, Ames, Iowa, 16-21 July 2000.

Hughes, D. (Colorado State University), "Detection of Corrosion in Aluminum Panels Under Paint and Primer," 27th Annual Review of Progress in Quantitative Nondestructive Evaluation, Ames, Iowa, 16-21 July 2000.

Davis, W.R. and B. Lasser, "Development of Real Time Ultrasonic Imaging," the 54th Meeting of the Machinery Failure Prevention Technology Society, 1-4 May 2000, Virginia Beach, Virginia.

Perez, I. and P. Kulowitch, "Thermography for Characterization of Corrosion Damage," the National Association of Corrosion Engineers (NACE) Expo 2000, 27-30 March 2000, Orlando, Florida.

Conference Sessions

4th International Aircraft Corrosion Workshop, hosted by Naval Air Warfare Center Aviation Division, Solomons Island, MD, 22-25 August 2000.

- 1 Dr. Perez chaired the session on Advanced Systems for Corrosion Detection and Monitoring Technologies

Patents

An application has been made for the issuance of a patent based on the oblique angle beam real-time ultrasound imaging system.

This page intentionally left blank

Paper presented at the 27th Annual Review of Progress in Quantitative Nondestructive Evaluation, Ames, Iowa, 16-21 July 2000 and published in *Review of Progress in Quantitative Nondestructive Evaluation*, Vol. 20, edited by D.O. Thompson and D.E. Chimenti, 2001.

DETECTION OF CORROSION IN ALUMINUM PANELS UNDER PAINT AND PRIMER

D. Hughes¹, N. Wang¹, T. Case¹, K. Donnell¹, R. Zoughi¹, R. Austin², M. Novack³

¹Applied Microwave Nondestructive Testing Laboratory (*amntl*), Electrical and Computer Engineering Department, Colorado State University, Fort Collins, CO 80523-1373

²Texas Research Institute Austin, Inc., Austin, TX 78733-6201

³Naval Surface Warfare Center, Carderock Division, Code 615, West Bethesda, MD 20817-5700

Abstract. Microwave nondestructive techniques have been used in the past to detect the presence of corrosion in steel plates under layers of paint and primer. This paper describes a similar investigation for the detection of corrosion in aluminum plates. Dielectric properties of paint, primer and aluminum oxide were determined. Theoretical calculations produced promising results. Experimental measurements on specially prepared panels showed that, using a multi-layer code simulating the reflection coefficient at a rectangular waveguide aperture, corrosion can be detected, even in the presence of pitting in the plate.

INTRODUCTION & BACKGROUND

The objective of this investigation has been to study the feasibility of using near-field microwave nondestructive testing (NDT) and evaluation (NDE) techniques to detect corrosion in aluminum panels under thin layers of paint and primer using open-ended rectangular waveguide probes. This technique has been shown to be effective in detecting corrosion in steel plates under paint and primer, as well as under thick composite laminate coatings [1-2]. A microwave signal reflects completely off of a metal surface, regardless of the type of metal. Therefore, the distinction between the present investigation and that of corrosion in steel plates lies solely in the potential difference between the dielectric properties of rust (Fe_2O_3) and aluminum oxide (Al_2O_3).

MEASUREMENT OF DIELECTRIC PROPERTIES

To perform the theoretical investigation, the thickness and the dielectric properties of paint, primer and aluminum corrosion products must be determined. Paint and primer samples in sheet form, as well as Al_2O_3 in powder form was obtained. These were measured using a two-port completely-filled waveguide transmission line technique [3]. The dielectric properties of paint and primer were measured at S-band (2.6-3.95 GHz), G-band (3.95-5.85 GHz), J-band (5.85-8.2 GHz), X-band (8.2-12.4 GHz) and Ku-band (12.4-18 GHz), while those of the naturally produced Al_2O_3 samples were measured at the same bands, with the exception of S-band. The average dielectric properties over all bands of interest were found to be (3.59-j0.10) for paint, (3.69-j0.12) for primer and (3.20-j0.225) for Al_2O_3 .

The dielectric properties, or dielectric constant, of a material is a complex quantity where the real part (permittivity) represents the ability of a material to store microwave energy, and the imaginary part (loss factor) represents the ability of a material to absorb microwave energy. Materials with loss factors lower than their permittivities, such as those used in this investigation, are known as low loss dielectric materials.

THEORETICAL RESULTS

The theoretical analysis of this investigation involved modeling the reflection properties of a microwave signal from an aluminum panel under a layer of paint and primer, with and without the presence of corrosion, using an open-ended waveguide probe. An additional layer of air is also included to account for standoff distance. Figure 1 shows the cross-section of a painted aluminum panel with corrosion. This model describes both the magnitude and phase of reflection coefficient (hereon known as magnitude and phase) referenced at the aperture of the waveguide. The Applied Microwave Nondestructive Testing Laboratory (*amntl*) has developed programs to formulate the reflection characteristics of an electromagnetic wave impinging upon a multi-layered structures using such probes, as shown in Figure 1 [4]. The parameters needed for this code include frequency of operation, thickness of each layer, the standoff distance and the dielectric properties of each layer. The average dielectric properties of paint, primer and corrosion found earlier were used, and thicknesses of 0.09 mm for paint, 0.06 mm for primer and 0.13 mm for corrosion product were used. These represent the expected thicknesses that would normally be encountered.

Simulations were made by varying the standoff distance and the frequency of operation. Since the individual layers are very thin and low loss, only the phase was used, as magnitude exhibited little change. The theoretical investigations were conducted in X-band, Ku-band, K-band and Ka-band. Within each of these bands, the phase was determined as a function of frequency with several different standoff distances. Figure 2 shows the phase as a function of frequency at X-band with a standoff distance of 4 mm. Figure 3 shows the same except at Ka-band (26.5-40 GHz) and with a standoff distance of 2 mm.

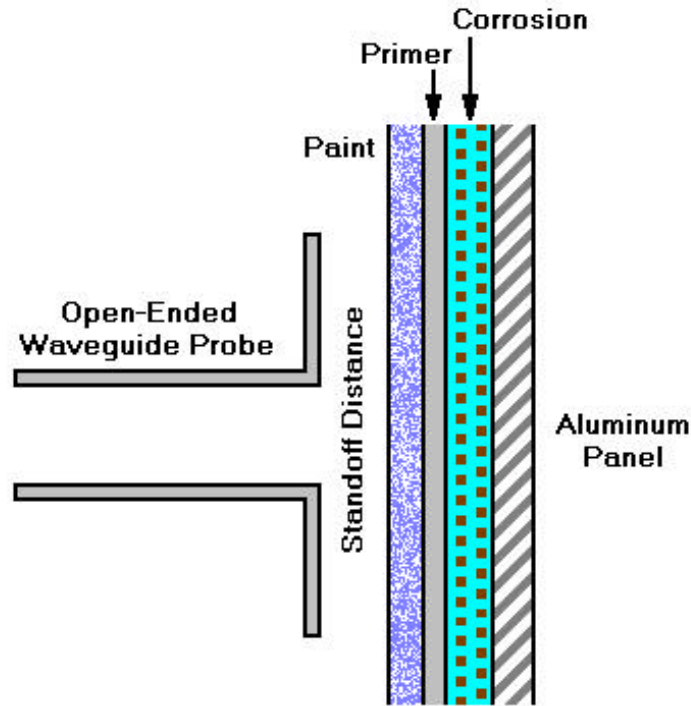


FIGURE 1. Cross-section of aluminum panel under a layer of paint, primer and corrosion.

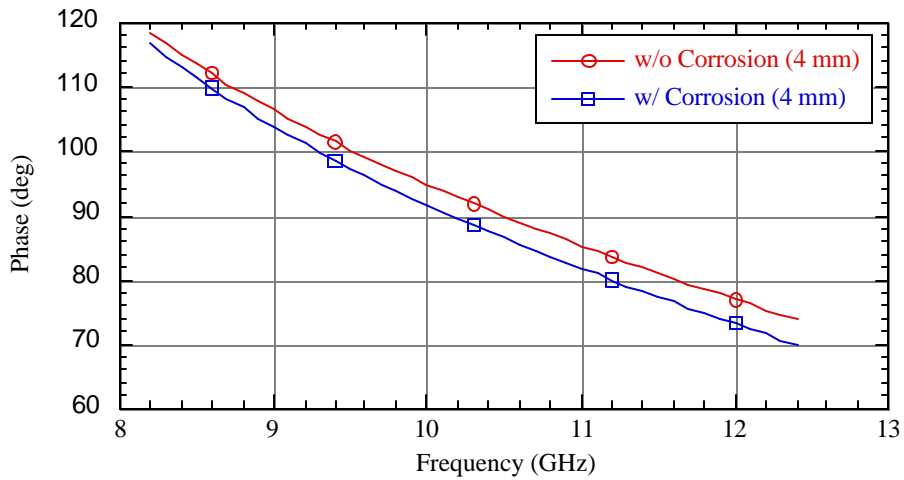


FIGURE 2. Phase of reflection coefficient at X-band with a standoff distance of 4 mm.

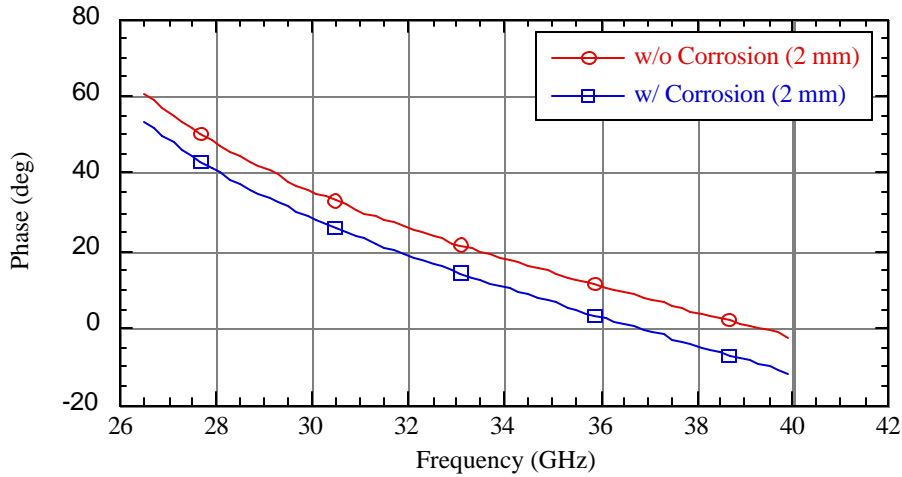


FIGURE 3. Phase of reflection coefficient at Ka-band with a standoff of 2 mm.

Note that, in both Figures 2 and 3, there is a difference in phase with and without a layer of corrosion. This difference indicates the possibility of detecting the presence of corrosion using an open-ended waveguide probe. Also, the difference in phase is much larger for Ka-band than for X-band. X-band had a difference in phase of up to 4 degrees, while Ka-band had a difference in phase of up to 10 degrees. The other simulations also showed an increase in the difference in phase as a function of increasing frequency.

Simulations were also conducted at two different frequencies within each band where the standoff distance was varied. This provided information used to determine the optimal standoff distance to detect corrosion, while also having the least amount of sensitivity due to standoff variation. The frequencies were chosen to represent the high and low frequencies of the band [5].

EXPERIMENTAL RESULTS

Three aluminum plates were specially prepared for the experimental investigation. One panel was provided without corrosion as a control sample. The other two panels (B and C) were halfway submerged in salt water in order to generate corrosion products. Both halves of the plate contained some corrosion products, however, the bottom halves had some pitting due to the presence of salt products, while the top half remained smooth. Excess salt was removed from the plates, and they were then sand blasted to remove the corrosion. Both the front and back panels of the plates had masks placed on them to retain areas of corrosion during sand blasting. The fronts of the panels were left with a strip of corrosion about 3 inches wide running down the center of the plate from top to bottom, and the backs of the panels were masked so that there was a square of corrosion on the pitted area. The plates were then primed and painted.

Most of the experimental investigation involved performing two dimensional area scans with an open-ended waveguide probe. The areas scanned included strips along the top of the plate (where no pitting was present), strips along the middle of the plate (where pitting was present), strips along both the top and middle of the plate (where there

contained areas with and without pitting). Scans of the entire plate were also performed. These scans were performed using different frequencies of operation, as well as adjusting the standoff distance of the waveguide probe [5].

Figure 4 shows an area scan of the top-middle strip of the front of panel B. The darker area of the image represents the corroded area in the panel. Pitting can also be seen in the lower half of the image. The frequency of operation was 24.1 GHz (K-band), and the waveguide probe was in contact with the surface (i.e. no standoff). Figure 5 shows the same scan as Figure 4, except the standoff distance was 5 mm in this case. Here, however, the lighter areas represent corrosion. Figure 6 shows an area scan of the top strip of the front of panel C. The frequency of operation was 24.1 GHz, and standoff distance was 5 mm. Again, the lighter area represents corrosion. Figure 7 shows an area scan of the middle strip of the front of panel C. Here, the darker area represents corrosion, and pitting can be easily seen. The frequency of operation was 33.5 GHz (K-band), and the standoff distance was 2 mm. Figure 8 shows an area scan of the top-middle strip of the front of panel C. The frequency of operation and standoff distance is the same as in Figure 7.

It was observed that as frequency of operation increased, the corroded area could be more easily distinguished from the non-corroded area. This observation matches the results from the theoretical analysis. Also, since the waveguide aperture is smaller at higher frequencies, pitting can be seen in greater detail as higher frequency bands are used.

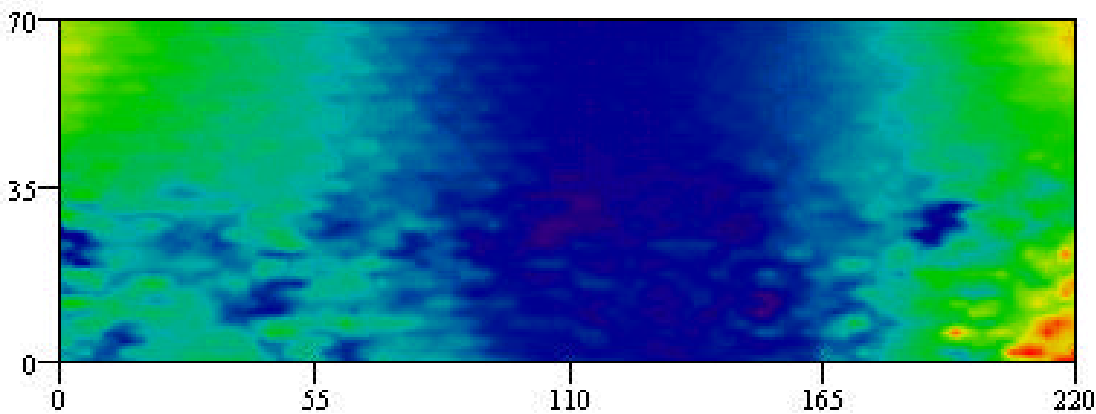


FIGURE 4. Image of the top-middle strip of the front of panel B, at a frequency of 24.1 GHz and at a standoff distance of 0 mm (i.e. in contact).

(Note: Dimensions are in mm).

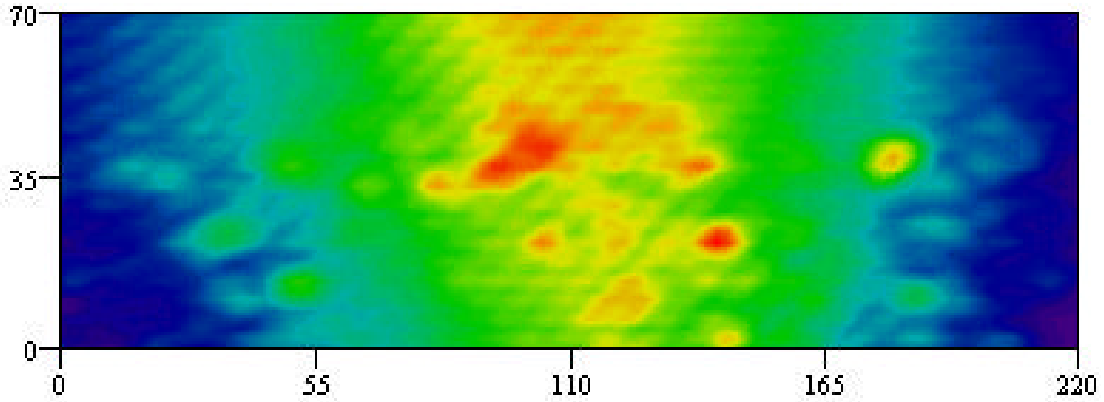


FIGURE 5. Image of the top-middle strip of the front of panel B, at a frequency of 24.1 GHz and at a standoff distance of 5 mm. (Note: Dimensions are in mm).

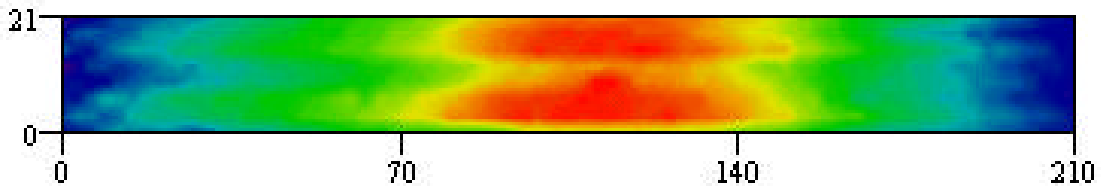


FIGURE 6. Image of the top strip of the front of panel C, at a frequency of 24.1 GHz and at a standoff distance of 5 mm. (Note: Dimensions are in mm).

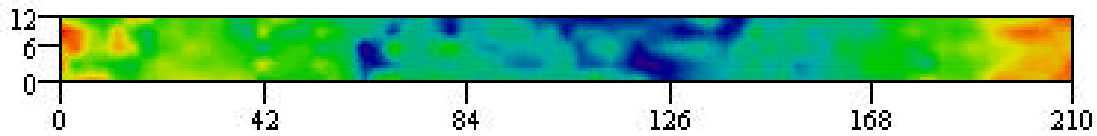


FIGURE 7. Image of the middle strip of the front of panel C, at a frequency of 33.5 GHz and at a standoff distance of 2 mm. (Note: Dimensions are in mm).

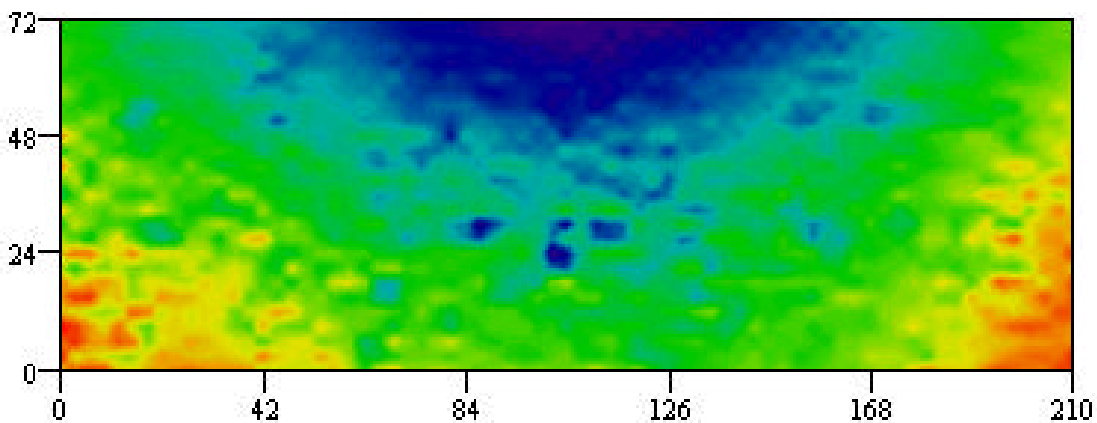


FIGURE 8. Image of the top-middle strip of the front of panel C, at a frequency of 33.5 GHz and at a standoff distance of 2 mm. (Note: Dimensions are in mm).

SUMMARY

The results of this investigation showed that there exists a high potential for detecting corrosion in aluminum under a layer of paint and primer using near-field microwave NDT techniques with open-ended rectangular waveguide probes. This was shown in both the theoretical simulations and experimental investigations performed using laboratory designed measurement systems.

The dielectric properties of paint, primer and naturally produced aluminum oxide were measured over a wide range of microwave frequencies (2.6-18 GHz). These materials were found to have low permittivities and low loss factors. Also, it was found that dielectric properties of aluminum oxide, paint and primer are very similar to each other. This is important since it is easier to detect corrosion under paint when the dielectric properties have a greater difference when compared to each other, as is the case with steel corrosion.

Theoretical investigation was performed using electromagnetic simulations of the reflection of a microwave signal off of a multi-layered structure using an open-ended rectangular waveguide probe. The simulations were also performed over a wide band (8.2-40 GHz), and at several standoff distances. These investigations showed that, for the frequency bands explored, higher frequencies produced better results. Standoff distances could also be adjusted to produce optimal results. The measurements generally had the most effective standoff distance occur at a few millimeters. It was also shown that the difference in phase with and without a layer of corrosion remained fairly constant regardless of frequency over a given band. This is important since it shows that frequency selection in a given band is not crucial, which allows for the use of commercially available components as opposed to custom-made components.

Three frequency bands were used in the experimental analysis (X, K and Ka). Several setups were used to produce 2-D images of various areas of two specially prepared samples. Images were produced at standoff distances ranging from in contact (i.e. 0 mm) to 5 mm, and at different frequencies. The pitting in the center strip of the plates could be seen, and in some instances, this masked the detection of corrosion in these areas. However, corrosion could easily be detected in areas devoid of pitting. Also, within the frequency bands investigated, utilizing higher frequencies allowed for greater possibility of detection of corrosion, as well as higher resolution of pitted areas.

ACKNOWLEDGEMENT

This work was supported in part by Dr. Charles Pellerin, Strategic Environmental Research and Development Program (SERDP) Office, Project No. PP-1134.

REFERENCES

1. Qaddoumi, N., Handjojo, L., Bigelow, T., Easter, J., Bray, A., and Zoughi, R., "Microwave Corrosion Detection Using Open-Ended Rectangular Waveguide Sensors," *Materials Evaluation*, vol. 58, no. 2, pp. 178-184, February 2000.

2. Qaddoumi, N., Shroyer, A., and Zoughi, R., "Microwave Detection of Rust Under Paint and Composite Laminates," *Research in Nondestructive Evaluation*, vol. 9, no. 4, pp. 201-212, 1997.
3. Bois, K., Handjojo, L., Benally, A., Mubarak, K., and Zoughi, R., "Dielectric Plug-Loaded Two-Port Transmission Line Measurement Technique for Dielectric Property Characterization of Granular and Liquid Materials," *IEEE Transactions on Instrumentation and Measurement*, vol. 48, no. 6, pp. 1141-1148, December 1999..
4. Bakhtiari, S., Ganchev, S., Qaddoumi, N., and Zoughi, R., "Microwave Non-Contact Examination of Disbond and Thickness Variation in Stratified Composite Media," *IEEE Transactions on Microwave Theory and Techniques*, vol. 42, no. 3, pp. 389-395, March, 1994.
5. Wang, N., Hughes, D., Donnell, K., Case, T., and Zoughi, R., "Feasibility Study of Corrosion Detection Under Paint in Aluminum Panels," Final Report, Texas Research Institute at Austion (TRI Austin), July 2000.

Paper presented at the 27th Annual Review of Progress in Quantitative Nondestructive Evaluation, Ames, Iowa, 16-21 July 2000 and published in *Review of Progress in Quantitative Nondestructive Evaluation*, Vol. 20, edited by D.O. Thompson and D.E. Chimenti, 2001.

MICROWAVE DETECTION OF COVERED SURFACE CRACKS IN METALS

N. Wang¹, K. Donnell¹, M. Castle¹, R. Zoughi¹, M. Novack²

¹*Applied Microwave Nondestructive Testing Laboratory (amntl), Electrical and Computer Engineering Department, Colorado State University, Ft. Collins, CO 80523-1373*

²*Naval Surface Warfare Center (NSWC), Carderock Division, West Bethesda, MD 20817-5700*

Abstract. This paper presents the results of detecting tight cracks under thin coatings, such as primer and paint, using open-ended coaxial probes and open-ended rectangular waveguide probes. For the latter case the properties of higher-order modes are utilized. Influences of crack size, probe size, operating frequency and coating thickness are investigated. Some of the issues related to the coaxial probe are also investigated theoretically.

INTRODUCTION

Surface crack detection in metallic structures is an important practical issue. This paper explores the effectiveness of using two kinds of microwave nondestructive testing (NDT) techniques, namely; open-ended coaxial probes and higher-order mode (HOM) rectangular waveguide probes, to detect cracks in metal surfaces. The detection is based on the change in the electric field at the aperture of the probe caused by the presence of the crack. For the coaxial probe, the change is reflected in the reflection coefficient and for the higher-order mode rectangular waveguide probe, the change is reflected in the generation of higher-order modes. Also, because of the ability of microwaves to penetrate into dielectric materials, these techniques are expected to be able to detect cracks under paint and primer. The result from scanning cracks for both covered and uncovered cases using these probes will be presented.

COAXIAL PROBE APPROACH

Theory

In this approach, the aperture of the coaxial probe is in contact with the specimen surface which is being scanned. For an exposed metal specimen, when the crack is outside of the coax aperture, the coax is effectively short-circuited and the reflection

coefficient is negative one. As the crack comes into the aperture of the coaxial probe, the interaction between the probe and the crack generates higher-order modes, and the reflection coefficient at the aperture changes. The more the crack comes into the coax aperture, the more the electric field is disturbed, and the change in the reflection coefficient becomes larger. When the crack coincides with the inner conductor the electric field is minimally disturbed and the change in the reflection coefficient decreases [1-2]. The details of this technique have been given elsewhere and for brevity will not be repeated here [1]. For the scanning of covered cracks, a similar explanation applies.

There is little radiation out of an open-ended coaxial probe into its surrounding environment. Such probes operate in a quasi-static mode. This means that the fields probing the surrounding environment around the coaxial probe are concentrated near the probe aperture and do not extend far beyond it. Thus, to detect a crack under a dielectric coating such as paint, it is important to first examine whether for the given paint thickness and dielectric properties the metal backing can be detected. If so, then any crack in the metal backing can be potentially detected, otherwise it may not. To this end, an existing electromagnetic formulation was used to determine the influence of paint thickness on the ability to detect a conducting layer under it [3]. This formulation provides for the magnitude and phase of reflection coefficient at the aperture of the coaxial probe given it is radiating into a conductor backed dielectric layer. The relative to free-space dielectric properties of the paint of interest had already been measured in a wide range of microwave frequencies to be $\epsilon_r = 3.48 - j0.12$ (the real part is the relative permittivity and the imaginary part is the relative loss factor). This paint is in the family of low permittivity and low loss dielectric materials. Also, the dielectric properties of the paint are similar to those of tissue paper which was subsequently used in the experimental testing. Figure 1 shows the phase and magnitude of reflection coefficient at several frequencies and as a function of paint thickness, respectively. The coaxial probe used here has an inner radius of 0.5 mm and outer radius of 1.5 mm (a commercially available coaxial line). Upon examining these figures, it becomes clear that when the paint exceeds a certain thickness the reflection coefficient approaches a non-changing level. This means that beyond this thickness it would be difficult to detect the conducting layer and hence any crack in it. It must be noted that the results shown in Figure 1 are figure-of-merit type information. That is to say that they do not take the incident microwave power into account. Thus, one may be able to penetrate more into the paint if the incident microwave power is increased. For our application, the typical paint thickness of interest is around 0.1 mm, and the results in Figure 1 show this thickness is well within the region where the reflection coefficient continues to change. Thus, for covered crack detection, the crack interacts with the electric field coupled into the dielectric layer, and its presence in the conductor backing can be detected.

Measurements Results

The measurements were conducted by moving the coaxial probe over a covered cracked metal specimen. For these measurements a custom-made phase detector was used which provided an output dc voltage proportional to the phase at the coaxial probe aperture.

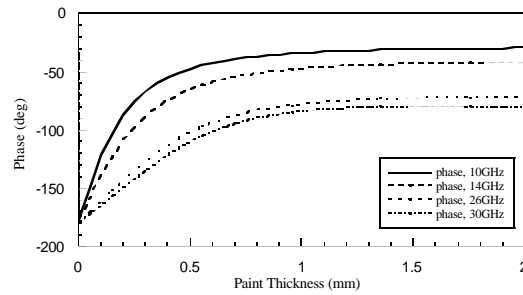


Figure 1a. Phase of reflection coefficient vs. paint thickness.

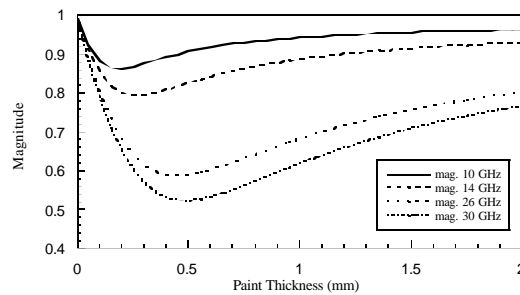


Figure 1b. Magnitude of reflection coefficient vs. paint thickness.

During the scanning process, the phase change in the reflection coefficient with respect to when the crack is out of the coax aperture, or the voltage proportional to this was recorded. This voltage as a function of the scanning distance is called the *crack characteristic signal*. Figures 2a and 2b show the influence of crack size and coaxial aperture dimensions on crack characteristic signal for two cracks/slots (not covered with paint) with the same widths but different depths and at a frequency of 11.3 GHz. The results shown in Figure 2a were obtained using a coaxial probe with an inner radius of 0.5 mm and an outer radius of 1.5 mm. Whereas, the results shown in Figure 2b were obtained using a coaxial probe with an inner radius of 1 mm and an outer radius of 4 mm. It can be seen that for the deeper crack the dynamic range of the detected signals is larger. In addition, the results clearly show the potential for crack depth evaluation. Theoretical analysis (for a fixed coaxial line dimension) has shown that as the depth of the crack exceeds approximately 1.5 mm, the sensitivity to depth reduces dramatically [1]. Comparing Figures 2a-2b, shows that the distance between the two peaks widens and the signal becomes more pronounced for the larger coaxial probe. To show the potential of this method for detecting tight surface cracks, a fatigue specimen with a 3 μm -wide crack was used using the smaller coaxial probe and at a frequency of 11.3 GHz, as shown in figure 3. The results clearly show the ability of this method to detect very tight fatigue cracks.

The goal of this investigation has been to detect covered cracks. Thus, to simulate varying paint thickness, sheets of 0.025 mm-thick tissue paper was used to cover cracks which were subsequently scanned. Figures 4a and 4b show the results for a crack/slot with a width of 0.250 mm and a depth of 1.0 mm and at a frequency

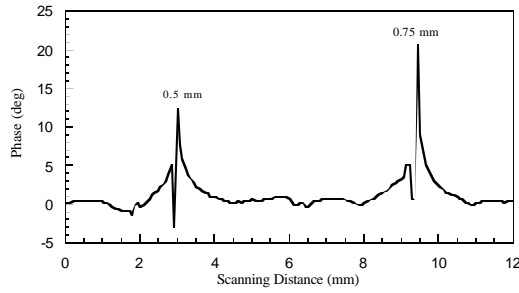


Figure 2a. Crack characteristic signal at 11.3 GHz for a slot with a width of ~0.200 mm and with different depths, coax inner radius of 0.5 mm and outer radius of 1.5 mm.

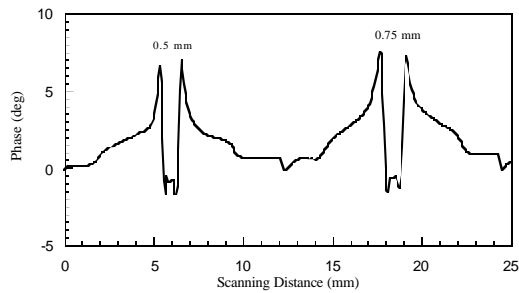


Figure 2b. Crack characteristic signal at 11.3 GHz for a slot with a width of ~0.200 mm and with different depths, coax inner radius of 1.0 mm and outer radius of 4.0 mm.

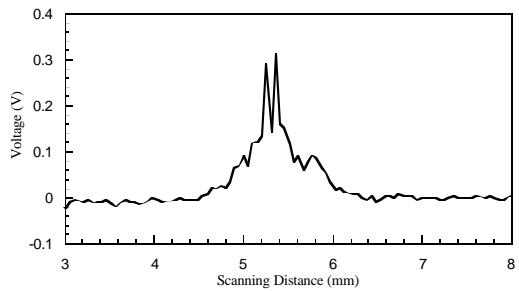


Figure 3. Crack characteristic signal for a fatigue crack with a width of ~3 micrometers and at a frequency of 11.3 GHz.

of 10.5 GHz for four different tissue paper thickness. It is obvious that as the coating thickness increases, the dynamic range of the detected signal decreases. Another point to note is that there is now only one peak in the crack characteristic signal while there are two peaks for the case when there is no coating. This is due to the fact that in this case the crack no longer directly interacts with the inner conductor of the coaxial probe. Consequently, the two peaks that were seen previously are combined into one. Figure 5 shows the effects of frequency and incident power in covered crack detection. At a frequency of for 11.37 GHz the detected dynamic range is larger than that at a frequency of 10.33 GHz. Measurements show that the optimal frequency for detection depends on the combination of the different crack size and

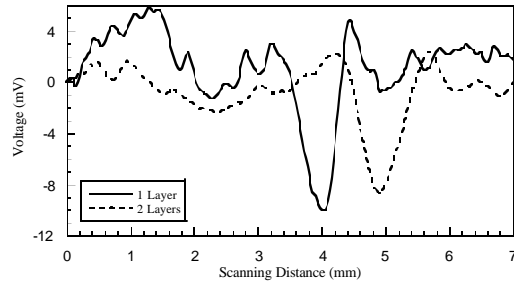


Figure 4a. Crack characteristic signal for covered crack with one and two layers of tissue paper.

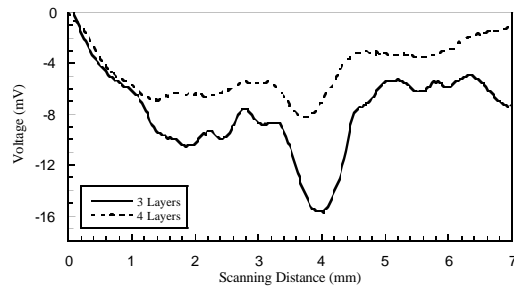


Figure 4b. Crack characteristic signal for covered crack with three and four layers of tissue paper.

coax size. Regarding incident power and as mentioned earlier, if the power is too low, the electric field may not be able to penetrate through the paint and reflected back to the coax aperture. In this case the crack will not be seen. Examining the signals at 11.37 GHz and different power input in Figure 5, it can be seen that the dynamic range increases with the increasing incident power.

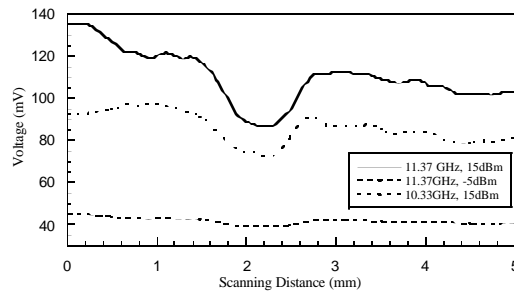


Figure 5. Influence of frequency and incident power on covered crack detection, for a slot with a width of ~0.150 mm and a depth of 0.750 mm and coating (tape) thickness of 0.110 mm.

HOM PROBE APPROACH

Theory

When a rectangular waveguide, operating in its dominant mode (TE_{10}), is terminated with a metal plate, it is effectively short-circuited and there is no electric field component along the direction of the broad side of the rectangular waveguide. However, if there is a crack in the metal plate, the crack changes the reflection properties of the plate and hence the waveguide is no longer short-circuited, the electric field is disturbed, and higher-order modes are generated. This causes electric field component in the direction along the broad side of the waveguide. By detecting this electric field, the presence of a crack can be indicated. This is a very sensitive method for detecting cracks. For brevity, the detailed discussion regarding the foundation of this method is given elsewhere [4-5]. Such a probe was used to examine the potential of this method for detecting covered cracks as well.

Measurements Results

Similar to the coaxial probe approach, measurements were conducted by moving the aperture of the probe along the surface under inspection. The recorded voltage is related to the power associated with the presence of higher-order modes as a result of the presence of a crack in a metal plate. Measurements were conducted in the Ka-band frequency range (26.5-40 GHz) which was previously determined to be a suitable frequency range for this purpose [5].

For the HOM crack characteristic signal, there are issues concerning the flange edge effect. When there is no dielectric layer between the waveguide and the metal plate, we expect two peaks as the two edges of the waveguide aperture come across the crack. However, when there is a dielectric layer between the waveguide and the metal plate, there may exist electric field propagating in the dielectric layer, and the detected signal changes four times as the two edges of the flange and two edges of the aperture scan across the crack [5-6]. The relative amplitude of the multiple peaks depends on the operating frequency, dielectric property and thickness of the coating, and also the probe location.

Figure 6 shows the results when scanning a slot on a brass sample at a frequency of 31.5 GHz. Figure 6a is for the case when the crack is uncovered. The airgap between the waveguide and metal plate caused the multiple peaks (more than two). Figure 6b and Figure 6c show the results from scanning the same crack under coating (clear tape) thickness of 0.05 mm and 0.15 mm. For all three cases shown in Figure 6, the signal level is very low in the region where the crack is outside of the waveguide aperture. Theoretically if there is no coating, there should be no signal detected, and the signal-to-noise ratio is infinity. The high signal-to-noise level is the most prominent characteristic of the HOM probe, which make it a very sensitive probe [5]. Also, the multiple peaks increase the probability of crack detection.

SUMMARY

Extensive sets of measurements over a wide range of cracks were conducted using coaxial and higher-order mode waveguide probes. Both coated and uncovered fatigue cracks and slots were used in this investigation. Some theoretical aspects of

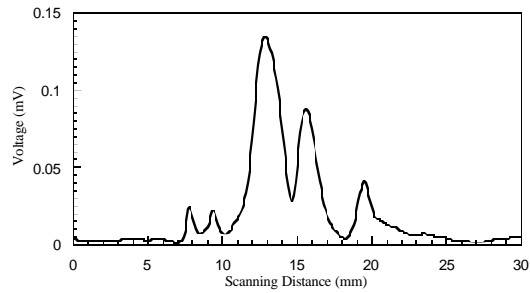


Figure 6a. HOM signal for an exposed crack with a width of ~ 0.10 mm and a depth of 0.90 mm.

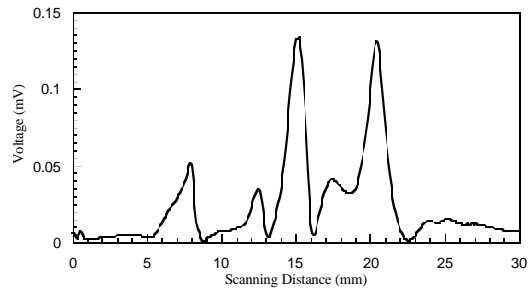


Figure 6b. HOM signal for a crack covered with a coating thickness of 0.05 mm and a crack with a width of ~ 0.10 mm and a depth of 0.90 mm.

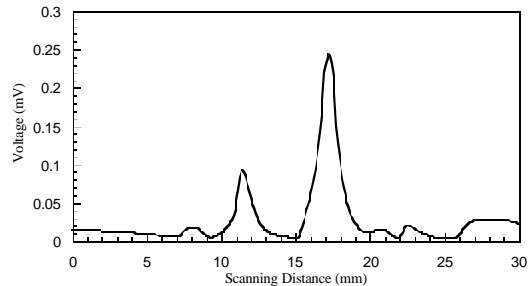


Figure 6c. HOM signal for a crack covered with a coating thickness of 0.150 mm and a crack with a width of ~ 0.10 mm and a depth of 0.90 mm.

the coaxial probe were also investigated. The results indicated that both probes have high potential for detecting cracks under coatings such as paint and primer. Each probe possesses its unique advantages and disadvantages. The coaxial probe was shown to easily be able to detect tight cracks under coatings of about 0.15 mm at relatively low microwave frequencies (X-band). This probe was also found to be less susceptible to edge effect issues. The HOM probe also showed to be capable of detecting similar cracks under similar coatings. However, the issue of edge effect and small changes in the standoff distance seem to be more of a concern when using this probe. Several issues regarding crack dimensions, frequency of operation, coating thickness, coaxial dimension and incident power were also investigated. Overall, the results of these investigations were found to be encouraging for detecting cracks under this dielectric coatings.

ACKNOWLEDGEMENT

This work was supported in part by Dr. Charles Pellerin, Strategic Environmental Research and Development Program (SERDP) Office, Project No. PP-1134.

REFERENCES

1. Y. Wang "Analysis of surface crack detection in metals using coaxial sensors" Ms. thesis, Department of Electrical and Computer Engineering, Colorado State University, 1999.
2. R. Zoughi, K. Hayes and S. Ganchev, "Microwave Detection of Hairline Surface-Breaking Cracks in Metals Using Open-Ended Coaxial Sensors: Preliminary Results", Proceedings of SPIE Symposium, Nondestructive Evaluation Techniques for Aging Infrastructure & Manufacturing Conferences, vol. 2945, pp. 444-450, Scottsdale, AZ, December 2-5, 1996.
3. Bakhtiari, S., S. Ganchev and R. Zoughi, "Analysis of the Radiation of an Open-Ended Coaxial Line into Stratified Dielectrics," *IEEE Transactions on Microwave Theory and Techniques*, vol. 42, no. 7, pp. 1261-1267, July, 1994.
4. C. Yeh, E. Ranu, and R. Zoughi "A Novel Microwave Method For Surface Crack Detection Using Higher Order Mode Waveguide Modes", *Materials Evaluation*, vol. 52, No. 6, pp676-681, June 1994.
5. Qaddoumi, N., E. Ranu, R. Mirshahi, P. Stepanek, V. Otashevich, C. Huber and R. Zoughi, "Development of Equipment for and Quantitative Analysis of Microwave Detection and Evaluation of Fatigue Induced Surface Cracks in Steel," Final Report, Federal Highway Administration (FHWA), Grant no. DTFH61-94-X-00023, p. 519, January, 1998.
6. Qaddoumi, N., E. Ranu, J.D. McColskey, R. Mirshahi and R. Zoughi, "Microwave Detection of Stress Induced Fatigue Cracks in Steel and Potential for Crack Opening Determination," *Research in Nondestructive Evaluation*, vol. 12, no. 2, pp. 87-103, 2000.

Paper presented at the 54th Meeting of the Machinery Failure Prevention Technology Society, 1-4 May 2000, Virginia Beach, Virginia, and published in the proceedings of the same meeting.

DEVELOPMENT OF REAL TIME ULTRASONIC IMAGING

William R. Davis

Naval Air Warfare Center, Aircraft Division
28066 Shaw Rd. Bldg. 2188 Code 4.3.4.2, attn.W.R.Davis
Patuxent River MD, 20670-5304

B. Lasser

Imperium Inc.
9700 Great Seneca Highway
Rockville, MD 20850

Abstract The paper investigates the real time imaging of corrosion and cracks on both the front and back surfaces of thin plate. A real time imaging system utilizing an innovative CCD camera to render the sound waves visible is used in conjunction with ultrasonic transducers as illuminators to generate video pictures of discontinuities. Longitudinal and shear waves are investigated as means to detect corrosion of various severities. Samples were fabricated in a salt fog environment to simulate corrosion under painted surfaces. Fatigue cracks were grown using reversed bending apparatus. Experimental results and video results of inspection are presented.

Key Words: Ultrasonic, NDI, Imaging, Corrosion, Inspection

Introduction: Imperium Inc. developed the concept of imaging sound waves in a water media using a modified infrared charge coupled device (CCD) during the 1997 time period. Since then continued development of the immersion “Acoustocam” system has taken place in partnership with Naval Aviation (NAVAIR) through small business innovative research (SBIR) contracts and with the Strategic Environmental Research and Development Program (SERDP). Hardware and enabling software have progressed to the point of providing clear real time TV images by several means using the camera.

Experimental Methods: The system utilizes a modified CCD camera fabricated by Imperium Inc (Figure 1). The CCD chip is coated with a piezoelectric material known as polyvinyl difluoride (PVDF) which enables the conversion of mechanical energy to charge the CCD chip. The system architecture is shown as Figure 2. An ultrasonic transducer is used to generate mechanical waves and is energized by a pulser. The timing for the pulse generation is provided by a delay card in the PC which gives a timed delay from the camera sync signal. The video output from the camera is either by analog signal or digital signal. The digital signal is fed to an imaging card in the PC. Initial work was performed by passing the sound energy directly through the test piece to the camera. This through transmission is the least complicated method which also had the benefit of requiring the least acoustic energy from the ultrasonic transducers and ultrasonic pulser utilized (Figure 3). Initial setup of the immersion tank involved the mounting of a low impedance diaphragm on one end of the tank for the camera to look through. The camera was manufactured with a block of aqualene cemented on the imaging chip. A suitable

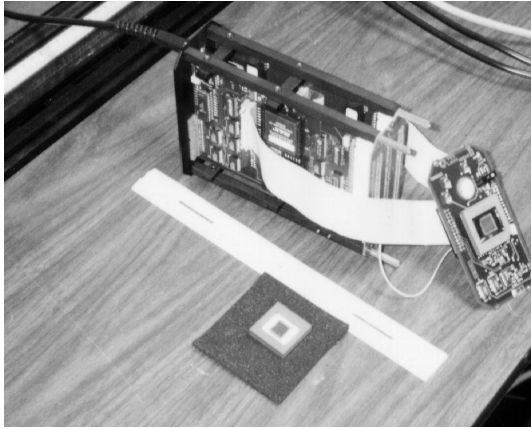


Figure 1. Camera Components

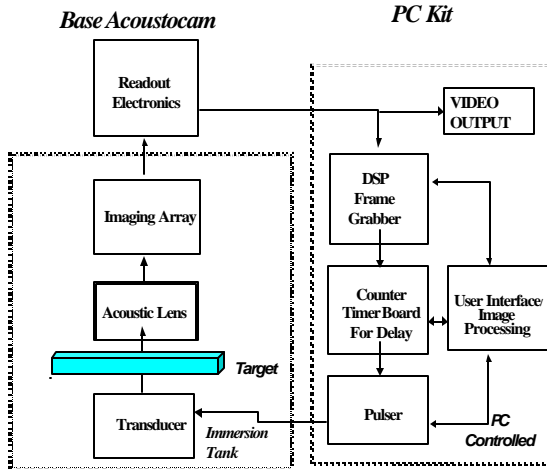


Figure 2. System Architecture

liquid or gel is applied to the diaphragm and the camera is moved into contact with the diaphragm, providing physical contact between the water and the CCD chip. A small PC manufactured in the “breadbox” configuration for ease of use was incorporated in the system to accommodate full size computer cards for control purposes and to display data. The ultrasonic transducer is energized by the pulser when triggered by the delay card in the PC. The pulse passes through the test item and reaches the CCD chip just as it is energized by the camera sync circuit. The electronic window for viewing the wave is kept small to minimize interference.

A second configuration was attempted by introducing the ultrasonic beam into thin aluminum sheet at an angle using a Lucite wedge (Figure 4). The beam was allowed to bounce several times within the sheet and exit back through the first side to the camera without going through the back surface. A thin sheet was glued to the back of the target

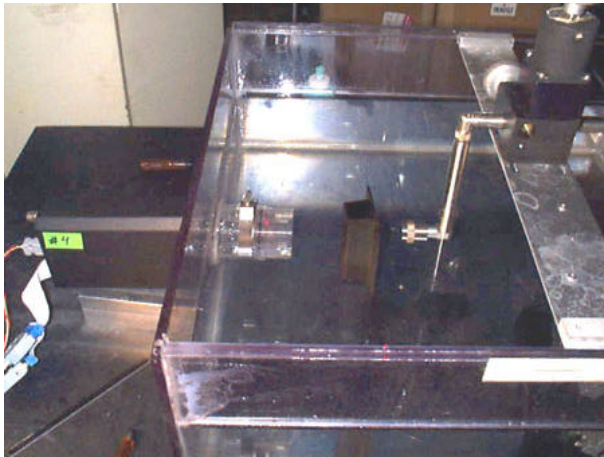


Figure 3. Through Transmission Imaging

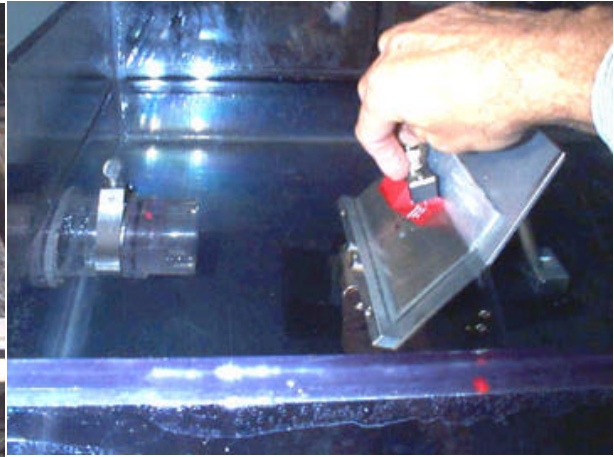


Figure 4. Angle Beam Imaging with Lucite Wedge

plate to provide an air gap behind the plate to eliminate signal loss through the back of the sheet. This allowed a 100% reflection of the beam from the back surface and simulated a hand held unit used outside the water tank to inspect the outer skin of

something like an aircraft. This method was successful but was replaced by an immerseable transducer mounted on a stand which had 5 modes of adjustment, allowing many configurations to be attempted. This configuration is shown as Figure 5. The UT beam was stronger using this configuration because of the elimination of an interface and the absorption by Lucite.

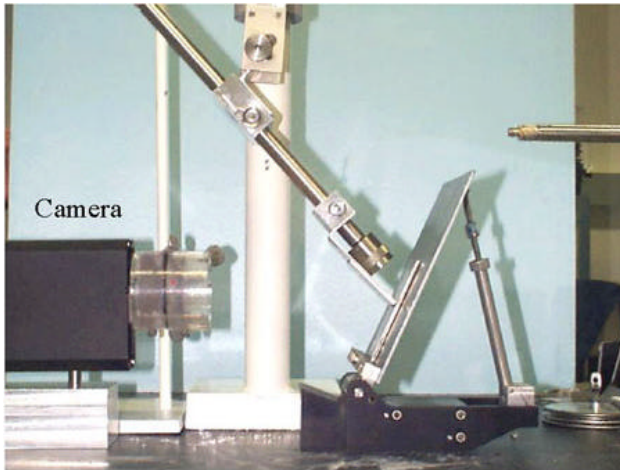


Figure 5. Adjustable Angle Beam Setup

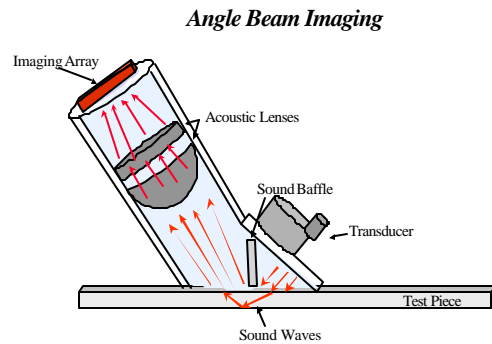


Figure 6. Architecture of the Portable Angle Beam Head

The configuration utilized in the immersion tank was redesigned as a portable unit when the success of the set up was established (Figure 6&7). The portable angle inspection head has been found to be as successful as it was when set up in the immersion tank.

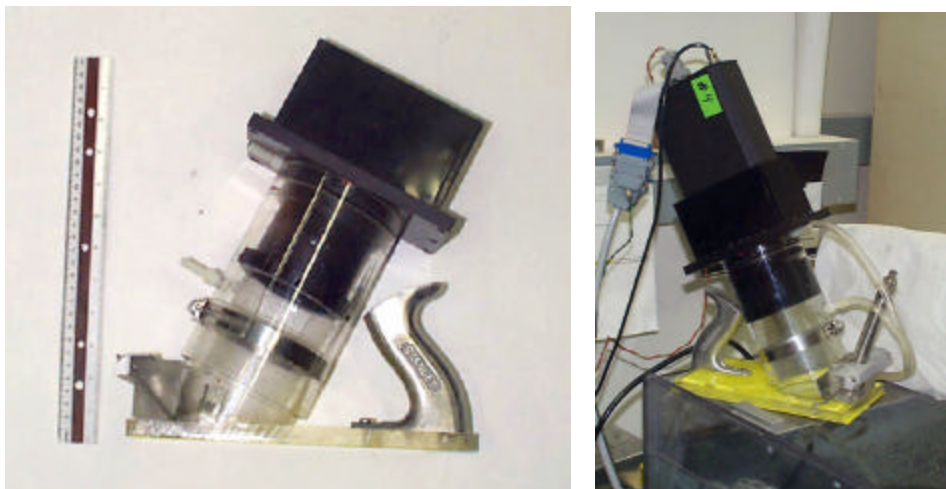


Figure 7. The Portable Angle Beam Inspection Head

Experimental Results:

Through Transmission Inspection Results: Imaging of targets by passing the ultrasonic beam through them is analogous to radiographic inspection in that a shadowgraph is formed. The image is remarkably similar to real time radiography with a few exceptions. Gamma radiation is attenuated proportionally to the thickness and density of the material it passes through. Sound waves are also attenuated proportionally to the thickness of the material, but are also reflected and refracted at interfaces like light waves. The reflection becomes total when a large mismatch of acoustic impedance between the two materials is involved. Air and any solid are one example of an interface that totally reflects.

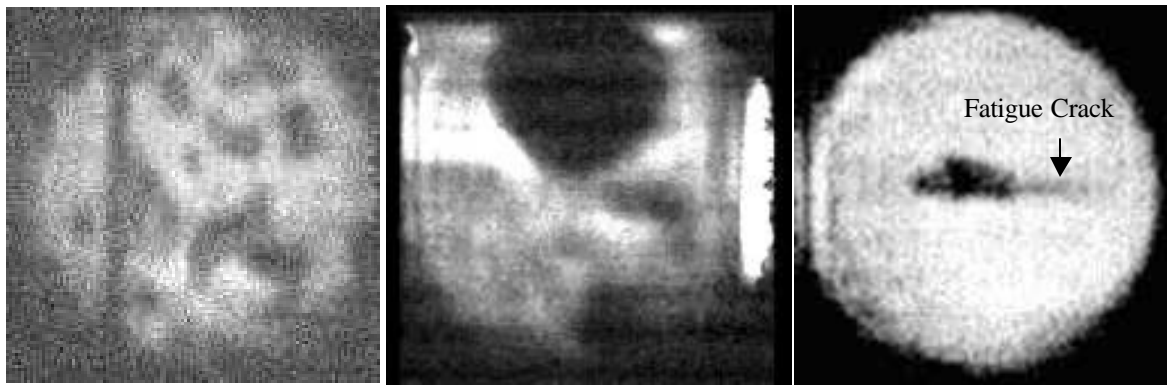


Figure 8. Exfoliation Corrosion (left), Riveted sheet (middle), and a Thin Fatigue Crack in 0.062 inch aluminum sheet (right)

The energy required to form a clear picture using the present first generation CCD chip developed by Imperium is somewhat more than that required for normal ultrasonic NDI inspection. The first pulser utilized was the MP215 manufactured by Tektronix. The 120 volt pulse generated provided clear images but was limited in application because of the need for more power. This was replaced by the MP275 with a pulse of approximately 250 volt was sufficient for many more trials, but was replaced by a pulser capable of 1,000 volts supplied by Imperium Inc. Through transmission studies showed that exfoliation corrosion was very easily imaged (Figure 8) as was detail in a riveted aluminum sheet or vertical cracks in thin aluminum sheet. Imaging of composite panels showed that the fibers themselves could be easily imaged in through transmission revealing fiber direction (Figure 9). Disbonds between composite layers were easily imaged because the crack interface does not allow the passage of sound resulting in dark areas in through transmission mode (Figure 10). Large areas of composite panels could be inspected in a short time because of the image clarity and the real time nature of the images. The size of the field imaged by the fabricated lenses was chosen to optimize the size while keeping the resolution required for optimal inspection. New CCD chips are under manufacture and will enable different inspection field sizes.

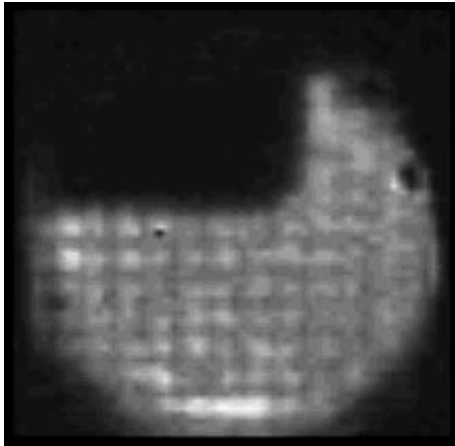


Figure 9. Image of Composite Fibers



Figure 10. Delaminated Composite Panel

Examination of an NDI Evaluation Repair Test Panel (Figure 11) showed remarkable definition of all aspects of the panel. The fibers themselves were clearly defined in the single layer areas at the outer fringes of the panel. The edges of the multiple circular patches applied to the panel were clearly defined as was the circular piece of Teflon tape (Figure 12) inserted between the patch layers. Penetration of the beam through the multiple layers presented no problem although the definition of the fibers within layers was lost when more than a few layers were imaged.

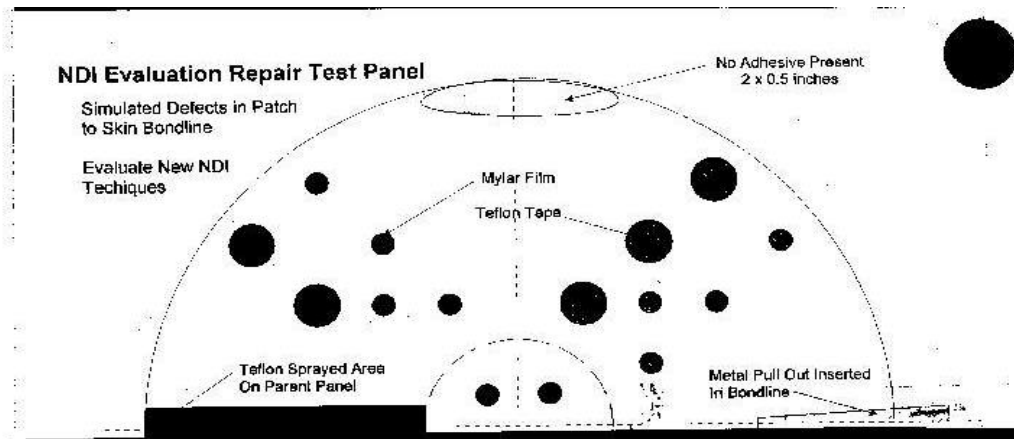
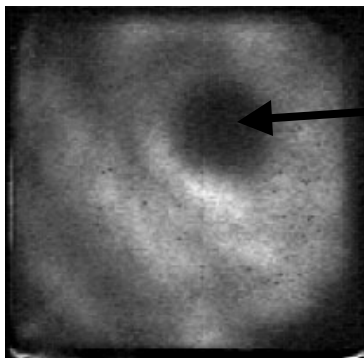


Figure 11. NDI Repair Test Panel



Teflon Tape Dot Shown in Figure 11

Figure 12. Sound image of the composite panel

Angle Beam Inspection Results: Angle beam inspection consists of introducing a sound beam into the part at an angle, allowing the beam to bounce from the bottom surface and then leave the part from the top surface (again at an angle) on the same side as it entered. Angle beam illumination of thin aluminum sheet was first successful on 9/2/99 in the imaging of flat bottom holes in 0.125 thick aluminum sheet. The trials were expanded to a successful simultaneous imaging of both near side and far side holes the same week. The method first utilized a plastic wedge commercially obtained with a 1"x 1/2" 5 MHz transducer for best imaging. This method gave a fixed angle beam which could be introduced into the plate wherever the wedge was held against the plate. The test jig shown in Figure 5 allowed the beam to be varied in placement and angle. A beam was found to give good results when aligned to refract at 60 to 70 degrees inside the plate, reflect between the back surface and front surface several times, refract at the front surface and then propagate into the camera. An angle between the test piece and the camera of approximately 28 degrees was found to maximize the brightness of the beam in this configuration. Initial trials used a 1/16 inch thick 7075 T6 plate with a 3/16 inch diameter flat bottom hole (FBH) 0.010 inch deep on both the front surface and the back surface of the plate. A thin sheet was glued to the back surface to exclude water. The near (top) surface is seen first followed by the back surface (Figure 13 left). The inspection is performed entirely from the front surface.

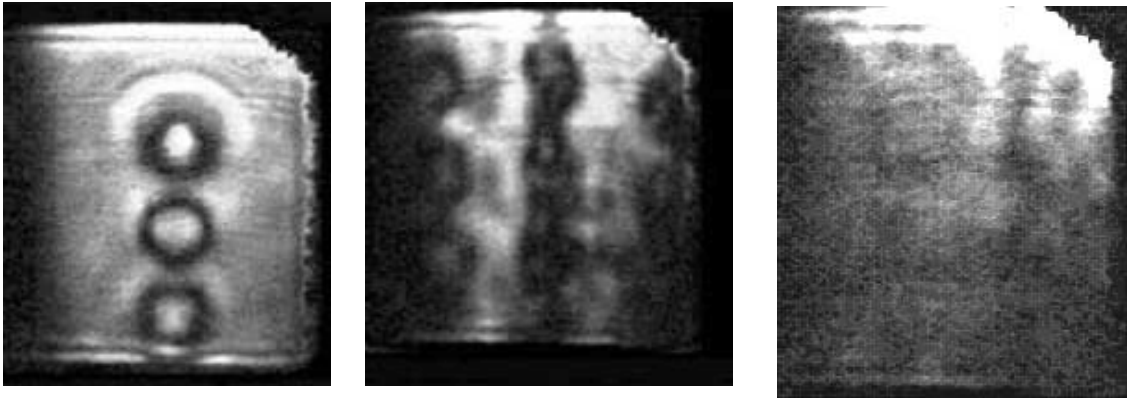


Figure 13. Angle Beam Images. A single back surface 0.010" deep 3/16" diameter flat bottom hole (left). Heavy back surface exfoliation corrosion (middle) and light back surface exfoliation corrosion (right). The multiple bounces of the beam cause multiple images of the discontinuities.

An extensive effort was made to make reproducible corrosion samples. One aluminum alloy (7075 T6) was chosen for the effort as being common in the aircraft industry and easily corroded. Trials using samples corroded in a salt fog environment showed that the degree of corrosion could be controlled by the duration of exposure and the corrosion could be produced in selected locations by protecting all the sample except those locations with a chromated primer and top coat of paint. Imaging of corroded samples representing as little as 1/2 % of weight loss were easily imaged using through transmission configuration. Angle beam inspection was not as clear but also showed the corrosion (Figure 13, right). Corrosion pits representative of 5% weight loss were exceedingly plain when imaged either in through transmission or angle beam (Figure 13,

middle). The angle beam images of flat bottom holes or larger corrosion pits (0.020 inch or so in diameter) appear as a string of discontinuities because of the bouncing of the beam between surfaces and the shadow formed by the defect. All images after the first one are the shadows. Smaller discontinuities have shadows which are obscured by beam scatter.

Discussion of Results: The goal of this project is the detection of corrosion and fatigue cracks on the second surface of thin aluminum sheet through paint. The first year has seen the development of through transmission inspection which gives very good penetration through a variety of materials including aluminum, carbon composites, thick glass fiber composites and some honeycomb structures with excellent images showing details as small as composite fibers and very small diameter pits in aluminum sheet.

A second inspection mode of either longitudinal or shear ultrasonic waves reflecting between the two surfaces of aluminum sheet has given very good results with good sensitivity through as much as three layers of paint when imaging pits 0.030 inch in diameter. The obvious advantage of this method over through transmission is that it requires access to only one surface. Airplane wings and fuselage components could therefore be inspected with no disassembly.

Imperium Inc. has had good results with a test head which directs the beam straight down into the target and images the reflected energy which bounces back up to the camera. This method has great promise for applications where the test object is thicker than the thin aluminum sheet used in aircraft, and may be useful for this with further improvement.

Conclusions: Ultrasonic inspections are performed daily by thousands of engineers and technicians in the United States alone. These individuals have never been able to make more than a guess about the nature of the discontinuities found in the sheet, plate, weld, composite panel, etc. because of the lack of information gleaned from the oscilloscope screen used (amplitude and time delay). Imaging of the same sound beam allows instant identification of the source of the signal with the possibility of accurate evaluation of the size, shape, and origin of the discontinuity. The great advantage of this is that the necessity for grinding out every signal source is negated. Only those discontinuities of a size, type, shape and placement which might cause failure need to be repaired.

Further development can now be concentrated on minimizing the size of the portable test heads developed and adapting the test heads to new specimen geometries such as curved (wing) surfaces. Other future applications might include heavy gauge welds in plate, corrosion in piping, welds in piping,

Acknowledgements: This work was supported by the Strategic Environmental Research and Development Program (SERDP).

References:

1. Lasser, M., Harrison, G. "A Novel High Speed, High Resolution Ultrasound Imaging System", QNDE Review of Progress In Quantitative NDE, Plenum Press, Volume 17B, pp. 1713-1719 (1997),
2. Lasser, M., Harrison, G., Kula, J., "Real-Time, Depth Sensitive C-scan Imaging System", 7th Annual research symposium transfer of emerging NDE technologies (1998)
3. Lasser, M., Lasser, B., Kula, J., Rohrer, G.," Latest Developments in Real-Time 2D Ultrasound Inspection for Aging Aircraft", 10th Annual AeroMat Conference & Exposition (1999)
4. Lasser, M., Lasser, B., Kula, J., Rohrer, G.," On-Line, Large Area Ultrasonic Imaging for Composite Manufacturing", American Society for Nondestructive Testing Conference (1999)
5. Lasser, M., "A Novel High Speed, High Resolution Ultrasound Imaging System", ASNT Fall Conference NDT- Keystone of Quality, published by ASNT, pp. 196-198 (1997) ,

Paper presented at the National Association of Corrosion Engineers (NACE) Expo 2000, 27-30 March 2000, Orlando, Florida, and published in the proceedings of the same meeting.

THERMOGRAPHY FOR CHARACTERIZATION OF CORROSION DAMAGE

Ignacio Perez and Paul Kulowitch
Naval Air Warfare Center, Aircraft Division
Patuxent River MD 20670

ABSTRACT

Thermography is a viable NDE technique for the characterization of corrosion in metallic materials. Thermography is a rapid, non-contact, wide area inspection technique that is easy to interpret and that is not significantly sensitive to material curvature. We have developed a portable system and have characterized the sensitivity of the technique. Results will be presented in this paper.

Keywords: Thermography, thermographic inspection, corrosion, naval aviation, corrosive environment, lateral heat effects.

INTRODUCTION

The Navy operates in the most corrosive environment of any of the DoD services or commercial aviation. As a result corrosion prevention, detection and repair are of outmost importance to the Navy. All the materials in our platform are designed and engineered to offer the maximum corrosion protection without limiting their structural characteristics. New paint systems are being developed that comply with EPA regulations while providing enhanced protection against the environment. No matter how much protection we provide to our platforms in the form of improved materials, sealants and paints, the environment ultimately will penetrate the coating and initiate corrosion. This process can be exacerbated or mitigated by the specific mission of the platform. Low flying antisubmarine aircraft will corrode at an accelerated rate when compared to high-altitude communications aircraft.

The cost of corrosion control is enormous and accelerating as our fleet ages. This is especially significant in today's environment of reduced budgets and decreasing personnel. With fewer new acquisitions, the Navy is increasingly being forced to extend the life of existing platforms beyond their original design life to meet mission requirements. In order to maintain fleet readiness and safety, improved inspection methods are required that can detect the occurrence of corrosion quickly and reliably.

New techniques are being developed at the Naval Air Warfare Center aimed at the reliable and rapid inspection of corrosion in Naval aircraft. One of such techniques is pulsed thermography. This is a wide area inspection technique which is especially suited for the detection of hidden corrosion. It requires no contact media to perform the inspection as opposed to more conventional techniques such as ultrasonic inspection. This technique relies on the thermal gradients that result from the interaction between the thermal fields and defects present in the structure. This technique is also significantly insensitive to curvature and is a relatively easy interpretation method.

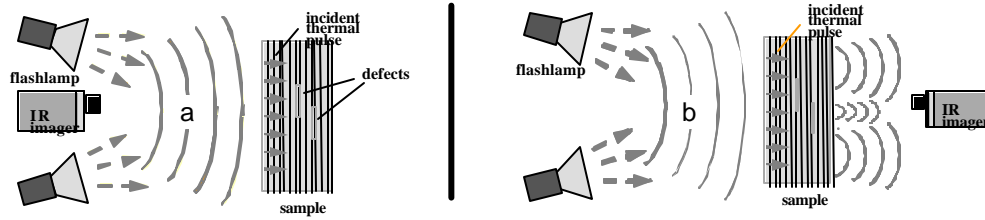


Figure 1. (a) Shows a standard single side inspection setup with the IR camera and the arc lamps in the same side. (b) Shows a through transmission setup which in general provides twice the depth of resolution.

EXPERIMENTAL

The minimum number of experimental components needed to perform pulsed thermography are a heat source and an infrared (IR) camera. The proper choice of heat source is paramount for a successful thermographic experiment. Such source must be chosen so as to maximize the thermal contrast between the defect and the surrounding material. In some cases one can maximize the thermal contrast by heating the defect exclusively without disrupting the surrounding material such as when using microwave energy for detecting water entrapped inside a ceramic material. The microwave energy will propagate through the ceramic material without heating it and finally will be absorbed by any water present in it. This approach is not always possible and one has to resort to exploiting other defect properties (such as geometrical features) to enhance the thermal contrast. The most common energy sources used to thermally excite materials are: air heat guns, microwave sources, infrared lamps and arc lamps. All the samples studied in this paper were thermally excited using a pair of xenon arc lamps, each one powered by a 5 KJoule capacitor bank with a 10 msec discharge time. The IR camera used in these experiments was a Amber Engineering InSb focal plane array (128 x 128) camera with silicon optics operating in the 3 - 5 micron spectral range. Figure 1a (single side inspection setup) shows the experimental configuration used to image all defects. Other experimental arrangements are possible such as the one shown on Fig. 1b (through transmission setup). This setup is not well suited for field inspections where only one side is typically exposed, but has twice the depth of resolution than single side inspection methods. Figure 2 shows the camera system and arc lamps used to acquire data for this paper.



Figure 2: Thermal imaging system used to acquire data.

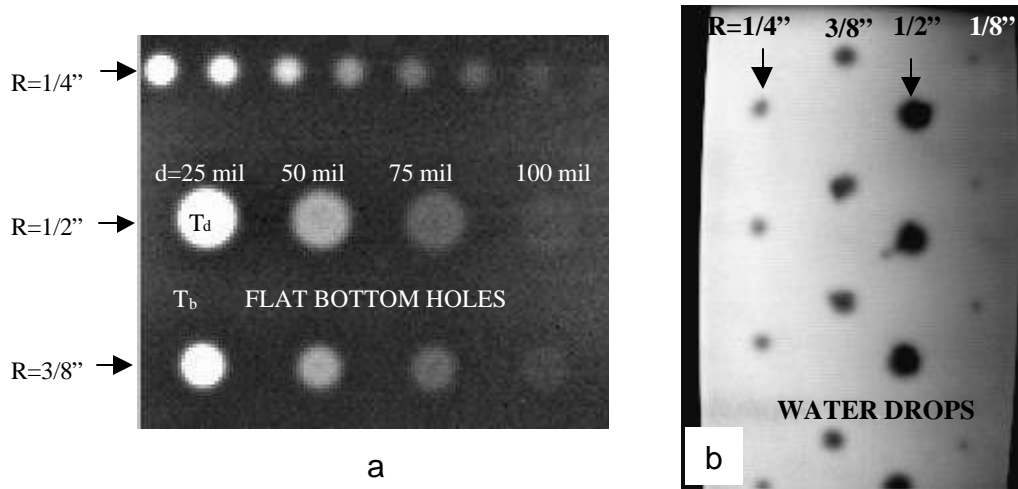


Figure 3. (a) Shows a 1/8" thick aluminum with flat bottom holes of different depth ranging from 25 mil to 100 mil and three different radii of $R=1/2''$, $3/8''$ and $1/4''$. (b) Shows a 1/32" thick aluminum panel with water drops of different radii and different water content.

Any material can be inspected thermographically (such as metals, ceramics and composites) but the outcome of the inspection will depend on many factors such as sample geometry, sample thickness, amount of heat used, surface emissivity, specific heat, material density, thermal conductivity, defect depth and the size of the defect and other parameters. To gain insight into the effect that several of these parameters have on the thermographic process we fabricated various aluminum 7075 T6 panels with embedded defects. One panel was fabricated with flat bottom holes while the others had water pockets on the back. Figure 3 shows two thermal images a few msec after exposure to a heat pulse. The figure on the left corresponds to a $t_o=1/8''$ thick aluminum panel with three different radii flat bottom holes ($R=1/2''$, $3/8''$ and $1/4''$ diameter). Flat bottom holes are a crude simulation to material loss that results from the corrosion process, but offer a simple means of generating standards for the characterization of the thermal process. The distance from the surface of the panel to the surface of the flat bottom holes (also referred as the defect depth "d") ranged from 25 mil to 100 mil. The largest contrast corresponds to the defect closest to the surface while the defect furthest from the surface showed the smallest thermal contrast. The thermal contrast is defined as the difference of the temperature above the defect (T_d on fig 3 a) from the temperature of a point away from the defect area (such as T_b on Fig. 3). The center to center distance between flat bottom holes was set to at least 2 diameters to minimize inter-hole proximity effects.

Water entrapment is a leading cause of corrosion and debonding in honeycomb structures. Early detection of it leads to economical repairs. Figure 3 b shows the thermal image a few msec after exposure of one of three panels (panel thickness were $t_o=1/32''$, $1/16''$ and $1/8''$) fabricated to model water entrapment. The panel shown on that figure corresponds to a $t_o=1/32''$ thick aluminum panel with water drops on the back of different diameters ($1/8''$, $1/4''$, $3/8''$ and $1/2''$ diameter) and with different amount of water in them. Water was contained on the back of the panels by gluing straws of different diameters to the surface and by filling them with water up to different levels. The heights of water used were $d = 1/16''$, $1/8''$, $3/16''$ and $1/4''$. It is clear from Figure 3b that the amount of water has little effect on the thermal contrast (notice the small contrast variation among drops of equal radii). The straws were staggered to maximize the spacing among them in order to minimize proximity effects. It is interesting to note the opposite nature of the thermal contrast effects when imaging flat bottom holes compared to when detecting water entrapment. When imaging flat bottom holes it is the thinner region above the defect what ultimately makes this region appear hotter (white region on Figure 3a). In contrast, it is the excess water acting as a heat sink what makes the region above the entrapped water appear colder (black region on Figure 3b).

RESULTS AND INTERPRETATION

Figure 4 shows the contrast data of all the samples studied, the graph on the left corresponds to flat bottom hole samples while the graph on the right corresponds to samples with water pockets on the back. From the graph 4a clear that the deeper the defect (or the smaller amount of mass loss) the smaller the contrast temperature will be. Also, as the diameter of the defect gets smaller the contrast temperature diminishes. These results have been previously explained^{1,2} using a simple lateral heat approximation model. The main result of the model is that the contrast temperature of a sample with a defect can be approximated by

$$\Delta T_{\text{contrast}} = \frac{Q}{\rho c} \left(\frac{1}{d} - \frac{1}{t_o} \right) \cdot \left[\frac{R}{2 d(t_o - d)} \right]^{1 - \frac{R}{2 d(t_o - d)}} \quad (1)$$

Where the parameters are shown in Figure 5 (left) and represent:

ΔT_{cont}	contrast temperature
Q	energy deposited on the surface of the sample per unit area
ρc	is the specific heat times the density of the sample
d	distance from surface of the sample to the defect
t_o	is the thickness of the sample
R	is the radius of the defect

This equation correctly accounts for all of the observed experimental results. The term before the square bracket provides the principal contribution to the thermal contrast from which the following can be verified:

1. The contrast temperatures (ΔT) increases linearly with the amount of energy deposited per unit area (Q).
2. The higher the specific heat-density of a material ($\rho c \uparrow$) the smaller the contrast temperature becomes ($\Delta T \downarrow$).
3. The closer the defect is to the surface ($d \rightarrow 0$) the larger the contrast temperature becomes ($\Delta T \rightarrow \infty$).
4. As the defect depth approaches the panel thickness ($d \rightarrow t_o$) the contrast temperature vanishes ($T \rightarrow 0$).
5. For a given defect depth d, the thicker the panel ($t_o \rightarrow \infty$) the larger the contrast temperature ($\Delta T \uparrow$).

The term in square brackets represent the lateral heat flow effects and the following can be verified:

6. As defects approach the surface ($d \rightarrow 0$) or as they approach the far end ($d \rightarrow t_o$), the lateral heat effects diminish ([lateral factor] $\rightarrow 1$) and the contrast temperature approaches

$$\Delta T = \frac{Q}{\rho c} \left(\frac{1}{d} - \frac{1}{t_o} \right).$$

7. When the defect size decreases ($R \rightarrow 0$), the lateral heat factor vanishes ([lateral factor] $\rightarrow 0$) and the thermal contrast disappears ($\Delta T \rightarrow 0$).
8. When the defect size increases ($R \rightarrow \infty$), then lateral isolation is approached and the lateral heat effects diminish ([lateral factor] $\rightarrow 1$) and the thermal contrast becomes

$$\Delta T = \frac{Q}{\rho c} \left(\frac{1}{d} - \frac{1}{t_o} \right)$$

9. When the thickness of the panel becomes very large ($t_0 \rightarrow \infty$), the contrast temperature has the limiting value given by $\Delta T = \frac{Q}{\rho c} \frac{1}{d} \left(\frac{R}{2d} \right)^{\frac{1}{2}}$

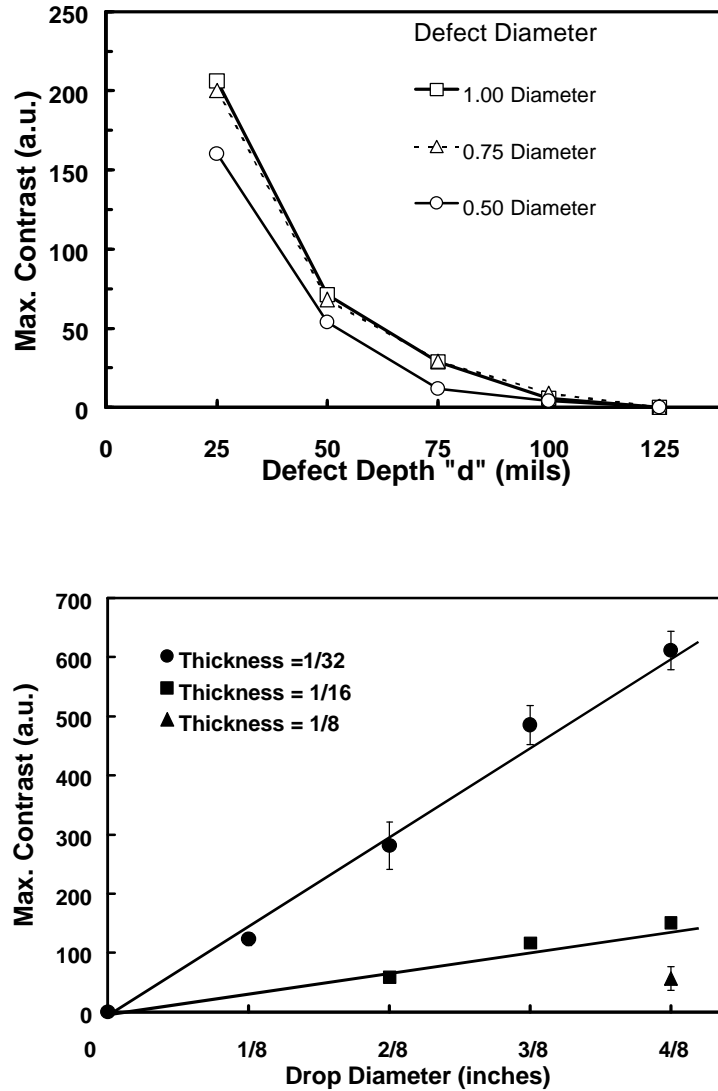


Figure 4. (Top) This graph shows the contrast temperature for all flat bottom holes shown in figure 3a. (Bottom) This graph shows the contrast temperature for all panels with simulated entrapped water shown in Figure 3b.

Similar analysis can be conducted for the problem of water entrapment. From the graph on Figure 4 (Top) it is clear that the thicker the panels are, the smaller the contrast temperature will be. Also, as the diameter of the defect gets smaller the contrast temperature diminishes. The error bars on the graph represent the effect that different amounts of water had on the thermal contrast. It is obvious from the smallness of the error bars that the effect of the amount of entrapped water on the thermal contrast is minimal. A simple model was previously obtained³ that used a simple lateral heat approximation. The main result of the model is that the contrast temperature of a sample with water entrapped can be

approximated by the following equation if a contact conductivity is used instead of the thermal conductivity, then

$$\Delta T_{\text{peak}} = \frac{Q}{\rho c} \frac{d}{r \cdot t_o^2} \cdot \left[\frac{h}{2k} \frac{R}{d} r \right]^{1 + \frac{h}{2k} \frac{R}{d}} \quad (2)$$

Where the parameters are shown in Figure 5 (right) and represent:

h	contact conductivity between aluminum and water
k	contact thermal conductivity of aluminum
r	specific heat-density ratio ($r = \rho c / \rho_w c_w$)
d	the height of the water drop
t_o	is the thickness of the aluminum sample
R	is the radius of the water drop

This equation correctly accounts for most of the observed experimental behavior of pulsed thermography as it relates to water entrapment. The terms before the square bracket provide the principal contribution to the thermal contrast from which the following can be verified:

1. The contrast (ΔT) increases linearly with the amount of energy deposited (Q).
2. The higher the specific heat-density of the substrate ($\rho c \uparrow$) the smaller the peak contrast ($\Delta T \downarrow$).
3. The contrast temperature (ΔT) is a linear function of the radius R for small values of the term in brackets.
4. As the amount of water grows indefinitely ($d \rightarrow \infty$) the contrast temperature saturates ($\Delta T \rightarrow Q / \rho_1 c_1 t_o^2$).

CHARACTERIZATION OF CORROSION

There are various types of corrosion present in metallic structures such as pitting, exfoliation, filiform, galvanic and crevice corrosion. Since the first means of corrosion protection is by painting the exposed surface or by sealing joined parts, corrosion will always start as hidden. Some of the locations where corrosion can be found are under the paint, around fasteners, inside lap joints, behind panels and on second layers. The ability to detect corrosion thermographically will depend on the amount of contrast generated relative to other contrast generating non-uniformities. Figure 7 shows a thermal image of an aluminum lapjoint with three rows of fasteners. The fasteners appear dark because they are much thicker than the structure being interrogated. Around several of the fasteners there are regions that clearly appear brighter than others as indicated in the figure. These regions can be interpreted as probable corrosion regions, but due to the proximity of the fasteners and the fact that sealant was used, it is difficult to determine if any mass has been lost. At the time of this paper the part could not be cut open in order to make a definite assessment of the defect. In order to make an exact determination of the cause for the hot regions a better knowledge of the part and finite element calculations are needed.

DETECTABILITY REGION

There is a “rule of thumb” that is regularly used to determine the ultimate depth to which a defect of a given size can be detected by thermal methods. This rule states that “those planar defects located at a depth smaller or equal to their cross sectional diameter can be detected thermographically”. In light of the simple models presented in this paper, this rule of thumb is not precise. From eq. 1 it can be seen that any planar defect, no matter what its location or cross section, can be detected thermographically provided that enough energy is deposited on the sample surfaces. This is direct consequence of the linear dependence of the thermal contrast on the amount of energy deposited on the surface. There is of course a practical limit of not depositing so much energy so as to damage the material.

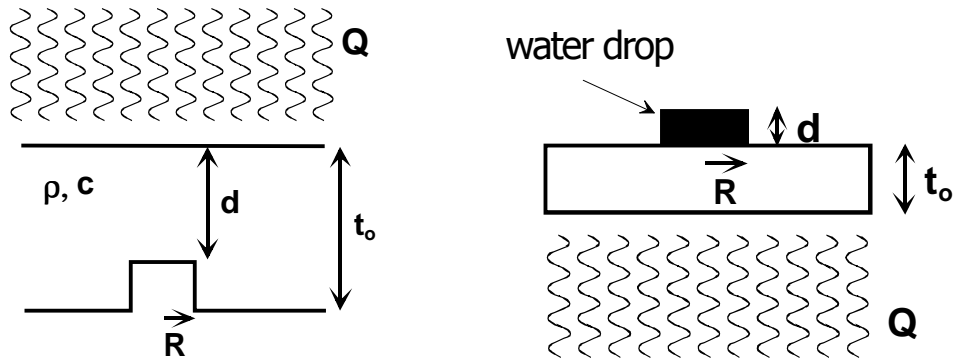


Figure 5. This illustration shows the main parameters used when modeling the thermographic process for mass loss due to corrosion (left) and water entrapment (right)

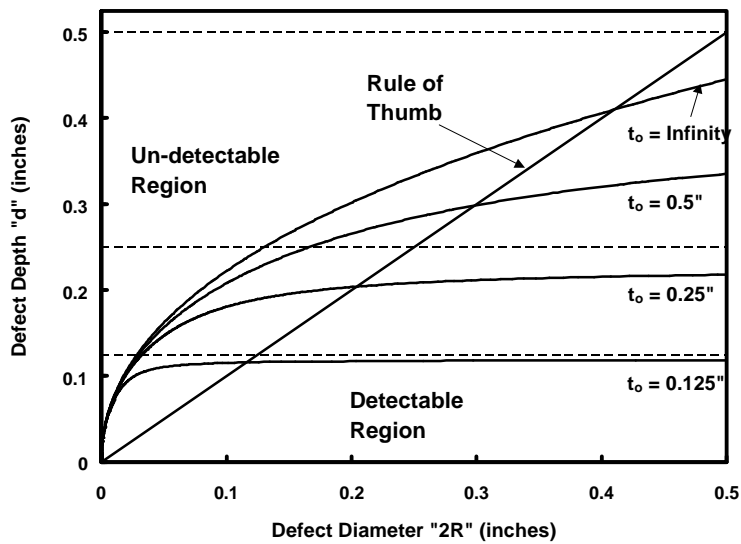


Figure 6. This graph shows curves that separate detectable from undetectable regions of defect of diameter 2R.

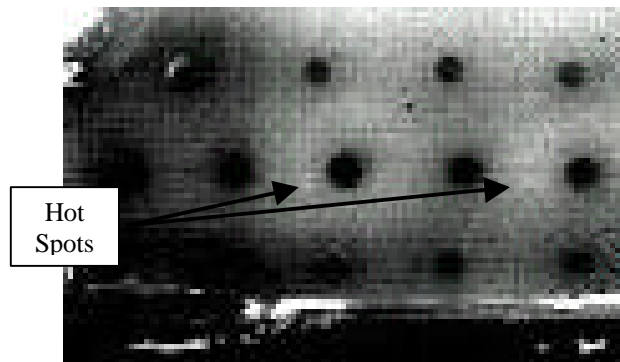


Figure 7. Aluminum lapjoint with three rows of fasteners. There is clear evidence of a hot spots around some fasteners.

More insight can be obtained into this matter by inverting eq. 1 and obtaining a relation between the size of the flaw “2R” and the distance of the flaw from the surface of the sample “d”. The following equation is obtained

$$R = 2 \frac{d(t_o - d)}{t_o} \cdot \text{finv} \left[\frac{\Delta T_{\text{contrast}} \rho c}{Q \cdot \left(\frac{1}{d} - \frac{1}{t_o} \right)} \right] \quad (3)$$

where the function “finv[x]” is the inverse of the transcendental function $y=x^{1/(1-x)}$. This equation can be used to divide the R-d space into “detectable” and “non-detectable” regions. That is, a defect whose radius “R” and location “d” are such that it falls inside the curve defined by equation 3 will be detectable thermographically. If the defect radius and position are such that they fall outside the curve, then for those experimental parameters the defect will be missed. Figure 6 shows boundary curves for various aluminum thickness. Also on that graph is the “rule of thumb” line. Clearly there is a strong discrepancy between the rule of thumb and the previous results.

SUMMARY

We have demonstrated that thermography can detect mass loss and water entrapment. We have presented predictive formulas that can assist the practitioner in determining what type of contrast levels will be obtained for a particular experimental arrangement. We have determined what the depth of resolution is for the detection of mass loss in aluminum 7075T6. When interrogating real structural components, these simple models can only provide approximate answers. For precise determination of the exact nature and extent of the defect a detailed knowledge of the part is required together with more detailed analysis such as finite element models.

ACKNOWLEDGMENT

This work was supported in part by Mr. Charles Pellerin of the Strategic Environmental Research and Development Program (SERDP) office under project number PP-1134 and by Mr. Jim Kelly of the Office of Naval Research by Work Request under document number N0001498WX20360.

REFERENCES

1. I. Perez, R. Santos, P. Kulowitch, M. Ryan, “Calorimetric modeling of thermographic data,” Proc. of the 1998 SPIE Thermosense XX Conference”, Orlando, April 6 - 9, 1998
2. I. Perez, P. Kulowitch, “Modeling of Pulsed Thermography in Anisotropic Media,” 25th annual Progress in QNDE, Snowbird, Utah., July 19 - 24, 1998
3. I. Perez, W. R. Davis, P. Kulowitch, “Thermographic modeling of water entrapment,” Proc. of the 1999 SPIE, Thermosense XXI Conference, eds. D.H. LeMieux & J.R. Snell, Jr. April 1999, p32-39

Subsurface Sensing Technologies and Applications Vol. 2, No. 4, October 2001 (©2001)

Microwave Nondestructive Detection of Corrosion Under Thin Paint and Primer in Aluminum Panels

D. Hughes,* N. Wang, T. Case,* K. Donnell, and R. Zoughi*¹

Applied Microwave Nondestructive Testing Laboratory (*amntl*), Electrical and Computer Engineering Department, Colorado State University, Fort Collins, CO 80523-1373

R. Austin

Texas Research Institute Austin, Inc., Austin, TX 78733-6201

M. Novack

Naval Surface Warfare Center, Carderock Division, Code 615, West Bethesda, MD 20817-5700

Received

Detection of corrosion, under paint and primer, in various metallic structural components, particularly when used in moist and salty environments is an important practical concern. Moreover, nondestructive testing techniques that do not require paint removal are desired. Near-field microwave nondestructive inspection techniques, employing open-ended rectangular waveguide probes, have shown tremendous potential for detecting and evaluating the presence of corrosion under paint in steel substrates. The objective of this investigation has been to investigate the potential of these techniques for detecting corrosion under paint and primer in aluminum substrates. To accomplish this goal, an electromagnetic formulation, simulating detection of corrosion in layered structure using open-ended rectangular waveguide probes, was used to gain an insight into the functionality of measurement parameters such as the frequency of operation and standoff distance. In conjunction with this simulation, the dielectric properties of paint, primer, real and chemically produced aluminum oxide were measured in a wide range of microwave frequencies (2.6–18 GHz). The results showed that the dielectric properties of paint, primer and aluminum oxide are very similar to each other. Subsequently, the theoretical simulation was conducted in a wide frequency band (8.2–40 GHz). The overall result of the

*Currently at the Applied Microwave Nondestructive Testing Laboratory (*amntl*), Electrical and Computer Engineering Department, University of Missouri-Rolla, Rolla, MO 65409.

¹To whom all correspondence should be addressed; e-mail: zoughi@ece.umar.edu

simulation effort was that higher frequencies and standoff distances of a few mm are more optimal for detecting thin corrosion layers under paint. Two specially prepared aluminum panels with induced areas of corrosion and surface pitting were produced as well. Using these panels and several phase sensitive measurement systems, experiments were conducted producing 2-D images of various areas of these panels. Images were produced at different standoff distances and at frequencies of 9, 11.725, 24.1, and 33.5 GHz. The overall results of the experimental investigation were extremely promising when detecting the thin regions of corrosion in these panels. This paper presents the approach and results of this investigation.

Key Words. Corrosion, aluminum, microwave techniques, nondestructive testing, paint, primer.

1. Introduction

Corrosion inducement in various metallic structural components, used in moist and salty environments, can significantly degrade their functionality. Detection of corrosion under paint and primer can be a challenging task, unless the corrosion has advanced to a level where the paint begins to blister and pitting in the metal substrate occurs [1–3]. Consequently, detection of corrosion under paint and other dielectric coatings is an important practical concern. Moreover, it is desirable to detect and evaluate the thickness and spatial extent of a corrosion layer without having to remove the paint. This is particularly important when lead-based paint is used, whose removal and disposal may have environmental consequences and when remediation measures and decisions are to be made. Therefore, a nondestructive detection and evaluation technique capable of operating in a non-contact fashion, quick, real-time, on-site and with local and large area inspection capabilities is desired.

Microwave nondestructive inspection techniques, when applied to layered composite structures (including conductor backed composites), have shown tremendous potential for evaluating the properties of the layered structure as well as determining critical information about its internal geometrical structure such as layer thickness and presence of disbonds and delamination [4–8]. Most of these investigations were conducted using open-ended rectangular waveguide probes. Paint, primer and corrosion products are all in the family of dielectric (insulating) materials. Therefore, these methods are also suitable for detecting and evaluating properties (i.e. presence and thickness) of corrosion layers under thin layers of paint and primer.

In the past few years several attempts have been made to detect corrosion under paint in steel [9–10]. Both of these investigations included a theoretical as well as an experimental phase. To perform the theoretical investigation, the dielectric properties of paint, rust (corrosion products) must be known as well as their respective thickness [4]. In the first investigation, the dielectric properties of chemically produced iron oxide were measured and used in conjunction with the model [9]. The results showed that the dielectric properties of chemically produced iron oxide and paint are very similar to each other. However, the experimental investigation conducted using a steel plate with real rust, showed higher sensitivity to the presence of corrosion compared to the theoretical results. Subsequently, in the second investigation, various types of real corrosion products (iron oxide) were obtained and their dielectric properties were measured [10]. The results showed that real iron oxide is a material with diverse dielectric

characteristics. More importantly, it was shown that the dielectric properties of real iron oxide and paint can be significantly different. In other words, there is more contrast between the dielectric properties of real rust and paint than chemically produced iron oxide and paint. This explains the reason for the experimental results, in the first investigation, having been more sensitive than the modeling results.

The relative to free-space dielectric properties (or constant) of a material is generally a complex parameter ($\hat{\epsilon}_r = \hat{\epsilon}'_r - j \hat{\epsilon}''_r$) whose real part (relative permittivity) indicates the ability of the material to store microwave energy (i.e., material's tendency to be polarized), while its imaginary part (relative loss factor) indicates the ability of the material to absorb microwave energy. In the second investigation, the dielectric properties of paint and primer were measured to be $\hat{\epsilon}_r = 3.48 - 0.12j$, whereas the dielectric properties of various real rust varied in relative permittivity between 5.33 to 12.58 and between 0.53 to 2.36 in relative loss factor. The dielectric properties of chemically produced iron oxide were measured to be $\hat{\epsilon}_r = 3.22 - 0.01j$ [10]. These results clearly show the increased contrast between the dielectric properties of paint and real rust when compared with chemically produced iron oxide powder. The success achieved through these investigations has prompted a look into using these near-field microwave nondestructive inspection techniques for detecting corrosion under paint and primer in aluminum panels.

2. Overall Approach

From an electromagnetic point of view, both steel and aluminum are considered excellent conductors. Therefore, any tangential electric field reaching the surface of either of these metals undergoes a complete reflection. However, the dielectric properties of aluminum oxide (Al_2O_3) may be markedly different than iron oxide (Fe_2O_3) and those of paint and primer. Therefore, the following tasks were conducted to examine the utility of near-field microwave nondestructive testing techniques, using open-ended rectangular waveguide probes, for detecting and evaluating corrosion under thin layers of paint and primer in aluminum panels:

- obtained specimens of paint, primer, real and chemically produced aluminum oxide (in powder form),
- measured their dielectric properties in a wide range of microwave frequencies, performed near-field theoretical simulations, using open-ended rectangular waveguide probes, as a function of frequency and standoff distance to gain an insight into the potential of this technique,
- prepared special aluminum panels with specific regions of induced corrosion,
- these panels were then painted and laboratory-designed microwave inspection systems were used to detect the corrosion regions in a wide range of microwave frequency and standoff distances.

The following sections present the highlights of the results for each task, along with a discussion of the results.

3. Results

3.1. Dielectric Property Measurements

The dielectric properties of the paint, primer, chemically produced and real Al_2O_3 specimens were measured using a two-port completely-filled transmission line (waveguide) technique conducive for measuring the dielectric properties of solids, liquids and powders [11]. In this approach a rectangular waveguide sample holder is filled with the dielectric material whose properties are to be determined. In the case of powders and liquids, two Plexiglas plugs are used to hold the sample in place. An incident signal is then impinged upon the specimen, a portion of which is reflected back and a portion of which transmits through the specimen [11]. The phase and magnitude of the reflected and transmitted signals once compared to those of the incident signal are used to calculate the dielectric properties of the specimen. The sample holder cross-section dimension is clearly a function of the frequency band used. Thus, at lower microwave frequencies this cross-section is larger, and more of a specimen is needed to fill the entire waveguide sample holder cross-section. Paint and primer specimens were produced in sheet form, and their dielectric properties were measured in *S*-band (2.6–3.95 GHz), *G*-band (3.95–5.85 GHz), *J*-band (5.85–8.2 GHz), *X*-band (8.2–12.4 GHz) and *Ku*-band (12.4–18 GHz), using the technique mentioned above. Table 1 presents the average value of the measured relative dielectric properties of paint and primer at all frequency bands. In addition, depending on how well a particular sample fits inside the waveguide sample holder the measured dielectric constant values may be slightly different than their actual values. Considering these factors and the fact that the corresponding measurement accuracy for the real and imaginary parts is about 5% and 10% respectively, the slight increase in the real part as a function of frequency is considered acceptable. The results also indicate that both paint and primer have very similar dielectric properties, and both are considered to be low permittivity and low loss dielectric materials. Moreover, and as is commonly expected, such dielectric materials possess a relatively constant permittivity and loss factor as a function of frequency. This fact is also indicated by the results shown in Table 1. Therefore, for the purpose of the theoretical investigation, the average permittivity and loss factor calculated throughout this wide frequency band (e.g. 2.6–18 GHz) was used.

Table 1. The Measured Average Dielectric Properties of Paint and Primer as a Function of Frequency.

Frequency (GHz)		Average value					
		Paint			Primer		
		Dielectric constant	Standard deviation		Dielectric constant	Standard deviation	
Real	Imag.		Real	Imag.			
<i>S</i> -Band	2.6–3.95	$3.121 - 0.116j$	± 0.052	± 0.032	$3.360 - 0.137j$	± 0.064	± 0.031
<i>G</i> -Band	3.95–5.85	$3.872 - 0.110j$	± 0.020	± 0.013	$3.425 - 0.105j$	± 0.009	± 0.006
<i>J</i> -Band	5.85–8.2	$3.932 - 0.080j$	± 0.032	± 0.009	$4.032 - 0.091j$	± 0.028	± 0.014
<i>X</i> -Band	8.2–12.4	$3.372 - 0.107j$	± 0.016	± 0.007	$3.847 - 0.143j$	± 0.012	± 0.005
<i>Ku</i> -Band	12.4–18.0	$3.633 - 0.111j$	± 0.029	± 0.007	$3.770 - 0.141j$	± 0.017	± 0.008

Real Al_2O_3 specimens were obtained from aluminum plates that had been corroded using salt spray. Subsequently, the surface of the plates were gently sponged to remove dirt and salt without scrubbing the corrosion product as much as possible. The remainder was then scraped from the plate using a razor blade. Table 2 shows the measured average relative permittivity and loss factor for the real Al_2O_3 specimen. As explained earlier, the measurements were not conducted at *S*-band due to the lack of sufficient amount of Al_2O_3 powder. The results also show that real Al_2O_3 is a low permittivity and low loss dielectric material. The permittivity of this material is very similar to that of paint and primer. However, the loss factor of real Al_2O_3 is just under two times larger than those of paint and primer. Nevertheless, the dielectric properties of real Al_2O_3 , paint and primer are considered to be quite similar. This is an important fact since the more dissimilar these dielectric properties are the better a layer of corrosion can be detected, particularly when considering that the thickness of each layer is very small as well.

Table 3 shows the measured average dielectric properties of the chemically produced Al_2O_3 as a function of frequency. The results indicate that compared to the real Al_2O_3 , this sample has a slightly lower permittivity and considerably lower loss factor. This fact was also found to be true for chemically produced iron oxide compared to real iron oxide [10].

There is an important ramification associated with these results. As discussed earlier, the dielectric properties of paint, primer and Al_2O_3 are very similar to each other. Considering the fact that these layers are also very thin, the distinction between when corrosion is present and when it is absent, in aluminum panels, is expected to be more difficult than the same case for steel panels.

Table 2. The Measured Average Dielectric Properties of Real Al_2O_3 as a Function of Frequency

Frequency (GHz)		Average value for real Al_2O_3		
		Dielectric constant	Standard deviation	
			Real	Imag.
<i>S</i> -Band	2.6–3.95	N/A	N/A	N/A
<i>G</i> -Band	3.95–5.85	4.036 – 0.430 <i>j</i>	±0.023	±0.015
<i>J</i> -Band	5.85–8.2	3.337 – 0.285 <i>j</i>	±0.033	±0.013
<i>X</i> -Band	8.2–12.4	3.495 – 0.357 <i>j</i>	±0.023	±0.011
<i>Ku</i> -Band	12.4–18.0	3.838 – 0.373 <i>j</i>	±0.029	±0.007

Table 3. The Measured Average Dielectric Properties of Chemically Produced Al_2O_3 as a Function of Frequency

Frequency (GHz)		Average value for real chemically produced (Al_2O_3)		
		Dielectric constant	Standard deviation	
			Real	Imag.
<i>S</i> -Band	2.6–3.95	2.243 – 0.032 <i>j</i>	N/A	N/A
<i>G</i> -Band	3.95–5.85	2.489 – 0.078 <i>j</i>	N/A	N/A
<i>J</i> -Band	5.85–8.2	2.306 – 0.124 <i>j</i>	N/A	N/A
<i>X</i> -Band	8.2–12.4	2.316 – <i>j</i> 0.049	±0.006	±0.004
<i>Ku</i> -Band	12.4–18.0	2.290 – 0.024 <i>j</i>	N/A	N/A

3.2. Theoretical Investigation

The theoretical aspect of this investigation involved simulating a painted aluminum panel, with and without corrosion, as a function of frequency and standoff distance, when using open-ended rectangular probes, as shown in Figure 1. The electromagnetic formulation for a multilayered structure such as that shown in Figure 1 has already been developed at the Applied Microwave Nondestructive Testing Laboratory (*amntl*) [4]. The results of this simulation are intended to give an insight into the influence of measurement parameters; namely, the frequency of operation and the standoff distance on corrosion detection. The theoretical analysis was used to investigate the difference in the phase of reflection coefficient, at the waveguide aperture as a function of frequency and standoff distance for the multi-layered composite structure shown in Figure 1. The simulations were performed with and without the presence of a thin layer of corrosion, and the two phases were compared to determine

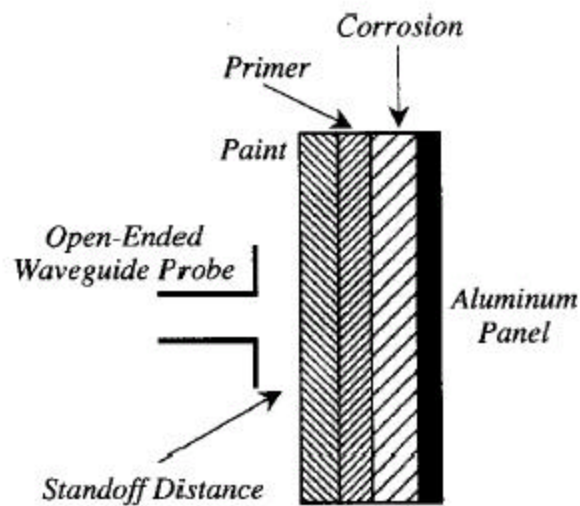


Figure 1. Schematic of an open-ended rectangular waveguide probe radiating into a typical aluminum panel with paint, primer, and rust.

potential for detecting the presence of corrosion. Since the layers are all thin and made of low permittivity and low loss materials the magnitude of reflection coefficient is not a sensitive parameter and was not used in this investigation. The simulations were performed across the entire X-band (8.2–12.4 GHz), Ku-band (12.4– 18 GHz), K-band (18–26.5 GHz), and Ka-band (26.5–40 GHz), as well as for standoff distances ranging from 0mm (i.e. in-contact) to 5 mm. The thickness of each layer was taken to be 0.089mm for paint, 0.064mm for primer, and 0.127mm for Al₂O₃. These thicknesses correspond to the values obtained for the experimental panels made for this investigation.

3.2.1. X-Band (8.2–12.4 GHz) Results

Figure 2 shows the phase as a function of frequency for a standoff distance of 0mm (i.e., in-contact) at X-band. Figure 3 shows the difference in these two phases as a function of frequency. The results show that there is a small difference between the phase with and without the presence of corrosion. It can be seen that the difference in phase increases as frequency increases. Similar results were obtained as a function of increasing standoff distance. Generally, in the range of 0-5 mm, the calculated phase difference showed to increase as a function of increasing standoff distance [12].

Standoff analysis was performed at the frequencies of 9 GHz and 11.725 GHz. These two frequencies were chosen to represent a high and a low frequency in the band, and were later used in the experimental analysis. At 9 GHz, the standoff distance of ~4mm was found to be optimal, while for 11.725 GHz the optimal standoff distance was found to be ~5mm [12]. It should be noted that the optimal standoff distances were

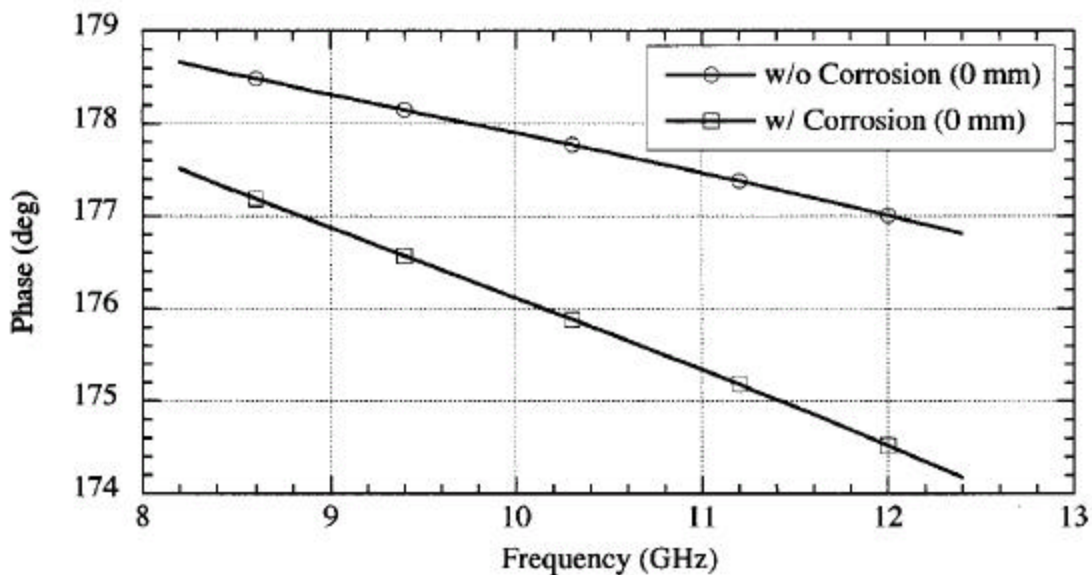


Figure 2. Phase as a function of frequency at a standoff distance of 0mm (i.e., in-contact) at X-band.

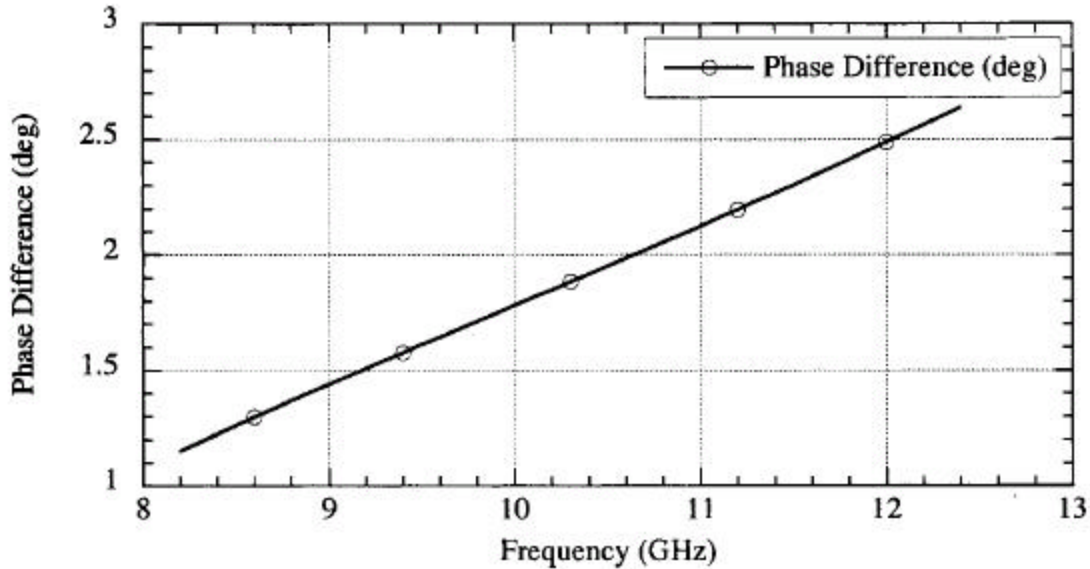


Figure 3. Phase difference as a function of frequency at a standoff distance of 0mm (i.e., in-contact) at X-band.

found when the phase was measured at the aperture of the waveguide. Since the actual probes used in the experimental analysis were uncalibrated, the phase will not be measured at the aperture of the waveguide. Consequently, these results do not correspond one-to-one to the experimental measurements. Rather, they provide an insight into the influences of changing standoff distance and frequency. Overall, the results for this band showed that, while it is possible to determine the presence of thin corrosion under paint and primer, there does not exist a high level of sensitivity to the presence of corrosion.

3.2.2. *Ku*-Band (12.4–18 GHz) Results

Figure 4 shows the difference in phase as a function of frequency at *Ku*-band and at a standoff distance of 4 mm. As with *X*-band, the phase difference increases as the frequency increases. Also, the difference is consistently higher in this band when compared with *X*-band. This increase in phase difference implies that at *Ku*-band one expects to have higher detection sensitivity to the presence of corrosion than at *X*-band. Nevertheless, this band produced only a modest increase in phase difference when compared with *X*-band. Waveguide probes at *Ku*-band also have the added advantage of having smaller aperture dimensions, resulting in higher spatial resolution when scanning for corrosion.

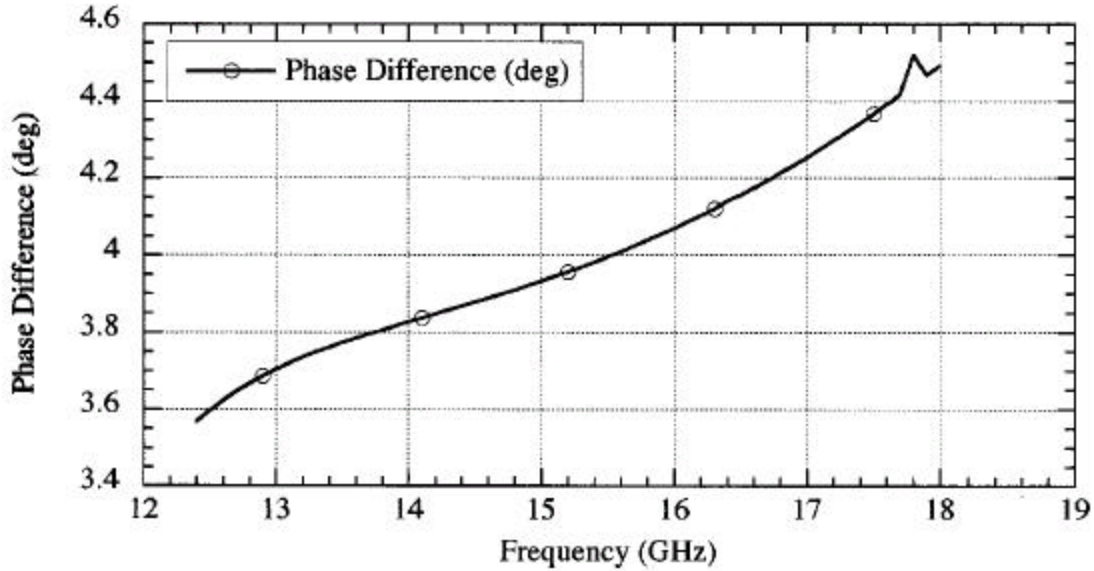


Figure 4. Phase difference as a function of frequency at a standoff distance of 4mm at *Ku*-band.

3.2.3. K-Band (18–26.5 GHz) Results

Figure 5 shows the phase difference as a function of frequency at *K*-band and at a standoff distance of 5 mm. As before, the difference in phase increases as a function of increasing frequency. Moreover, this increase in phase difference is higher than those obtained at the previous two bands. The maximum phase difference is greater than 8° , which is a large enough difference for corrosion detection purposes. To show the influence of standoff distance, standoff analysis was performed at a fixed frequency of 24 GHz, and the results are shown in Figure 6. In this case, the optimal standoff distance occurs at ~ 1.5 mm. This frequency was chosen since microwave components are relatively readily available at or near this frequency.

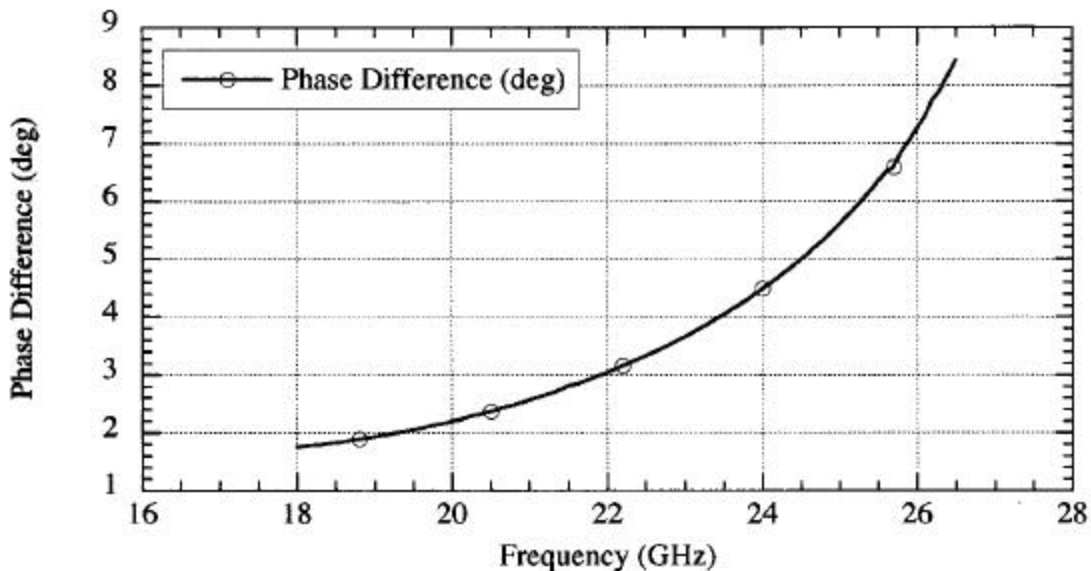


Figure 5. Phase difference as a function of frequency at a standoff distance of 5mm at *K*-band.

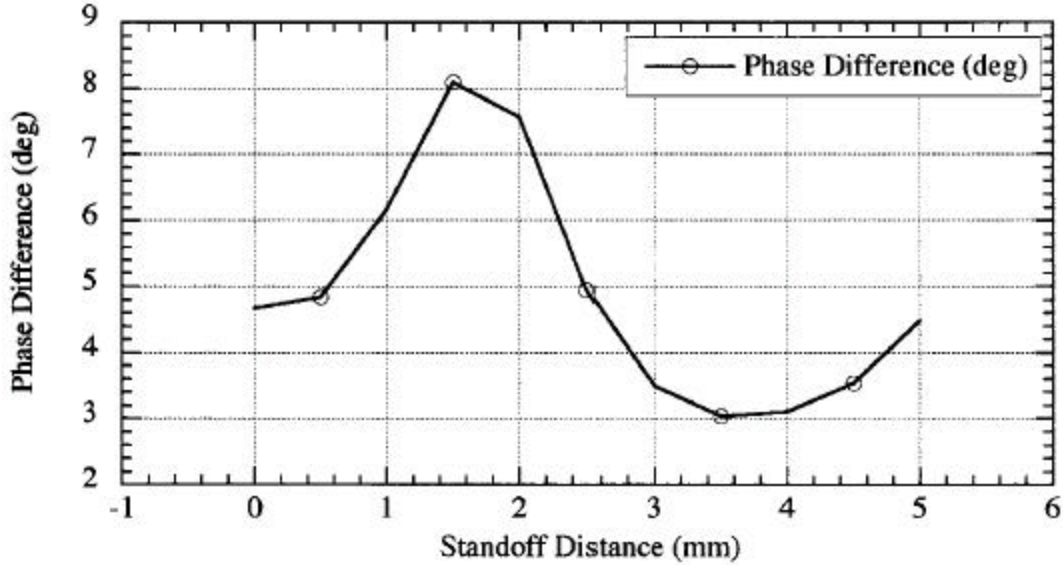


Figure 6. Phase difference as a function of standoff distance at a frequency of 24 GHz.

3.2.4. Ka-Band (26.5–40 GHz) Results

The highest frequency band explored in the theoretical investigation was *Ka*-band. Figure 7 shows the phase difference as a function of frequency at a standoff distance of 3 mm. As can be seen, the maximum phase difference is greater than 11° in the higher frequency portions of this band. This implies that *Ka*-band is the most optimal of the frequency bands explored. Standoff analysis was also performed at a frequency of 33.5 GHz. Figure 8 shows the phase difference as a function of standoff distance at this frequency. It can be seen that, regardless of standoff distance, the difference in phase is at least $\sim 6^\circ$, and that several standoff distances produce differences of over 11° . This implies that at this frequency some level of standoff distance variation may be tolerated without much loss in detection sensitivity.

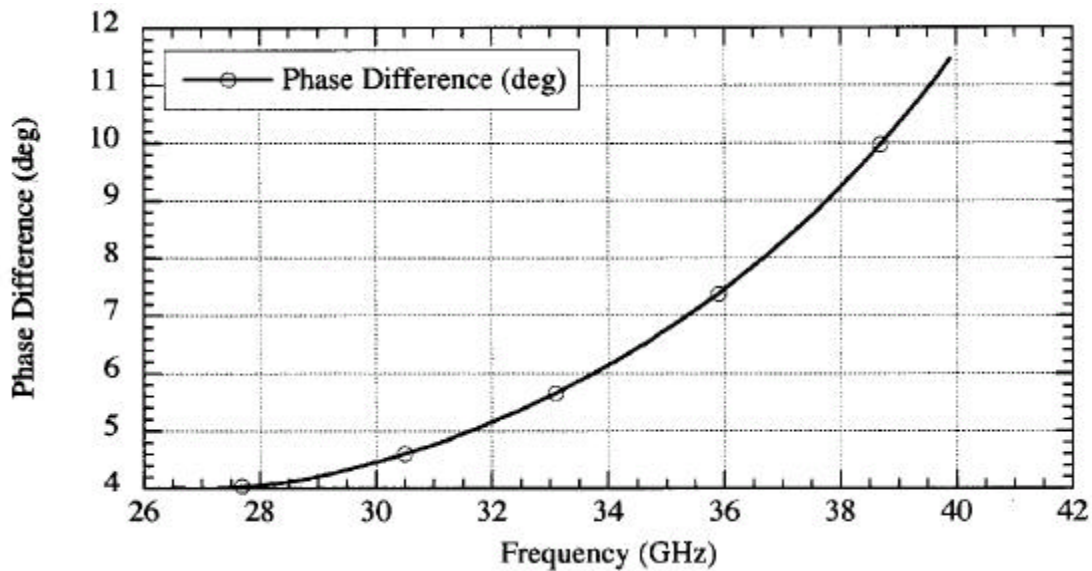


Figure 7. Phase difference as a function of frequency at a standoff distance of 3mm at *Ka*-band.

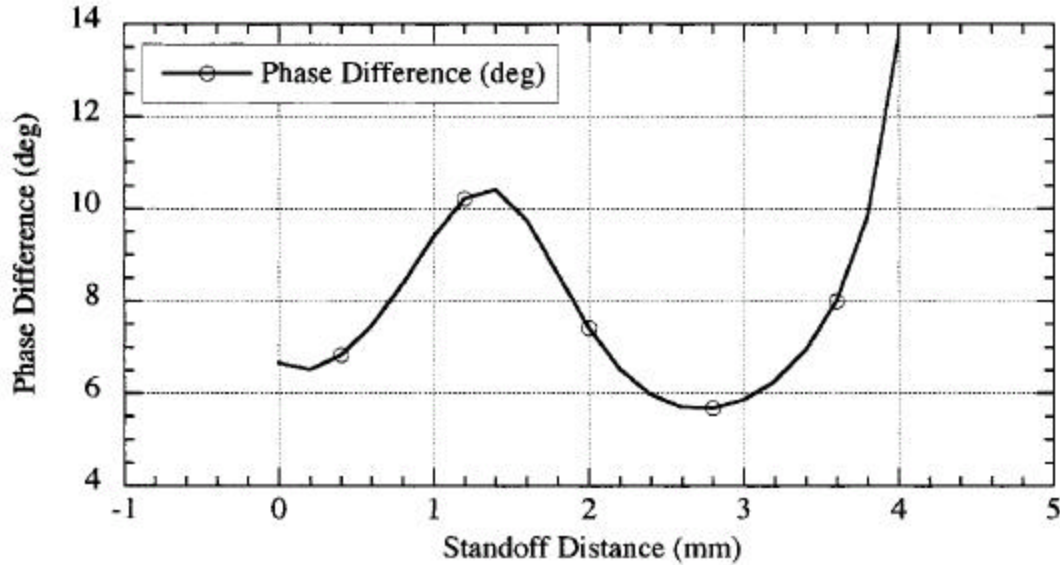


Figure 8. Phase difference as a function of standoff distance at a frequency of 33.5 GHz.

The results of the theoretical formulation showed that the phase difference increased as a function of increasing frequency. The utility of this formulation for optimizing the standoff distance was also effectively demonstrated. This parameter plays a much larger role in lower frequencies, where phase differences of only a few degrees occur even at the higher frequencies in these bands. At higher frequencies, the minimum calculated phase difference was larger, regardless of standoff distance. Because of this, choosing a specific standoff distance is less consequential, although using the optimal standoff distance provides a larger dynamic range in phase difference, allowing for better detection.

3.3. Experimental Investigation

For the experimental analysis, two-dimensional scans were performed using open-ended rectangular waveguide probes similar to those simulated in the theoretical analysis. The scans were performed on two aluminum panels (labeled “B” and “C”) that contained sections of corrosion, as seen in Figure 9. The corrosion was created by partially submerging the plates in a salt bath in order to encourage corroding. The panels were then immersed in fresh water to remove excess salt that had deposited on the sections of the panels that were near the surface of the bath. Masks were then placed vertically down the panels, and the panels were then sand blasted to remove corrosion from the unmasked regions. The darker vertical strips down the middle in Figure 9, show the remaining corrosion. Pitting occurred due to the buildup of salt on the panels. This can be seen as the dark patches across the middle of the panels. Scans were performed in three areas of the panels. The top portion of the panels contained no pitting, and were scanned in order to test for corrosion alone. The middle portions were scanned to determine if corrosion could be found in the presence of pitting. The top-middle portion was also scanned to show the difference, if any, in detection of corrosion both with and without the presence of pitting. Laboratory designed phase detectors, generating a

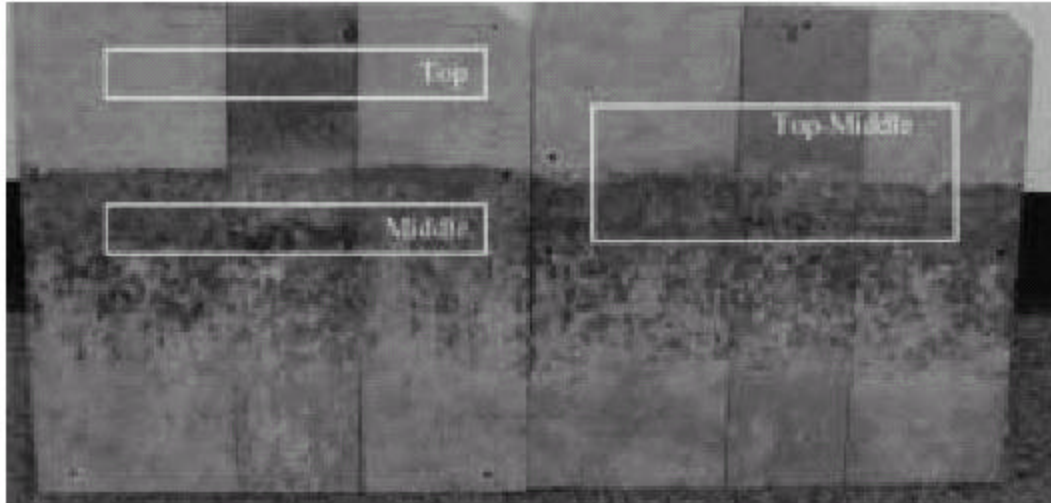


Figure 9. Sample plates showing corrosion before being painted, with areas scanned highlighted.

voltage proportional to the phase of reflection coefficient, were used to generate the experimentally obtained images.

Figure 10 shows an area scan of the top of panel B. This scan was performed at a frequency of 9 GHz, and at a standoff distance of ~0mm (i.e., in-contact). The scans were conducted by placing the waveguide probe over the panel which was placed on a computer controlled scanning table. In this way a raster scan of the panel was obtained. Normalizing the output voltage of the phase detectors and assigning various gray scales to these normalized voltages produced the images shown in this section. The white region represents corrosion, while the black region represents the sand blasted areas. The gray areas in between these two regions are due to the integrating effects of the waveguide aperture as it scans over different portions of these two areas simultaneously. The dimensions in these images is in millimeters which correspond well with the size of a particular corrosion region. It should also be noted that white does not always represent corrosion. Rather, the change in gray scale is more important than the actual color.

Figure 11 shows the top-middle region of panel B, scanned at a frequency of 24.1 GHz and at a standoff distance of ~0mm (i.e., in-contact). Here, the black regions represent the sand blasted areas, while the light gray regions represent corrosion. Pitting can be seen as white spots on the bottom portion of the image. This is encouraging since corrosion can still be distinguished despite the presence of pitting. Figure 12 shows the top region of panel C, scanned at a frequency of 24.1 GHz and at a standoff distance 5 mm. Again, the black regions indicate sand blasted areas, while the white represents corrosion. These are very similar results to those obtained by scanning plate B, indicating the robustness of this microwave technique. Compared to the results at 9 GHz shown in Figure 10 this image produced a higher spatial resolution (i.e., the white area corresponding to the corrosion region is better identified and its dimensions match the actual corrosion region closer).

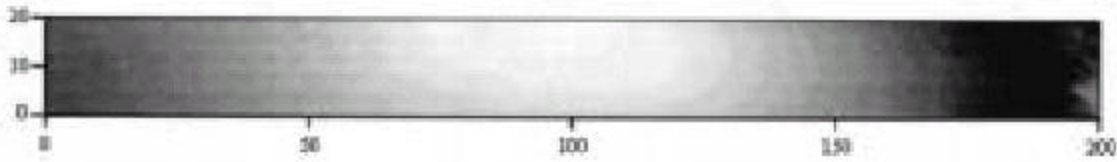


Figure 10. Area scan of top strip of panel B, scanned at a frequency of 9 GHz and at a standoff distance of ~0mm (i.e., in-contact).

Figure 11 shows the top-middle region of panel B, scanned at a frequency of 24.1 GHz and at a standoff distance of ~0mm (i.e., in-contact). Here, the black regions represent the sand blasted areas, while the light gray regions represent corrosion. Pitting can be seen as white spots on the bottom portion of the image. This is encouraging since corrosion can still be distinguished despite the presence of pitting. Figure 12 shows the top region of panel C, scanned at a frequency of 24.1 GHz and at a standoff distance 5 mm. Again, the black regions indicate sand blasted areas, while the white represents corrosion. These are very similar results to those obtained by scanning plate B, indicating the robustness of this microwave technique. Compared to the results at 9 GHz shown in Figure 10 this image produced a higher spatial resolution (i.e., the white area corresponding to the corrosion region is better identified and its dimensions match the actual corrosion region closer).

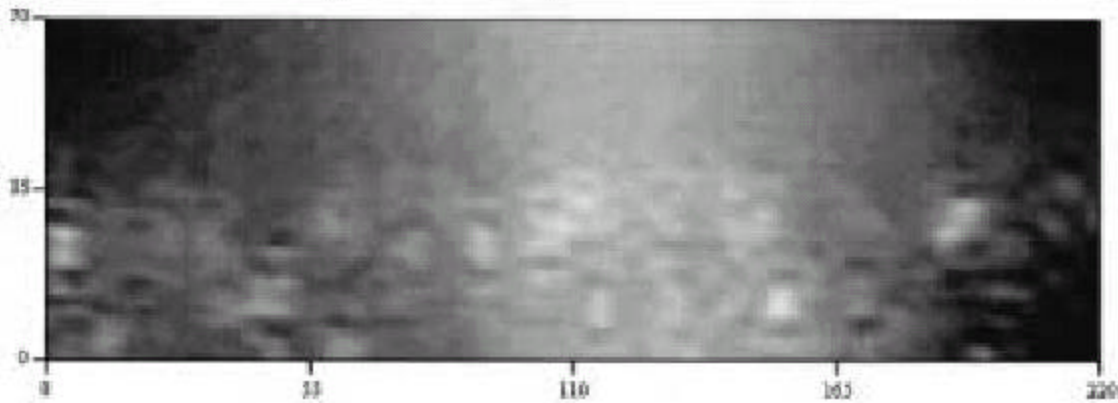


Figure 11. Area scan of top-middle strip of panel B, scanned at a frequency of 24.1 GHz and at a standoff distance of ~0mm (i.e., in-contact).



Figure 12. Area scan of top strip of panel C, scanned at a frequency of 24.1 GHz and at a standoff distance of 5 mm.



Figure 13. Surface plot of the top-middle strip of panel B, scanned at a frequency of 33.5 GHz and a standoff distance of 4.3 mm.

Figure 13 shows a surface plot of a scan of the top-middle region of panel B. This scan was made at a frequency of 33.5 GHz, and at a standoff distance of ~4.3 mm. The black areas indicate non-corroded (i.e., sand blasted) portions of the panel, while light gray represents corrosion, and whitish gray represents pitting. Individual pits can also be clearly seen, although the effect of these is not enough to obscure corrosion. The higher resolution in this image when compared to previous images, particularly with the pitting, is due to the smaller aperture of the waveguide at *Ka*-band (0.711 cm by 0.356 cm). Of the bands investigated, *Ka*-band produced the best results, having both the largest dynamic range for detection as well as the highest spatial resolution.

4. Summary and Conclusions

Overall, the results of this investigation showed the potential of near-field microwave NDT techniques, using open-ended rectangular waveguide probes, for detecting thin corrosion patches under paint and primer in two aluminum panels. This potential was shown both theoretically and experimentally using laboratory designed measurement systems.

The dielectric properties of paint, primer, real aluminum oxide, and chemically produced aluminum oxide were measured at a relatively wide range of microwave frequencies (2.6–18 GHz). The results indicated that all of these materials are low permittivity and low loss. More importantly the results showed that the dielectric properties of paint, primer, and aluminum oxide are very similar to each other. This is important since the detection of thin corrosion under thin paint is easier when their dielectric properties are more distinct from one another. This had previously been shown to be the case for steel corrosion products [10].

The electromagnetic formulation for interrogating multi-layered structures was used to examine the influence of measurement parameters such as the operating microwave frequency and standoff distance on corrosion detection, using open-ended rectangular waveguide probes. This theoretical investigation was conducted in a wide frequency band (8.2–40 GHz). The overall conclusions of this investigation was that higher frequencies and standoff distances of a few millimeters are more optimal for detecting thin corrosion layers under paint when the phase of reflection coefficient is

employed. Due to the low loss nature of these layers, the magnitude of reflection coefficient was not of much use. The results also showed that the phase difference as a function of frequency in a given band, between when there is corrosion and when there is not, remained fairly constant (within a few degrees). This is important from a practical point of view since it points to the fact that frequency selectivity within a given band is not crucial and commercially available components as opposed to custom ordered components can be utilized. It was also shown that given a frequency of operation, one is still able to optimize for the standoff distance using this code. However, the standoff distance selectivity was not that great (i.e., phase difference remained within a few degrees), unlike for the case of corrosion in steel.

Experimentally, three frequency bands (X , K , and Ka) were chosen. Several phase sensitive measurement systems were arranged and used to produce 2-D images of various areas of two specially prepared panels. Images were produced at different standoff distances and at frequencies of 9, 11.725, 24.1, and 33.5 GHz. The pitting in the panels ended to mask the presence of corrosion over pitted regions. This is due to the fact that the reflection (or scattering) from the pits is larger than a layer of corrosion. However, the corrosion regions devoid of pits were all detected. In some cases the corrosion in the pitted regions were also detected when a relatively large scan of the area of a panel was produced. Higher frequencies produced higher spatial resolution results. Their respective (corrosion) detected areas in these images also closely estimated the dimensions of the corrosion patches.

The overall results of this investigation indicates the robust capability of near-field microwave nondestructive testing and evaluation techniques, using open-ended rectangular waveguide probes.

Acknowledgment

This work was supported in part by Dr. Charles Pellerin, Strategic Environmental Research and Development Program (SERDP) Office, Project No. PP-1134.

References

1. Baboian, R. (ed.), 1995, Corrosion tests and standards: application and interpretation'', American Society for Testing and Materials, Philadelphia, PA.
2. Funke, W., 1981, Blistering of paint films, *in* Corrosion Control by Organic Coatings, H. Leidheiser, Jr. (ed.), National Association of Corrosion Engineers, Houston, TX, p. 97–102.
3. Collins, J.A., 1993, Failure of Materials in Mechanical Design, 2nd edn, Wiley Interscience, New York, NY.
4. Bakhtiari, S., Ganchev, S., Qaddoumi, N., and Zoughi, R., 1994, Microwave non-contact examination of disbond and thickness variation in stratified composite media: IEEE Transactions on Microwave Theory and Techniques, v. 42, no. 3, p. 389–395.
5. Bakhtiari, S., Ganchev, S., and Zoughi, R., 1993, Microwave frequency optimization for accurate thickness or dielectric property monitoring of conductor backed composites: Materials Evaluation, v. 51, no. 6, p. 740–743.
6. Ganchev, S., Qaddoumi, N., Ranu, E., and Zoughi, R., 1995, Microwave detection optimization of disbond in layered dielectrics with varying thicknesses: IEEE Transactions on Instrumentation and Measurement, v. IM-44, no. 2, p. 326–328.
7. Qaddoumi, N., Zoughi, R., and Carriveau, G.W., 1996, Microwave detection and depth determination of disbonds in low-permittivity and low-loss thick sandwich composites: Research in Nondestructive Evaluation, v. 8, no. 1, p. 51–63.
8. Gray, S. and Zoughi, R., 1997, Dielectric sheet thickness variation and disbond detection in multilayered composites using an extremely sensitive microwave approach: Materials Evaluation, v. 55, no. 1, p. 42–48.
9. Qaddoumi, N., Shroyer, A., and Zoughi, R., 1997, Microwave detection of rust under paint and composite laminates: Research in Nondestructive Evaluation, v. 9, no. 4, p. 201–212.
10. Qaddoumi, N., Handjojo, L., Bigelow, T., Easter, J., Bray A., and Zoughi, R., 2000, Microwave corrosion detection using open-ended rectangular waveguide sensors: Materials Evaluation, v. 58, no. 2, p. 178–184.
11. Bois, K., Handjojo, L., Benally, A., Mubarak, K., and Zoughi, R., 1999, Dielectric plugloaded two-port transmission line measurement technique for dielectric property characterization of granular and liquid materials: IEEE Transactions on Instrumentation and Measurement, v. 48, no. 6, p. 1141–1148.
12. Wang, N., Hughes, D., Case, T., Donnell, K., and Zoughi, R., 2000, Feasibility study of corrosion detection under paint in aluminum panels, Final Report, Texas Research Institute at Austin (TRI-Austin), p. 78.
13. Qaddoumi, N. and Zoughi, R., 1997, Preliminary study of the influences of effective dielectric constant and non-uniform probe aperture field distribution on near-field microwave images: Materials Evaluation, v. 55, no. 10, p. 1169–1173.

Distribution

	<i>Copies</i>		<i>Copies</i>
DoD - CONUS		INTERNAL DISTRIBUTION	
OFFICE OF NAVAL RESEARCH		CODE 0115 (MESSICK)	1
ATTN CODE 332 (I PEREZ)	1	CODE 60 (MORTON)	1
BALLSTON CENTRE TOWER ONE		CODE 61 (DENALE)	1
800 NORTH QUINCY ST		CODE 61S (REPORT ARCHIVE)	1
ARLINGTON VA 22217-5660		CODE 611 (CHIODO)	1
		CODE 612 (APRIGLIANO)	1
NAVAL SEA SYSTEMS COMMAND		CODE 613 (HAYS)	1
ATTN SEA 05ME (R KOK)	1	CODE 614 (CZYRYCA)	1
PMS 450 (M NOVACK)	1	CODE 615 (DELOACH)	1
2531 JEFFERSON DAVIS HWY		CODE 615 (LIPETZKY)	5
ARLINGTON VA 22242-5160		CODE 62 [OMB NO. 0704-0188]	1
		CODE 63 [OMB NO. 0704-0188]	1
NAVAL AIR WARFARE CENTER		CODE 64 [OMB NO. 0704-0188]	1
AIRCRAFT DIVISION		CODE 65 [OMB NO. 0704-0188]	1
ATTN CODE 4342 (W R DAVIS)	1	CODE 66 [OMB NO. 0704-0188]	1
22347 CEDAR POINT ROAD		CODE 3442 TIC	1
PATUXENT RIVER MD 20670-1161			
DEFENSE TECHNICAL INFORMATION			
CENTER	1		
8725 JOHN KINGMAN ROAD			
SUITE 0944			
FORT BELVOIR VA 22060-6218			

